Characterization of a novel interaction between Islr2 and Vasorin and its role in retinal axon routing at the vertebrate optic chiasm

Dissertation

der Mathematisch-Naturwissenschaftlichen Fakultät
der Eberhard Karls Universität Tübingen
zur Erlangung des Grades eines
Doktors der Naturwissenschaften
(Dr. rer. nat.)

vorgelegt von
Paolo Panza
aus Camposampiero, Italien

Tübingen
2015

Gedruckt mit Genehmigung der Mathematisch-Naturwissenschaftlichen Fakultät der Eberhard Karls Universität Tübingen.

Tag der mündlichen Qualifikation: 11.06.2015
Dekan: Prof. Dr. Wolfgang Rosenstiel
1. Berichterstatter: Prof. Dr. Christiane Nüsslein-Volhard
2. Berichterstatter: Prof. Dr. Alfred Nordheim

Portions of this thesis are published in the following articles:

Panza, P., Maier, J., Schmees, C., Rothbauer, U. and Söllner, C. (2015). Live imaging of endogenous protein dynamics in zebrafish using chromobodies. Development 142, 1879–1884.
https://doi.org/10.1242/dev.118943

Panza, P., Sitko, A. A., Maischein, H-M., Koch, I., Flötenmeyer, M., Wright, G. J., Mandai, K., Mason, C. A., Söllner, C. (2015). The LRR receptor Islr2 is required for retinal axon routing at the vertebrate optic chiasm. Neural Development 10.
https://doi.org/10.1186/s13064-015-0050-x

Abbreviations

AC	Anterior commissure
ADAM17	A disintegrin and metalloprotease domain 17
AMV	Avian myeloblastosis virus
AVEXIS	Avidity-based extracellular interaction screen
CB	Chromobody
cDNA	Complementary DNA
CH1	Heavy chain constant domain 1
Comm	Commissureless
Csf1ra	Colony stimulating factor 1 receptor A
CSPG	Chondroitin sulfate proteoglycans
DCC	Deleted in colorectal carcinoma
ddH2O	Double distilled water
DMF	Dimethylformamide
DNA	Deoxyribonucleic acid
dNTP	Deoxynucleotide triphosphate
dpf	Days post fertilization
DRG	Dorsal root ganglion
ECM	Extracellular matrix
EGF	Epidermal growth factor
eLRR	Extracellular leucine-rich repeat
EMT	Epithelial-to-mesenchymal transition
EXT1	Exostosin glycosyltransferase 1

F-actin	Filamentous actin
FP	Floor plate
FRAP	Fluorescence recovery after photobleaching
GFAP	Glial fibrillary acidic protein
GFP	Green fluorescent protein
hpf	Hours post fertilization
Hs2st	Heparan sulfate 2-O-sulfotransferase
HSPG	Heparan sulfate proteoglycan
IgG	Immunoglobulin G
IgSF	Immunoglobulin superfamily
indel	Insertion/deletion
Islr2	Immunoglobulin superfamily containing leucine-rich repeat 2
LB	Lysogeny broth
LGN	Lateral geniculate nucleus
MESAB	Ethyl 3-aminobenzoate methanesulfonate salt
MLF	Medial longitudinal fasciculus
mRNA	Messenger ribonucleic acid
mTOR	Mechanistic target of rapamycin
Mycbp2	MYC binding protein 2
NCAM	Neural cell adhesion molecule
Ngf	Nerve growth factor
NGS	Normal goat serum
Nr-CAM	NgCAM-related cell adhesion molecule
Nrp1	Neuropilin 1
Ntrk1	Neurotrophic tyrosine kinase receptor type 1
OC	Optic chiasm
ON	Optic nerve
ORF	Open reading frame

OT	Optic tract
PBS	Phosphate buffered saline
PCNA	Proliferating cell nuclear antigen
PCR	Polymerase chain reaction
pLLP	Posterior lateral line primordium
pME	Gateway middle entry clone
POC	Postoptic commissure
PTU	1-phenyl 2-thiourea
Rb1	Retinoblastoma 1
RFP	Red fluorescent protein
RGC	Retinal ganglion cell
RNA	Ribonucleic acid
Robo	Roundabout
RT	Room temperature
SC	Superior colliculus
Sema6D	Semaphorin 6D
SOC	Super optimal broth
SPR	Surface plasmon resonance
SSEA-1	Stage-specific embryonic antigen 1
TALEN	Transcription activator-like effector nuclease
TGF-beta	Transforming growth factor beta
TILLING	Targeting induced local lesions in genomes
Tp53	Tumor protein 53
TrkA	see Ntrk1
TUNEL	Terminal deoxynucleotidyl transferase dUTP nick end labelling
UAS	Upstream activating sequence
Vasn	Vasorin, alias Slit-like2
VEGF	Vascular endothelial growth factor

VHH	Variable domain of camelid single-heavy chain antibodies
VT	Ventrotemporal
WT	Wild-type
YFP	Yellow fluorescent protein
ZFIN	Zebrafish information network
ZFN	Zinc-finger nuclease

Contents

Zusammenfassung **1**

Summary **3**

Introduction **5**

Cellular strategies of axon pathfinding 5
Visual system development in vertebrates 8
Midline crossing in the visual system as a model for axon guidance 9
The ipsilateral projection in rodents 10
Default midline crossing in the visual projection . . . 13
Guidance of retinal axons in zebrafish 16
Cell surface LRR proteins in development and disease 19
Protein detection in living organisms 21

Results **24**

Isolation of *islr2* as candidate gene with roles in retinal axon pathfinding 24
Optimization of a lipophilic dye-based axon tracing technique 27
Phenotyping of *islr2* mutants 29
Islr2 and Robo2 act independently in retinal axon guidance 44
Screening for Islr2-interacting partners 44
Biochemical characterization of the Islr2-Vasna interaction 48

The Vasorin paralogs are expressed in the zebrafish visual system 50
vasna and *vasnb* mutants: generation and analysis . . 55
A first application of the chromobody technology in vertebrates 60

Discussion **70**
Identification of new players in retinal axon guidance 70
Redundancy at the optic chiasm 71
Function of Islr2-Vasorin signalling 74
The glial knot, an anatomical feature required for retinal axon midline crossing? 78
Divergence in midline crossing strategies of zebrafish and rodent retinal axons 81
Chromobodies as a complementary method to investigate endogenous protein dynamics 83

Materials and methods **89**
Zebrafish animal maintenance 89
Embryological techniques 89
Genotyping of zebrafish individuals 90
cDNA preparation 91
Amplification from cDNA 91
Cloning 92
Transformation 92
Plasmid preparation 93
Sequencing 93
RNA preparation 93
In situ hybridization 93
Immunohistochemistry 94
Whole-eye fills by lipophilic dye injection 94
AVEXIS 95
Rabbit antisera production 95
Generation of targeted knockout lines 95
Generation of transgenic fish lines 95
Imaging 96

Histological methods 97
Antibodies 98

Appendix **99**

Contributions **104**

Acknowledgements **106**

Bibliography **107**

List of Figures

1 Retinal axon pathfinding in the zebrafish embryo . . 17

2 *islr2* expression in the embryonic zebrafish retina . . 27
3 PTU treatment does not affect retinal axon guidance 30
4 Retinal axon projection phenotype in $islr2^{sa82}$ 33
5 Chronological progression of the $islr2^{sa82}$phenotype . 34
6 Embryonic axon tracts do not display overt defects in $islr2^{sa82}$mutants 35
7 Unaltered retinal lamination in $islr2^{sa82}$mutants . . . 36
8 The diencephalic anatomy of *islr2* mutants is unaffected 37
9 The number of differentiated RGCs is decreased in *islr2* mutants 41
10 Null mutations in *tp53* do not rescue optic nerve hypoplasia of *islr2* mutants 42
11 Optic nerve hypoplasia in *islr2* mutants 43
12 *islr2* and *robo2* act independently in retinal axon guidance 45
13 Vasna and Vasnb transiently bind to Islr2 47
14 Mapping of the interacting domains in Islr2 and Vasna 50
15 Detection of *vasna* and *vasnb* expression in 36 hpf zebrafish embryos 51
17 Vasna and Vasnb protein localization in 48 hpf embryos 54
16 Vasna and Vasnb protein localization in 36 hpf embryos 54
18 *vasna*/*vasnb* double mutants do not display overt defects in retinal axon guidance 57
19 *vasna* and *vasnb* alleles are null mutations 58
20 *islr2* mutants do not display mispatterning of cellular populations at the optic chiasm 60

21 Wild-type morphology in embryos ubiquitously expressing chromobodies 62
22 Chromobodies colocalize with target endogenous antigens 64
23 Actin-CB can trace endogenous Actin dynamics *in vivo* 67
24 PCNA-CB and human PCNA-GFP trace identical structures *in vivo* 68
25 PCNA-CB reveals cell cycle progression in *wnt1*-positive progenitors 69

26 The *Islr2/Linx* knockout mouse phenotype 75
27 The interaction between chromobodies and their antigens is transient 86
28 Actin-CB and PCNA-CB trace dynamic behaviours of intracellular structures 88

List of Tables

1 List of immunoreagents used in this study 98

2 Type-I transmembrane LRR proteins in zebrafish . . 99

Zusammenfassung

Eine herausragende Eigenschaft von embryonalen Nervenbahnen ist ihr hohes Niveau an axonaler Wegfindungs-Stereotypie. Um neue Kandidatenmoleküle mit potentieller Funktion in der Wegfindung von Axonen der Retina zu identifizieren, fokussierten wir uns auf die extrazelluläre „leucine-rich repeat“ (eLRR) Proteinfamilie in Zebrafisch. eLLR Proteine sind dafür bekannt spezialisierte und dynamische Funktionen an den Membranen von axonalen Wachstumskegeln auszuüben. Die Zusammenstellung eines eLRR Genkatalogs und die Analyse ihrer Expressionsmuster ermöglichte die Identifikation von *islr2* als Kandidat mit möglicher Funktion in der Regulation von früh in der Entwicklung stattfindenden Wegfindungsprozessen von retinalen Axonen. Um die *in vivo* Funktion von Islr2 zu studieren, machten wir uns folgende Vorteile des Modellsystems Zebrafisch zu Nutze: Die schnelle Entwicklung der retinotektalen Projektion und die sehr gute Zugänglichkeit für bildgebende Methoden. *islr2*^{sa82} Mutanten sind gekennzeichnet durch das Vorhandensein von ektopischen ipsilateralen Projektionen, wohin gegen Zebrafische normalerweise über komplett gekreuzte retinale Axonprojektionen verfügen. Diese Daten deuten darauf hin, dass *islr2* das Kreuzen von retinalen Axonen in die gegenüberliegende Gehirnhälfte bewerkstelligt. Durch die Zuhilfenahme eines neuartigen Protein-Protein-Interaktion-Screeningverfahrens, das die Detektion von Bindeereignissen mit niedriger Affinität ermöglicht, konnten wir Vasorin A und B als spezifische Islr2 Bindepartner identifizieren. Wir generierten Immunoreagenzien, um die Lokalisation der entsprechenden Proteine in Zebrafischembryonen zu ermitteln und konnten zeigen, dass ihre Expressionsdomänen eng mit den Leitungsbahnen von reti-

nalen Axonen assoziiert sind. Besonders Vasnb wird von einer kleinen Zellpopulation im anterior-ventalen Bereich der diencephalischen Mittellinie exprimiert, ein Standort, der auf den „Glia-Knoten“ (glial knot) hindeutet. Der Knoten ist eine anatomische Struktur, die in Maus und Huhn identifiziert wurde und von der angenommen wird, dass sie retinale Axone an der Mittellinie umleiten oder beeinflussen kann. *vasna/vasnb* Einzel- und Doppelknockout-Zebrafische weisen jedoch keine offensichtlichen Phänotypen in der Sehnervkreuzung auf. Zum Abschluss schlagen wir daher vor, dass zusätzliche durch Islr2 wirkende Faktoren an der Mittellinienkreuzung von retinalen Axonen beteiligt sind. Diese kompensieren das nicht Vorhandensein von Vasna und Vasnb *in vivo*, ein Szenario, das aufgrund der beschriebenen hohen Redundanz der Signalübertragung am Chiasma opticum nicht wirklich überrascht.

In einem parallelen Projekt generierten wir induzierbare transgene Zebrafischlinien, die „Chromobodies“ exprimieren. Chromobodies sind Antikörper, die aus einer einzelnen Domäne bestehen, abgeleitet von schwerkettigen IgG2 und IgG3 aus Kameliden. Gegen Aktin und PCNA gerichtete Chromobodies können intrazellulär exprimiert werden, wodurch endogene Zielmoleküle ohne den Gebrauch von Protein-Tags oder Überexpressionsmethoden verfolgt werden können. Diese Methode kann in lebenden Zebrafischembryonen angewendet werden, dabei repräsentieren diese intrazellulären Immunoreagenzien eine komplementäre Methode für Proteinlokalisationsstudien. Durch das Verwenden von Aktin-CB konnten wir detailgetreu die dynamischen Prozesse des Zytoskeletts, während schnellen Verhaltensänderungen, in den Zellen verfolgen. Darüber hinaus erlaubte die Verwendung von PCNA-CB das akkurate Verfolgen von DNA-Replikationsgabel-Foci im Zellkern, wodurch die Zellzyklus-Progression *in vivo* analysiert werden kann. Diese molekularen Werkzeuge verursachen überraschenderweise keine morphologischen oder entwicklungsbiologischen Beeinträchtigungen während der frühen Embryonalentwicklung und können auch in erwachsenen Tieren exprimiert werden. Hierbei handelt es sich um den ersten Bericht zur Anwendung der Chromobody-Technologie in lebenden Vertebraten.

Summary

A striking feature of embryonic axon tracts is their high level of guidance stereotypy. To isolate new candidate molecules with putative functions in retinal axon pathfinding we focused on the extracellular leucine-rich repeat (eLRR) protein family in zebrafish. eLRR proteins are known to convey specialized, dynamic functions at the axon and growth cone membranes. The compilation of an eLRR gene catalogue and the analysis of their expression patterns allowed the identification of *islr2* as a candidate putatively involved in early guidance decisions undertaken by retinal axons. We used the zebrafish to model Islr2 behaviour *in vivo*, taking advantage of the rapid development of its retinotectal projection and amenability to imaging. *islr2*^{sa82} mutants display the presence of ectopic ipsilateral projections, although zebrafish normally have a completely crossed retinal axon projection. These data suggest that *islr2* facilitates retinal axon crossing to the opposite side of the brain. Taking advantage of a novel protein-protein interaction screening method, dedicated to detecting low affinity binding events, we identified Vasorin A and B as specific Islr2 binding partners. We generated immunoreagents in order to describe these proteins' localization in zebrafish embryos and found that their expression domains are closely associated to the retinal axon pathway. Vasnb, in particular, is expressed by a small population of cells at the anterior ventral diencephalic midline, a location reminiscent of the glial knot. The knot is a structure identified in mouse and chick which was anatomically thought to redirect retinal axon fibers at the midline. *vasna/vasnb* single and double knockout animals, however, do not show overt phenotypes in the optic nerves traversing the chiasm. In conclusion, we propose

that other midline factors act through Islr2 allowing retinal axons to cross the midline. They compensate for the absence of Vasna and Vasnb function *in vivo*, a scenario that is not surprising when considering the high level of signalling redundancy characteristic of the optic chiasm.

In a parallel project, we created transgenic zebrafish lines expressing chromobodies in an inducible fashion. Chromobodies are single-domain antibodies derived from heavy-chain IgG2 and IgG3 of camelids. Actin- and PCNA-directed chromobodies can be expressed intracellularly, allowing to trace endogenous targets without the need of protein tagging or overexpression. This technique can be applied in live zebrafish embryos, introducing intracellular immunoreagents as a complementary technique for protein localization studies. Using Actin-CB we were able to follow detailed cytoskeletal dynamics during rapid cellular behaviours in living animals. Additionally, PCNA-CB allows accurate tracing of DNA replication forks foci in the nucleus, making it possible to discern cell cycle progression *in vivo*. These tools surprisingly do not cause morphological or developmental defects throughout the duration of early development and can be expressed to adulthood. This is the first report of the applicability of the chromobody technology to living vertebrates.

Introduction

Cellular strategies of axon pathfinding

A common theme in developmental biology is how the morphogenesis of a certain structure is often observed to be highly stereotyped: a morphogenetic process is reliably carried out in the same way in different individuals of a certain species, at times even in different species. Genetic analysis of essential developmental processes has recently started to unravel that stereotypy is a consequence of elaborate cellular and molecular systems of emergent robustness, to the level that removal of regulatory components is compensated. This strategy of self-stabilizing regulation is able to confront environmental variables that would otherwise affect organismal development. Stereotypy and redundancy are central themes in this dissertation. Such reproducible, stereotyped modes of development particularly underlie the formation of early embryonic axon tracts, a founding observation in developmental neurobiology. The extraordinary precision of nervous systems connectivity is illuminated by models of axon guidance. This field investigates how axons are precisely guided to appropriate targets and aims at identifying the molecular signals that instruct this type of decisions.

The growth cone is a spread-out cellular compartment found at the tip of growing axons and its structural and functional integrity is required for axon navigation. Growth cones are organized in a central and a peripheral domain (C- and P-domain), which greatly differ in form and molecular processes they host (Lowery and Van Vactor, 2009). The C-domain shares with the axon a scaffold made of stable microtubules, which are required for long-range vesicular transport. This region is also enriched in mitochondria and exocytic vesicles.

In contrast, the growth cone periphery opens up with a fan-like shape and it is the main site of Actin dynamics, although sparse dynamic microtubules do venture in this area. Growth cone advancement through the surrounding environment is seen as a consecution of stages which include protrusion, engorgement and consolidation through establishment of focal adhesions (Lowery and Van Vactor, 2009; Vitriol and Zheng, 2012). The direct mediator of every growth cone's ability to steer and chemotactically crawl is a combination of Actin (de)polymerization at the leading edge – allowing the formation of lamellipodia and filopodia, which endow the growth cone with ameboid movement – and microtubule dynamics. The global directionality of an advancing growth cone is governed by the localized (de)stabilization of cytoskeletal elements, which is the common downstream effector of guidance receptors displayed on the growth cone plasma membrane (Lowery and Van Vactor, 2009; Vitriol and Zheng, 2012). Several additional dynamic processes essentially contribute to the growth cone function, for example specific mRNA localization to the growth cone, local protein synthesis and degradation (Holt and Schuman, 2013; Jung et al., 2012), and asymmetric membrane recycling (Tojima et al., 2010; Vitriol and Zheng, 2012). The environment traversed by elongating axons is presented to the growth cone as a complex combination of adhesive molecules, repellent substrate-bound cues and diffusible chemotropic molecules, which is constantly interpreted to generate advancement in a certain direction or asymmetric retraction. One can therefore conceive the growth cone as a "travelling signal integrator", because exogenous signals detected through guidance receptors will be integrated at the level of second messengers or cytoskeletal effectors to produce a median output (Lowery and Van Vactor, 2009). Thus, the growth cone allows axons to discriminate their path by filtering signalling noise and averaging the environmental guidance cues; as a result, axons appear to follow a highly stereotypic route. It has been noticed, however, that the stereotypy of axon tracts is a property emerging from an additional variety of environmental features and strategies adopted by migrating axons (Raper and Mason, 2010).

The presence of an appropriate substrate for axonal growth is often a determining factor in axon guidance and can orient outgrowing axons (Randlett et al., 2011) or form corridors for their extension (Silver and Rutishauser, 1984). These prepatterned routes facilitate axon migration through complex environments, especially during the genesis of embryonic commissures, and are contributed by distinct cellular populations, which can express permissive factors controlling axon-substrate adhesion or acquire the capacity to redirect axons. In zebrafish, cells expressing glial markers form a bridge, which temporally precedes the extension of the postoptic commissure (POC) (Barresi et al., 2005). Another prominent cellular formation, the "glial sling", has been described to be required for the contralateral growth of callosal commissural axons in mouse (Silver et al., 1982). In this case, cells of the glial sling function as a barrier, redirecting growth cones to the opposite brain hemisphere. Along their route axons need to change directionality, at times dramatically; however, cellular barricades are not always the preferred strategy to change the course of axon fibers. In the nerve cord of both protostomes and deuterostomes, for example, after traversing the midline, axons turn to align themselves along the longitudinal embryonic axis and extend at a close distance from the midline. In this process, axons reach and contact a special set of medial cells that express specific guidance cues, thereby instructing growth cones to surpass the midline (Evans and Bashaw, 2010) and then immediately follow their postcrossing path (Stoeckli, 2006). Cellular landmarks with guidance function have been collectively named "guidepost cells". Outgrowing axons can additionally rely on pre-existing tracts for their guidance, by exploiting axon-axon interactions. The stereotyped trajectory of several embryonic tracts has been described to be dependent on the successful navigation of pioneering axons (Chitnis and Kuwada, 1991; Bak and Fraser, 2003). Once the earliest growth cones have pioneered a non-innervated tract, subsequent axons, named "followers", can partly rely on fibre-fibre adhesion and fasciculation for appropriate navigation (Pittman et al., 2008). There is another dimension to the phenomenon of stereotypy of axon tract development. These

fundamental central nervous highways must also be stable over time and mostly remain unaltered to adulthood. However, in many systems it has been recognized that axons at times commit guidance mistakes. These misprojections will not be functional at later stages of development and therefore must be removed by error correction mechanisms (Hutson and Chien, 2002; Poulain and Chien, 2013). Accordingly, most misprojections are pruned during development, a process that ensures that the only remaining axons are functional and are positioned correctly.

Visual system development in vertebrates

Animals critically rely on the precise establishment of eye-brain wiring to exert any visually-evoked behaviour. As a consequence, it is primarily important that axon tracts transporting visual information to processing areas of the brain are properly guided during early embryonic development. The simplest architecture of a visual projection comprises retinal ganglion cells (RGCs) as central relays of visual information transfer to the brain. RGCs are the first neuronal cellular type differentiating in the retina and integrate information indirectly derived from photoreceptor cells and filtered by other retinal cells (Erskine and Herrera, 2014). RGCs grow out axons that fasciculate into one of the earliest commissural tracts which develop in the embryonic brain, the optic nerve. Retinal axons must exit the eye (Stuermer and Bastmeyer, 2000; Oster et al., 2004), cross the midline of the ventral diencephalon through the anterior hypothalamus (Jeffery and Erskine, 2005; Petros et al., 2008) and grow posteriorly and dorsally to processing brain areas, the lateral geniculate nucleus (LGN) and superior colliculus (SC) in mammals or the optic tectum in other vertebrates (Erskine and Herrera, 2014). Once axons reach these target tissues, they arborize and form stable synaptic contacts with other neurons, which are distributed in laminae and send information for motor output or sensory integration in the mammalian cortex (Xiao and Baier, 2007; Xiao et al., 2011; Feldheim and O'Leary, 2010). A very special property of the retinal axon tract is that it transports topographic information. RGCs

located in different quadrants of the retina receive positional visual stimuli, whose relative spatial arrangement must be preserved at the arrival of visual information in the brain. Axons of the optic nerve maintain the retinal topography and project it onto the dorsal midbrain, establishing a so-called topographic map, which reproduces the perceived visual space with correct orientation. The topography of visual systems is instructive for the actuation of visually-evoked behaviours in animals (Sperry, 1943).

Midline crossing in the visual system as a model for axon guidance

Midline crossing is one of the most prominent decisions axons have to take on their way to appropriate targets. Axons of all commissural tracts encounter the embryonic midline, which acts as an intermediate target fundamentally required for extension to the contralateral side of the brain. The behaviour of axons at the midline is considered a simplified readout of guidance, because the variety of decisions axons take is limited. As a consequence, paradigms for the investigation of midline crossing take advantage of loss- and gain-of-function conditions to characterize a particular molecule as attractant or repellent for traversing axons. The classical model for midline crossing is the interaction of commissural axons with midline glia of the ventral nerve cord in *Drosophila* (Evans and Bashaw, 2010). Midline cells at the same time secrete Netrin, a potent axon attractant and growth stimulator, and Slit, a repellent molecule. Precrossing axons are drawn to the midline by effect of Netrin binding to its receptor, Frazzled (a DCC ortholog). Commissureless (Comm) is an endocytic sorting factor that prevents Roundabout (Robo) receptors to reach the growth cone membrane and it is highly expressed in precrossing axons. Upon contacting midline cells, Comm expression is downregulated, causing the targeting of Robo receptors to the growth cone, which can successfully transduce repellent signals with the effect of pushing crossing axons away from the midline (Keleman et al., 2002, 2005). A similar mechanism is at work in ensuring that commissural axons of the vertebrate spinal cord cross the floor plate, albeit the

absence of Comm orthologs. Robo3 receptors are transcribed into two functionally different transcript isoforms. The first is expressed in precrossing axons and downregulates Robo1/Robo2-mediated repulsion, until at the midline a translational or trafficking switch induces the stabilization of a second Robo3 isoforms, which cooperates with the other Robo receptors to transduce Slit signals (Chen et al., 2008). A similarly well-studied model for midline crossing is the vertebrate retinal projection (Petros et al., 2008; Jeffery and Erskine, 2005), although the cellular and molecular regulation of forebrain commissures development is different (Lindwall et al., 2007; Chédotal, 2011). More evidently, in contrast to spinal cord commissures, numerous binocular animals possess optic nerves that upon arriving at the optic chiasm (the X-shaped region where projections from each eye cross the midline) diverge to form an ipsilateral and a contralateral axon bundle. The ipsilateral component of the optic nerve is dedicated to transmit visual information from the part of the visual field which is shared between the eyes of binocular organisms. Accordingly, RGCs from the ventronasal region of the retina specifically project ipsilateral fibers that correlate in size with the degree of binocularity observed in different mammals. The contrary, however, is not always true. Fish and birds generally have completely crossed retinal projections, although specific predators have centrally-located eyes and highly binocular fields of view. These animals may lack ipsilateral projections, but can compensate by directing visual information to higher processing centers or by taking advantage of different strategies for connectivity. Amphibian tadpoles have laterally-located eyes and fully contralateral optic nerves, although at metamorphosis they acquire ipsilateral projections, as the eyes relocate in frontal position (Nakagawa et al., 2000).

The ipsilateral projection in rodents

Research heavily concentrated in the last decades on the ontogeny of the rodent ipsilateral retinal projection. Indeed, the divergence of axons at the midline is the most evident strategy to achieve final integration of the monocular visual fields. The early descriptive

analysis of retinal fibre trajectories at the chiasm (Godement et al., 1990; Sretavan, 1990) prompted the investigation of the properties of midline tissue related to retinal axon growth and guidance. *Ex vivo* experiments using membranes derived from the murine optic chiasm revealed that these cells express a chemorepellent or chemosuppressive factor, which specifically affects ventrotemporal (VT) retinal axons (Wizenmann et al., 1993). Later experiments clarified that chiasmatic cells exhibit a contact-dependent repulsive activity towards ventrotemporal axons (Wang et al., 1995). In addition, it was determined that secreted factors derived from midline tissue make it generally inhibitory to axon growth, a property shared with the floor plate of the spinal cord (Wang et al., 1996). These results could explain the observations of retinal growth cones slowing down when approaching the midline (Godement et al., 1994). In particular, growth cone morphology appears to change when axons transit from more lateral to medial positions of the optic pathway. This is due to the fact that growth cones are frequently found in a pausing state near the midline, and this phase is characterized by adoption of complex, spread-out morphologies that are indicative of an "exploratory" behaviour. This condition is in sharp contrast with the streamlined form of growth cones when axons advance, phases that have a reduced duration in the vicinity of the chiasm (Mason and Wang, 1997). These findings opened two main research directions, one involving the characterization of how the chiasmatic tissue is exactly patterned, the other investigating which specific molecules trigger midline repulsion. The work of Wizenmann et al. (1993) included a suggestion that midline radial glial cells might selectively repel ventrotemporal retinal axons. This was demonstrated two years later (Marcus et al., 1995), by using an anti-RC2 (Nestin) antibody to highlight radial glial cells. In addition, it was shown that at stages when ipsilateral axons diverge at the midline (E15-E17) a raphe of cells is present at the very midline, inside the chiasmatic RC2-positive radial glia population. These cells express SSEA-1, an antigen found in embryonic stem cells, and ipsilateral axons never proceed beyond them (Marcus et al.,

1995). At earlier embryonic stages (E12.5-E13.5), SSEA-1 is expressed by a subset of cells which are marked by CD44 (Marcus and Mason, 1995). This CD44-positive cell population was described to border posteriorly the chiasm, forming an inverted V-shaped territory. Interestingly, beside CD44, which inhibited axon growth *in vitro*, these neurons also expressed L1, a well-known axon growth-promoting molecule (Sretavan et al., 1994). Therefore, the role of such cells for chiasm formation appeared controversial. However, when CD44-positive cells were subjected to complement-mediated ablation, retinal axons failed to enter the anterior hypothalamus, suggesting that this cellular population is required for chiasm formation (Sretavan et al., 1995). The characterization of tissue types and their molecular markers in the ventral diencephalon highlighted the fact that different cellular populations seem to contribute in specific ways to retinal axon guidance. Because axons from the ventrotemporal quadrant of the retina avoid the midline raphe of SSEA-1-positive cells, it is conceivable that this particular cell population expresses contact-dependent repellents that deflect axons to the ipsilateral tract. Nakagawa et al. (2000) showed that molecules of the Ephrin-B class begin to be expressed at the chiasmatic midline in metamorphic *Xenopus* larvae. It is at this timepoint that the larval retinal projection, fully contralateral, is paralleled by the appearance of an ipsilateral projection, which develops to accommodate the newly acquired binocularity. Interestingly, Ephrin-B is also expressed in the mammalian chiasm, but not in chick or fish, suggesting that it could be critical for the development of the ipsilateral projection (Nakagawa et al., 2000). Blocking the function of Ephrin-B2 in semi-intact chiasm preparations reduced the number of ipsilateral axons, indicating that Ephrin-B2 is necessary for the formation of the ipsilateral projection (Williams et al., 2003). Ephrin-B2 is the only Ephrin specifically expressed in a subset of midline radial glial cells and its transcript level peaks at the stage when most ipsilateral axons are navigating. Consistent with the specific repulsive effect of Ephrin-B2 for axons programmed to project ipsilaterally, the Ephrin-B2 receptor – EphB1 – was found to be ex-

pressed by ventrotemporal RGCs and to be required for ipsilateral growth of their axons. Indeed, *EphB1* knockout mice display an increase in the number of axons crossing the midline, at the expenses of the ipsilateral projection (Williams et al., 2003). Interestingly, however, *EphB1* mutant mice do not completely lack ipsilateral axons and residual innervation in the ipsilateral tract is still present in the *EphB1*, *EphB2*, *EphB3* triple knockout, suggesting that these receptors are not redundant in transducing repulsive cues from the midline (Williams et al., 2003). Additional investigations established that the transcription factor Zic2 marks postmitotic ventrotemporal RGCs and controls their ipsilateral guidance program (Herrera et al., 2003) by inducing *EphB1* at the transcriptional level (Lee et al., 2008). Islet-2, instead, is expressed by the majority of RGCs, projecting their axons to the contralateral side of the brain. This transcription factor represses the ipsilateral program by controlling the levels of Zic2 and – directly or indirectly – of EphB1 (Pak et al., 2004).

Default midline crossing in the visual projection

Whereas a genetic program driving the formation of the ipsilateral retinal projection has been characterized, it is still not completely understood how the majority of retinal axons cross the midline. This event is common to the ontogeny of the visual system in most animals, however it appears in contradiction with data describing axon growth *in vitro*. These experiments show that the chiasmatic tissue once explanted is generally inhibitory to axon growth (Wang et al., 1996, 1995). As a consequence, two models have been put forward to explain why retinal axons might cross the midline by default. (1) The first model implies that RGCs, which do not express the Ephrin-B2 receptor EphB1, are insensitive to midline repellents. This scenario accounts for the redirection of the largest set of ventrotemporal (ipsilateral) axons to cross the midline in *EphB1* mutant mice (Williams et al., 2003). The model implies that midline crossing is a passive property of RGCs, which are capable of ignoring inhibitory cues and exert crossing by default. (2) A second

model proposes that contralateral growth of retinal axons is instead an active process, making use of one or several molecules that allow axons through the midline. As a consequence, genetic conditions determining an increase in the ipsilateral component of the optic nerve should be found, since mutants rarely show true axon stalling at the midline choice point.

Explant culture systems alone are unlikely to yield a solution to the controversy, especially because they may not fully reproduce the spatiotemporal arrangement of cellular and molecular cues that are intimately associated to the retinal projection in the optic stalk and ventral diencephalon (Marcus et al., 1995; Silver et al., 1982; Silver and Rutishauser, 1984). For instance, explanted RGCs change their growth properties when confronted with a uniform culturing environment (Zolessi et al., 2006). Work on the development of retinal projections, instead, suggested that oriented cellular populations can be fundamental for axon guidance, often giving rise to spatially-definite signalling domains. In the chick embryo retinal axons selectively associate along their ventral diencephalic course to endfeet of neuroepithelial cells of radial morphology, which display pial immunoreactivity to neural cell adhesion molecule (NCAM). Interfering with NCAM antigen presentation *in vivo* results in the perturbation of retinal axon guidance, indicating that NCAM marks a preformed adhesive pathway for the retinal projection (Silver and Rutishauser, 1984; Silver et al., 1987). In another example, the region bordering posteriorly the mouse chiasm consists of CD44/SSEA-1-positive neurons that locally support retinal axons. When these neurons are ablated, axons cannot proceed further into the ventral diencephalon (Sretavan et al., 1995). Collectively, these data demonstrate that the chiasmatic tissue is not exclusively refractory to axon extension. However, it is not known whether CD44/SSEA-1-positive cells influence midline crossing of retinal axons, in that a possible phenotype would be masked by the stronger effect of cell ablation (Mason and Sretavan, 1997). Specific molecules with direct functions in midline crossing have not been identified until very recently. A first indication of active systems promoting

midline crossing came from the blockade of Nr-CAM in semi-intact chiasm cultures. Predominantly expressed by contralateral RGCs in mouse, Nr-CAM appeared to cell-autonomously facilitate axon extension through the chiasm. *Nr-CAM* mutant embryos displayed alterations in the retinal projection only after retrograde lipophilic labelling of the tract, showing an increased number of ipsilaterally-projecting ventrotemporal RGCs at E18.5 (Williams et al., 2006). The work of Kuwajima et al. (2012) finally demonstrated that Nr-CAM and Plexin-A1 on retinal axons can independently transduce repulsive Semaphorin6D (Sema6D) signals derived from the midline. Surprisingly, Nr-CAM and Plexin-A1 are also required at the chiasm, where their presence determines the conversion of Sema6D effect from repulsion to growth promotion. The two receptors in RGCs are also required for the transduction of Sema6D growth-promoting effect. How changing the sign of a guidance cue might be functionally relevant to midline crossing and spatiotemporally regulated remains to be established. Another receptor implicated in retinal axon midline crossing is Neuropilin 1 (Nrp1). *Nrp1* knockout mice display an increase in size of the ipsilateral projection, a phenotype shared with vascular endothelial growth factor (VEGF164) mutants. A *Nrp1* allele abolishing receptor binding to all class 3 Semaphorins, conversely, did not show similar defects. VEGF164 indeed is expressed at the chiasmatic midline (whereas class 3 Semaphorins are not) and appears to function as chemoattractant for murine retinal axons (Erskine et al., 2011).

In conclusion, an appropriate view of retinal axon midline crossing might emerge from the joint consideration of both models described here. In rodents, contralateral RGC axons are indeed lacking the genetic program that makes them sensitive to important midline repellents; however, they require specific receptor molecules that endow them with the capability of recognizing and surpassing the midline.

Guidance of retinal axons in zebrafish

The eyes of zebrafish are positioned laterally from embryonic to adult stages, conferring only poor binocularity, but at the same time a large field of view, probably required for predator avoidance and positional recognition of conspecifics. As a consequence, zebrafish retinal axons all project to the opposite side of the brain. The development of RGCs and their axonal projections follows in this animal a somewhat rigid timeline (Burrill and Easter Jr, 1994; Stuermer, 1988), in that these cells begin to differentiate at about 28 hpf, from the ventronasal retinal quadrant, proceeding to nasal, dorsal and temporal retinal partitions. At about 48 hpf, differentiated RGCs are for the first time homogeneously distributed in the appropriate retinal layer. From the time of their cell cycle withdrawal, RGCs immediately project an axon which ultimately will grow outside the eye. The site of axon emergence is specified by contact with Laminin substrate (Zolessi et al., 2006; Randlett et al., 2011). The retinal fibers invade the optic stalk and reach at 34-36 hpf the prospective chiasmatic midline. At about 48 hpf pioneering growth cones have reached the rostral border of the optic tectum. Along the optic tract retinal axons have organized in a ventral and dorsal branch, which respectively contain axons from dorsal and ventral RGCs (Baier et al., 1996). During the second and third day of development, tectal connectivity and a topographic map of the visual field are established (Stuermer, 1988). Thanks to the rapid development of the retinal projection, external fertilization and embryonic growth, transparency, and genetic tractability, the zebrafish – together with *Xenopus* – has been chosen as ideal model for the analysis of retinal axon guidance (Fadool and Dowling, 2008).

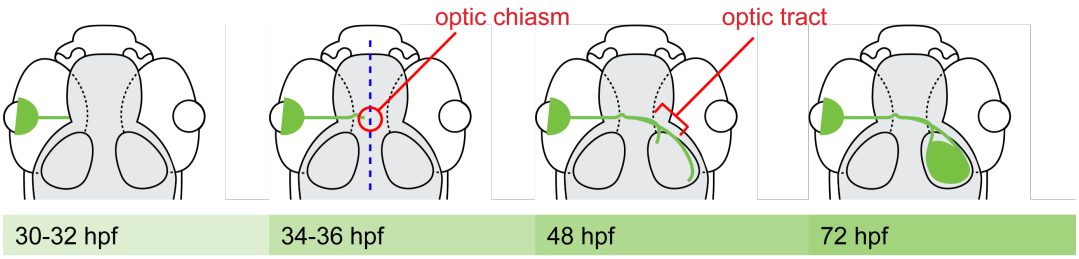

Figure 1. Retinal axon pathfinding in the zebrafish embryo
Chronology describing the morphogenesis of the retinal axon projection in zebrafish. RGC differentiation begins at about 28-30 hpf from the ventrotemporal portion of the retina. These cells immediately project axons that navigate the retinal tissue and recognize the prospective optic nerve head. Retinal axon outgrowth continues through the 36 hpf stage, when pioneering axons contact the ventral diencephalic midline for the first time. As soon as the first cohort of retinal axon fibers cross the midline, the optic chiasm is established. Retinal axons exit the chiasm and join a permissive corridor along the lateral pial surface, the optic tract, which brings axon fibers from the ventral diencephalon to the dorsal midbrain. Along their course, retinal axons redistribute into two *brachia*, one ventral and one dorsal, from which target innervation will initiate. From about 48 hpf through the third day of development, retinal axons arborize in the optic tectum and target synaptic contacts are refined. The final product is a functional topographic map of the visual world projected onto the animal brain. Note: for simplicity, the morphology of embryos at different developmental stages is invariant in the schematic.

In order to identify new guidance molecules with distinct *in vivo* phenotypes, contrarily to the more traditional *in vitro* systems used, a large forward genetic screen to isolate mutants with defects in retinotectal pathfinding or topography has been conducted (Baier et al., 1996; Karlstrom et al., 1997; Trowe et al., 1996). The majority of mutations mapped so far strikingly hit essential signalling factors implicated in brain patterning, combining guidance defects with more pronounced morphological abnormalities of the neural tissue (Poulain et al., 2010). In particular, several of these mutations affected the Hedgehog signalling pathway, which is required for midline patterning in vertebrates (Chiang et al., 1996) but also has a direct role in axon guidance (Charron et al., 2003). The laborious characterization of mutants thought to act cell-autonomously culminated with the identification of *astray/robo2*, an RGC receptor ensuring the anteroposterior containment of the retinal projection,

prevention of recrossing and chiasm formation (Fricke et al., 2001). These findings prompted the investigation of the function of Robo ligands (Slit) in retinal axon pathfinding. Slit1 and Slit2 indeed cooperate to form a corridor of surrounding repulsion for retinal axons in mouse, thereby prohibiting inappropriate ectopic axon crossing (Plump et al., 2002). More detailed work on *astray/robo2* showed that Slit2 and Slit3 are the plausible partners of this receptor in zebrafish retinal axon guidance. Surprisingly, Robo2 appeared to be required both before and after midline crossing and a function in guidance error prevention and correction was identified. Although *astray* mutant embryos displayed larger and more complex growth cones and an overall increase in axon guidance mistakes (mainly at the midline) that were not corrected, ipsilateral neurites were always pruned like in control siblings. These data suggested that a mechanism for correction of ipsilateral misprojections exists and is unaffected in *robo2* mutants (Hutson and Chien, 2002).

When considering the collection of mutants displaying defects in midline crossing, only few do not concurrently show general patterning phenotypes, an indication that these genes could be specifically required for guidance, likely cell-autonomously. One of them, *esrom*, encodes truncations in MYC binding protein 2 (Mycbp2), an intracellular scaffolding protein that controls axon guidance and synapse formation from invertebrates. These zebrafish mutants display phenotypes at different levels of the retinal projection: they have a defect in midline crossing, as only a subset of fibers proceeds beyond the midline (Karlstrom et al., 1996), their axons are insufficiently fasciculated, and the segregation into separate roots for tectal innervation is affected (D'Souza et al., 2005). Unfortunately, Mycbp2 appears to have complex functions that comprise interacting with mTOR signalling, inhibiting adenylate cyclases, functioning as E3 ubiquitin ligase, controlling responsiveness to axon guidance cues by controlling the level of their receptors, and modulating microtubule and F-actin dynamics (Po et al., 2010; Hendricks and Jesuthasan, 2009; D'Souza et al., 2005). As a consequence, the exact cause for the observed *esrom* phenotypes has not been identified yet. An-

other mutant isolated in the forward genetics screen effort, *space cadet/rb1* shares many characteristics with the *islr2* mutant condition discussed in the present work. *Space cadet* has been initially identified for a locomotor behaviour phenotype, the inability to perform fast turning movements due to axonal defects in a subset of hindbrain commissural neurons (Lorent et al., 2001). These mutant larvae also display peculiar phenotypes of the retinotectal projection, for instance the retinal axons' failure to exit the retina, a hypoplastic optic nerve and ipsilateral projections (Lorent et al., 2001). The *rb1* mRNA is ubiquitously expressed during embryonic development in the retina, however the basic histology of this structure appears unaltered in homozygous embryos. *Space cadet* mutants nonetheless display a decrease in the number of early-born RGCs due to a combined increase in apoptosis and delayed cell cycle exit of the progenitors (Gyda et al., 2012). To this point, the direct cause of the specific pathfinding defects displayed by mutant larvae is still unknown.

Cell surface LRR proteins in development and disease

Cell surface and secreted proteins constitute a great portion of the human proteome, which reflects their functional relevance in most cellular processes. Among these proteins, the extracellular leucine-rich repeat (eLRR) superfamily has recently attracted attention, based on its disproportionate expansion in mammals (Dolan et al., 2007). eLRR proteins display a wide range of specific neural and immune tissue expression patterns, suggesting their involvement in mediating specialized functions at the cell membrane and in the extracellular milieu. The extensive usage of this protein-protein interaction module shows correlation with the increased complexity of mammalian nervous system connectivity and organization. The high evolvability empirically inferred from genome-wide surveys concentrating on the eLRR superfamily, has its structural basis on the properties of the LRR domain itself. The LRR motif is composed by 20 to 30 amino acids including Leucine at conserved positions. This amino acidic stretch is found to be repeated in tandem for a vari-

able number of iterations to finally form the complete domain. The emerging three-dimensional fold resembles a banana-shaped structure with a large concave surface consisting of beta-sheets and a less structurally conserved convex part. Variations at the level of single motif length and total number of repeats affect the final curvature of the interaction domain, which can therefore accommodate a large diversity of globular ligands (de Wit et al., 2011). eLRR proteins have been implicated in all aspects of neural connectivity establishment, from axon guidance and tract positioning, to target selection, to synaptogenesis. In addition, these proteins' roles in regulating (negatively for the most part) myelination and synaptic plasticity have been under investigation as putative causative factors in human neurological and psychiatric disorders, such as obsessive-compulsive disorder, schizophrenia and epilepsy (de Wit et al., 2011). Importantly, certain functions, for example the pivotal role of Slit/Robo signalling in midline crossing and longitudinal tract positioning, are conserved in *Drosophila* and mammals. Conversely, eLRR proteins mediating target selection or synaptogenesis appear to radically differ between invertebrates and mammals, reflecting the higher degree of diversity in strategies employed to regulate these processes.

Despite the functional attractiveness of the eLRR protein class – important mediators of dynamic cell-cell and cell-ECM interactions and signalling – they are often underrepresented in most interactomics studies. Indeed, the analysis of cell surface and secreted proteins is complicated by several factors, precluding their final characterization. The purification of superfamily members containing transmembrane domains remains laborious. Disulphide bonds, post-translational modifications and glycosylation are usually required for the replication of functional surfaces, for which reasons large-scale expression systems are normally not suitable. eLRR proteins are known to sustain low-affinity interactions, which fail to be detected by most methods. In the present work, we tackle these limitations by merging the expression data available for most eLRR genes in zebrafish, to large-scale interaction screening results produced using an assay optimized for the detection of low-affinity interactions.

Using this strategy, we identified *islr2* as new candidate gene to regulate axon guidance in the retinal projection. Islr2 (alias Linx) is a type-I transmembrane protein containing a LRR and an immunoglobulin domain in its extracellular portion. Its transcripts are found in localized populations of postmitotic neurons distributed along the whole nervous system. *Islr2* is expressed in the chick and mouse motor column, subsequently appearing in neurons of the dorsal root and sympathetic ganglia (Gejima et al., 2006). Homma et al. (2009) additionally detected *Islr2* transcripts in the nasal placodes, cranial ganglia and dorsal neuroretina of the E10 mouse embryo. This gene was identified from a microarray analysis of factors downregulated in the *Ngf* mouse knockout condition, where most TrkA-positive DRG axons are lost. Indeed, Islr2 was found to colocalize with TrkA in explanted DRG neurons (especially in axons) and could be immunoprecipitated with the neurotrophin receptor. *Islr2* knockout mice display sensory and motor projection abnormalities, like thinning and increased branching, which partially phenocopy *Ret* and *Ngf* null conditions. This effect did not depend on programmed cell death and was consequently imputed to the function of Islr2 in modulating neurotrophin signalling (Mandai et al., 2009). Recent work identified the requirement of Islr2 for the formation of the internal capsule, a major brain tract comprising thalamocortical and corticofugal projections (Mandai et al., 2014). Although the expression of *Islr2* is globally similar in chick and mouse, and this factor appears to be expressed in RGCs (Blackshaw et al., 2004), its function in retinal axon guidance has not been investigated thus far. In the first part of this dissertation, I will characterize Islr2 function in the formation of the zebrafish retinal axon projection.

Protein detection in living organisms

The investigation of protein localization and dynamics is central to the characterization of protein function. Traditionally, the examination of protein distribution in cells and tissues has relied on immunohistological protocols that are based on the introduction of immunoreagents inside the cell. While this type of approach is con-

sidered the "gold standard" for protein localization description, it can give rise to artifactual results, given the dramatic tissue alterations induced by fixation/permeabilization procedures (Schnell et al., 2012). In order to circumvent these limitations, the comparison with live cell imaging data has been deemed indispensable. Target protein fusions to genetically-encoded fluorescent tags are indeed capable of tracing protein dynamics in an intact, living system, with the advantage of minimally interfering with the physical properties of the tissue in analysis. Unfortunately, however, a notable pitfall of this methodology is the effect of a direct modification of the polypeptide of interest. Most protein localization studies take advantage of fluorescent protein fusions that are introduced either at the N- or C-terminus or in an internal site of the target protein. Although generally reliable, this strategy has been reported to cause artifacts of different kind. Among the complications derived from using fluorescent proteins as tags is steric hindrance, which might underlie conditions where functional surfaces or interaction sites of the targeted protein are masked or overall protein folding is affected. Protein tags can induce aggregation or artifactual multimerization, as was the case of a YFP-fused MreB actin homolog in *E. coli* (Swulius and Jensen, 2012). A global analysis of protein localization in *S. cerevisiae* has been conducted by inserting a GFP tag at the C-terminus of target ORFs by homologous recombination. This work showed that proteins which require modification of C-terminal domains for their localization were often mislocalized, probably because of altered secretion and transport (Huh et al., 2003). In summary, the negative effects of protein tagging can contribute to altering endogenous protein localization and dynamics (Khmelinskii et al., 2012). In this context, where comparison between immunolabelling and live imaging of fluorescent fusions is highly recommended, chromobodies stand out as the most promising complementary reagent to reveal endogenous proteins with limited interference. Chromobodies are fluorescent fusions of nanobodies (Rothbauer et al., 2006), derivatives of single-chain antibodies present in camelids (Hamers-Casterman et al., 1993). In these an-

imals, IgG2 and IgG3 antibody classes retain their natural ability to recognize and bind antigens though their hypervariable domain (VHH), however they do not associate with light chains given the loss of CH1 domains required for this interaction (Muyldermans, 2013). The nanobody repertoire of an immunized or naïve animal can be isolated by cloning of the V gene repertoire from peripheral blood lymphocyte cDNA and the identification of functional nanobodies is carried out by panning of phage display libraries against an antigen of interest. Positive clones can be exogenously expressed in bacteria or mammalian cells, so that – once fused to fluorescent proteins – the result is a genetically-encoded functional antibody expressed intracellularly, which is capable of detecting endogenous proteins (Rothbauer et al., 2006). This is achieved in the absence of target protein overexpression or tagging. In combination with the transient binding mode displayed by commercial chromobodies, these reagents are likely to reproduce endogenous protein characteristics with minimal functional interference. In the second part of my thesis, we asked whether chromobodies can be used in an intact, living organism.

Results

Isolation of *islr2* as candidate gene with roles in retinal axon pathfinding

In a previous study (Söllner and Wright, 2009), a large fraction of the zebrafish repertoire of cell surface LRR and IgSF proteins was cloned and screened for transient protein-protein interactions. With the ultimate aim of establishing which binding partners were suitable for further investigation, mRNA expression patterns were compared to infer putative embryonic functions. Double fluorescent *in situ* hybridization data were collected for most of the interacting protein pairs (Söllner and Wright, 2009), revealing the relative distribution of receptor- and ligand-expressing cells in zebrafish embryos. Interacting cell surface proteins were found to be expressed by the same cells or by adjacent tissues, implying different mechanisms of action. Importantly, these data assisted the identification of the developmental time window and location at which the binding protein pairs could exert physiological functions in the embryo. To identify novel proteins required at the membrane for normal retinal axon pathfinding, we focused on the cell surface LRR family, because of these proteins' reported functional relevance in neural development. Contrarily to the method exposed above, we assembled a comprehensive list of type-I cell surface LRR receptor genes in the zebrafish genome, by following orthology relationship to the mammalian protein family surveyed in Dolan et al. (2007). We screened the subset of genes with annotated expression patterns in the zebrafish model organism database, ZFIN (Bradford et al., 2011), in search of hits transcribed in RGCs, the first neurons that differentiate in the zebrafish retina and the cell type responsible for the transmission of

visual information to higher processing centers. Among the 116 genes analysed, 23 were described to be expressed in the RGC layer (Table 2 on page 99). We based our analysis on these genes, because of both their clear expression in differentiated neurons, indicative of specialized functions (i.e. axon guidance), and their transmembrane structure, suggesting their involvement in signal transduction at the membrane. The earliest RGC differentiation and axon outgrowth events follow a rigid time course in zebrafish. RGCs terminally withdraw the cell cycle starting at about 30 hpf in the ventronasal portion of the neural retina, a location that is associated with the ventral choroid fissure, which provides an anatomical blueprint for migration out of the eye. Immediately after differentiation, RGC axons start to form at about 32 hpf and immediately grow towards and inside the brain, to first reach the diencephalic midline at about 36 hpf. Between the second and third day of development, most zebrafish retinal axons – now forming the optic nerve – follow their postcrossing route in the optic tract and establish functional innervation with specific targets in the optic tectum. We took advantage of the stereotyped time series of events in the development of the zebrafish retinal projection to assign putative functions to candidate LRR receptors expressed in RGCs. To our surprise, most genes are transcribed by the retinal neurons at 48 hpf and afterwards. Only one gene displayed specific RGC expression at 36 hpf, the stage at which the optic chiasm first forms: *islr2*. As a consequence, we considered Islr2 a candidate receptor for early guidance decisions of retinal axons in zebrafish. We analysed *islr2* expression in more detail, by resolving the timepoint at which its transcripts first appear in RGCs, and characterized how the *islr2*-positive expression domain changed over time in zebrafish embryos. Our results indicate that *islr2* can be detected in the very first RGCs that differentiate in the eye (Figure 2A). These cells contribute to a large population of pioneering axons that explore the prospective course of the optic nerve, and have been described to have critical roles ensuring proper guidance of follower axons (Pittman et al., 2008). Interestingly, we found that *islr2* expression appears in RGCs following a pattern

reminiscent of the consecution of cell differentiation for this retinal cell type. In zebrafish the first RGCs differentiate ventro-nasally and this process continues as a circular wave to the temporal retinal portion. At 48 hpf, *islr2* transcripts mark the complete RGC layer, which is evenly populated by differentiated cells at this stage. 24 hours later, the expression level of *islr2* is generally reduced in the retina (Figure 2B). Faint staining is present in a subset of sparse amacrine cells, which share with RGCs common progenitors (Jusuf et al., 2012). These data would not support a functional role of Islr2 in late events of visual system development, such as target innervation, synaptic development or establishment of a topographic map. Rather, these results are consistent with a putative function played by Islr2 in axon guidance, as RGCs – once differentiated – immediately project axons in a directed fashion towards the optic nerve head. RGCs whose axons reach the prospective chiasm at 36 hpf transcribe *islr2* mRNA, introducing the possibility that Islr2 is required in cellular recognition events that take place at the diencephalic midline.

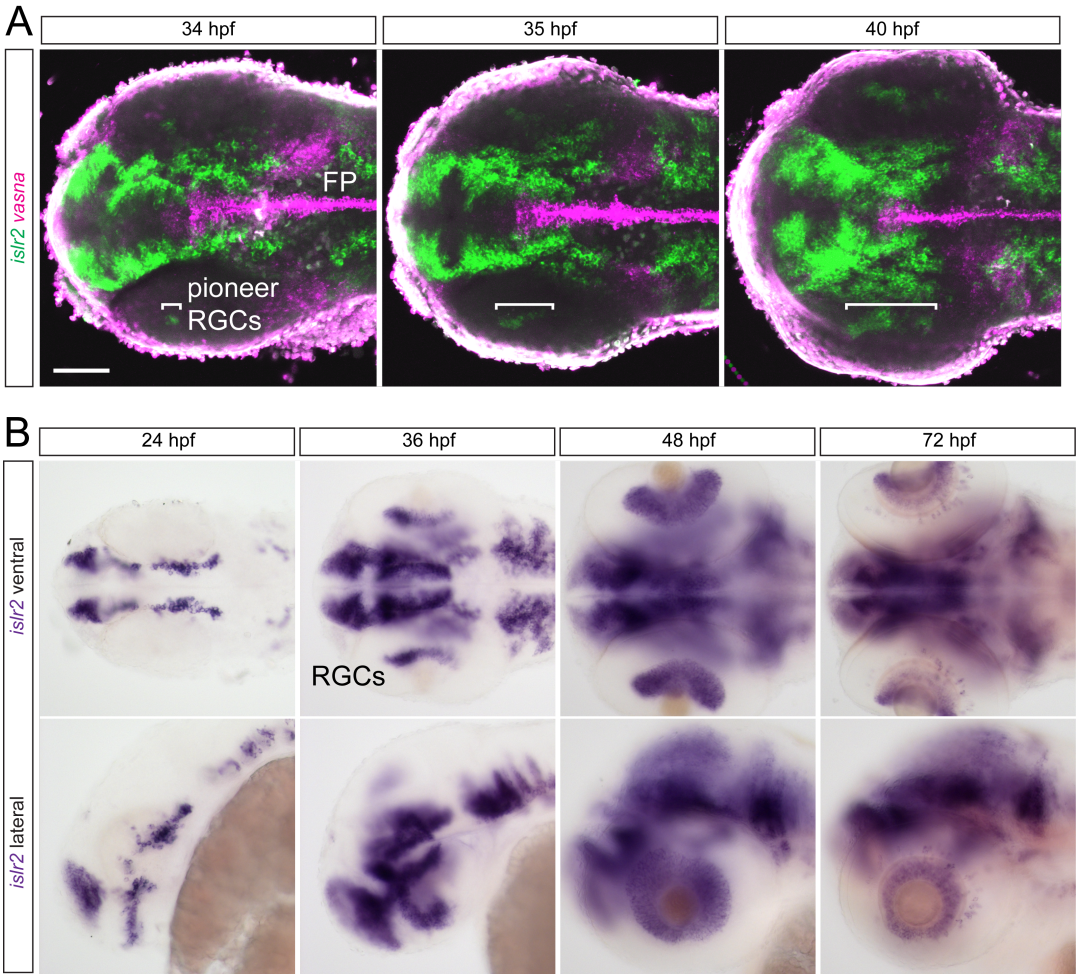

Figure 2. *islr2* expression in the embryonic zebrafish retina
(A) Double fluorescence *in situ* hybridization for *islr2* (green) and *vasna* (magenta). *islr2* transcripts appear in early-differentiating ventronasal RGCs and extend to the dorsal and temporal retinal quadrant, following the wave of RGC differentiation. This early *islr2*-positive RGC population contributes pioneering axons to the optic nerve. *vasna* is used here as a marker of the floor plate (FP), which marks the embryonic midline. Z-projections of confocal datasets. Dorsal views. Anterior is to the left. Scale bar: 100 µm. (B) Whole mount *in situ* hybridization for *islr2* (purple) at embryonic and larval stages. *islr2* is generally expressed by differentiated neurons in the brain and retina and specifically marks RGCs until larval stages. Ventral and lateral views. Anterior is to the left.

Optimization of a lipophilic dye-based axon tracing technique

In order to label the retinal projection and be able to differentiate the two optic nerves, we adopted a lipophilic dye retinal injection tech-

nique (Godement et al., 1987). This method relies on the injection of carbocyanine dyes behind the lens, in the RGC layer. The fluorescent compounds intercalate the surface membrane lipids and diffuse along the plasma membrane. Because the RGC layer surrounds the lens, it is easily targetable, so that most dye injected behind the lens will be selectively absorbed by RGCs – the only cell type sending axons outside the retina – and will diffuse to their full projections over time, thereby anterogradely labelling the optic nerve. Although the conditions for this technique have been previously described with the aim of labelling the zebrafish retinal projection, we experienced a number of technical issues affecting the reproducibility of this tracing method. First, the conditions of tissue fixation appeared to have a strong impact in the final quality of the staining. Insufficient fixation time caused difficulties in the injection procedure, because the retinal tissue did not become sufficiently rigid. Excessive fixation led to poor diffusion of the dye and leakage to neighbouring cell membranes, especially in the optic chiasm region. In this region reliable staining conditions were obtained with difficulty, because it is likely that zebrafish retinal fibers from different eyes intermix to a certain degree at the midline. At 5 dpf, this effect should be minimized by the presence of basal lamina and myelination surrounding the optic nerve, which physically separate the two projections. However, in many instances we detected dye leakage to structures neighbouring the nerve, for example to endothelial cells of head vessels and *trabeculae cranii*. Second, the temperature at which the injected samples were stored during overnight incubation influenced the speed of dye diffusion in the tract. High temperatures facilitated dye mobility and therefore increased staining background. Last, imaging conditions were optimized to have a clear view of the complete retinal projection, which approximates 100 µm x 200 µm in dimensions. It is a challenge to record at the highest resolution this axonal projection, because no clearing method can be employed, for the majority of these protocols are incompatible with DiI labelling. The opacity of the tissue, together with pigment cells in the animal skin, noticeably increased light scattering effects, preventing the imaging of the reti-

nal projection in its full dorsoventral extent. In order to circumvent these limitations, we treated zebrafish larvae with phenylthiourea (PTU), a chemical inhibitor of Tyrosinase, an enzyme required for melanin production. In these conditions, zebrafish embryos have non-pigmented melanophores. Our preliminary experiments indicated that PTU treatment does not affect guidance of retinal axons (Figure 3). Additionally, our protocol for sample mounting includes the surgical removal of the lower jaw structures and paired imaging from the dorsal side, to image RGC axons arborizing in the optic tectum, and from the ventral side, to record with the highest resolution settings the optic chiasm, where normally the signal is very intense. Four different carbocyanine dyes are commercialized: DiI, DiO, DiD, DiA. Their spectral properties are distinct, so that DiO fluoresces in green, DiI and DiA in orange and DiD in far red. Extensive testing indicated that DiD exhibits enhanced diffusivity, a property that is likely due to the particular chemical structure and interaction with solvent molecules. This dye was reputed not suitable for our experimental purpose, as it mostly gave rise to elevated background. DiI and DiO are the most used dyes according to the literature and the most stable. DiO displays a slightly increased tendency to diffuse out of axon tracts, compared to DiI. Several protocols exist, describing the lipophilic dye injection technique in the zebrafish retina (Burrill and Easter Jr, 1994; Baier et al., 1996; Hutson et al., 2004; Poulain et al., 2010). The most notable difference among them is the type of solvent these dyes are dissolved in. We tested different dye/solvent combinations, resulting in the final choice of commercially available Vybrant dyes, normally used for cell culture applications. Vybrant DiI is dissolved in ethanol, while DiO in dimethylformamide (DMF). They are both purified through a 0.2 nm filter. These dyes show the best intensity/diffusivity ratio compared to other ethanol, DMF or chloroform solutions alone.

Phenotyping of *islr2* mutants

In order to analyse the physiological role of *islr2* in zebrafish, we examined an *islr2* TILLING allele (*islr2*^{sa82}). This allele encodes a

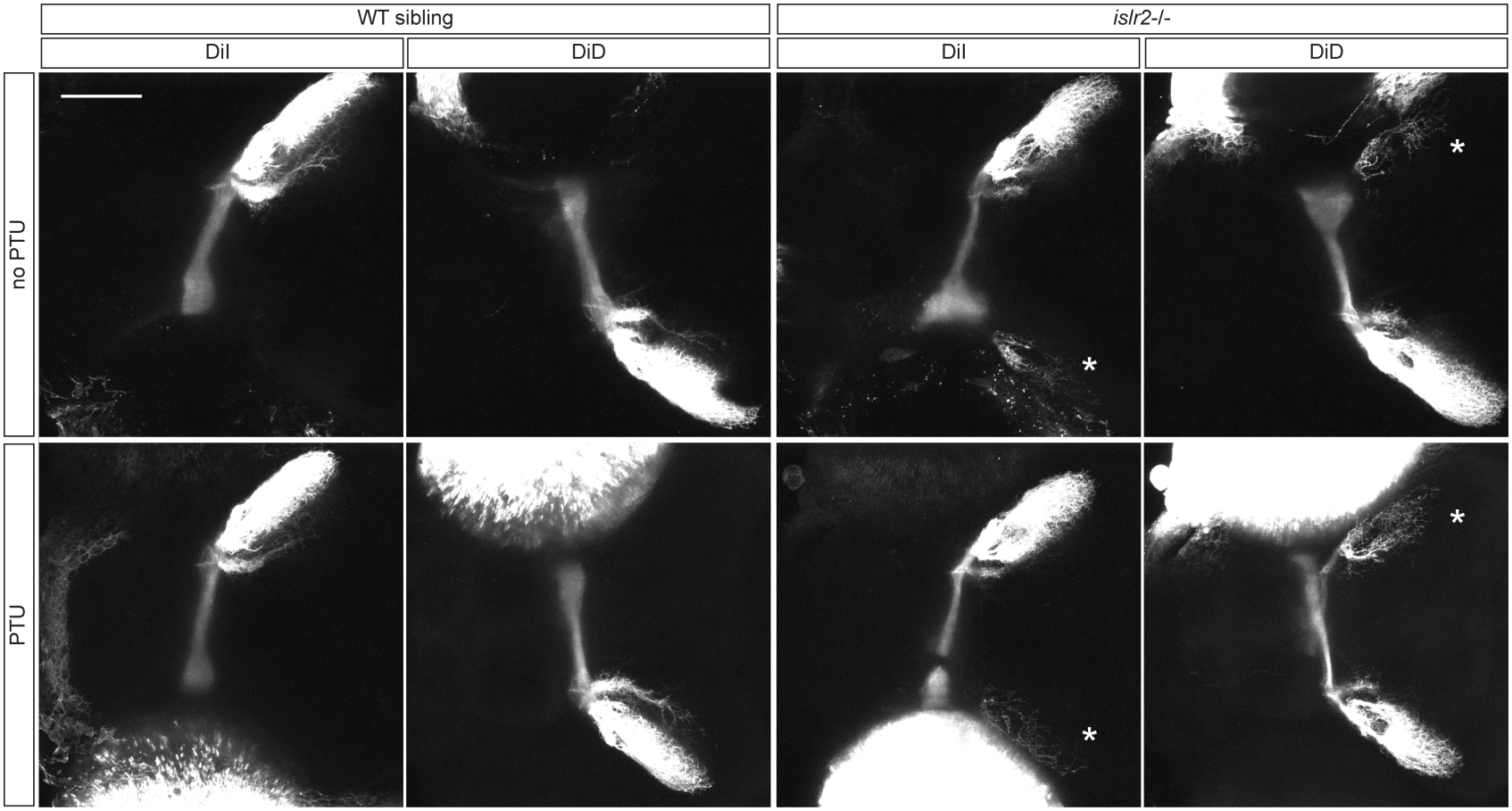

Figure 3. PTU treatment does not affect retinal axon guidance
Incubation of zebrafish embryos in medium containing 0.003% PTU from 8 hpf to 5 dpf does not perturb retinal axon guidance, as both wild-type and mutant projections can be reliably identified and do not appear qualitatively altered. Asterisks indicate ectopic innervation of the ipsilateral optic tectum, a phenotypic hallmark of *islr2* mutants. Z-projections of confocal datasets. Dorsal views. Anterior is to the left. Scale bar: 100 µm.

prematurely truncated Islr2 polypeptide, devoid of transmembrane domain (Figure 4A) and was identified by targeted retrieval of mutations in the *islr2* ORF induced by chemical mutagenesis. Any phenotype associated with the mutation is therefore likely due to the mutation itself and not to genetic background. We labelled the retinal projection to score for mutant phenotypes at the larval stage of 5 dpf. At this developmental time point, any remodelling of the projection has ceased and the axon pathway is stable (Hutson and Chien, 2002). Retinal injections of lipophilic dyes showed the presence of ipsilaterally-projecting retinal axons in *islr2* mutant larvae, in contrast to heterozygous siblings that always display a fully contralateral wild-type projection. Following the ipsilateral neurites from the dorsal side of the larval brain to the chiasm indicates that most – if not all – ipsilateral axons derive from the diencephalic midline (Figure 4B). In order to chronologically characterize the appearance of *islr2* mutant defects, the retinal projection was labelled at consecutive stages starting from 2 dpf. At this time point, only 12 hours after the first retinal axons reach the prospective chiasm, a defect in axon outgrowth can already be identified in selected mutants. At times, retinal growth cones appear to stray from their normal course, especially at the midline, and lag behind compared to wild-type siblings. From about 3 dpf, ipsilaterally-directed growth cones can be recognized (arrow in Figure 5). Finally, ventral views of the chiasm in 5 dpf *islr2* mutants clearly show a subset of axons invading the ipsilateral optic tract from the midline (arrowheads in Figure 5).

The retinal axon phenotype of *islr2* mutants appears surprisingly specific, given that mutant larvae in their 5th day of development cannot be distinguished from their siblings and are therefore mostly normal from a morphological (Figures 7, 8) and basic behavioural point of view. Because *islr2* expression is shared between RGCs and other neuronal subtypes in the brain and spinal cord, we investigated the possibility that Islr2-deficient larvae would display co-occurrence of other axonal or, more generally, neuronal phenotypes. Acetylated Tubulin stainings at different developmental time points, however,

failed to highlight obvious defects in other axon tracts (Figure 6). Strikingly, the earliest commissures that form in the embryonic vertebrate brain appeared normal. Furthermore, the absence of defects in motor behaviours indicates that motor neuron projections are normal and functional in *islr2* mutants. Collectively, these data suggest that *islr2* null larvae have specific and highly penetrant defects in the retinotectal projection.

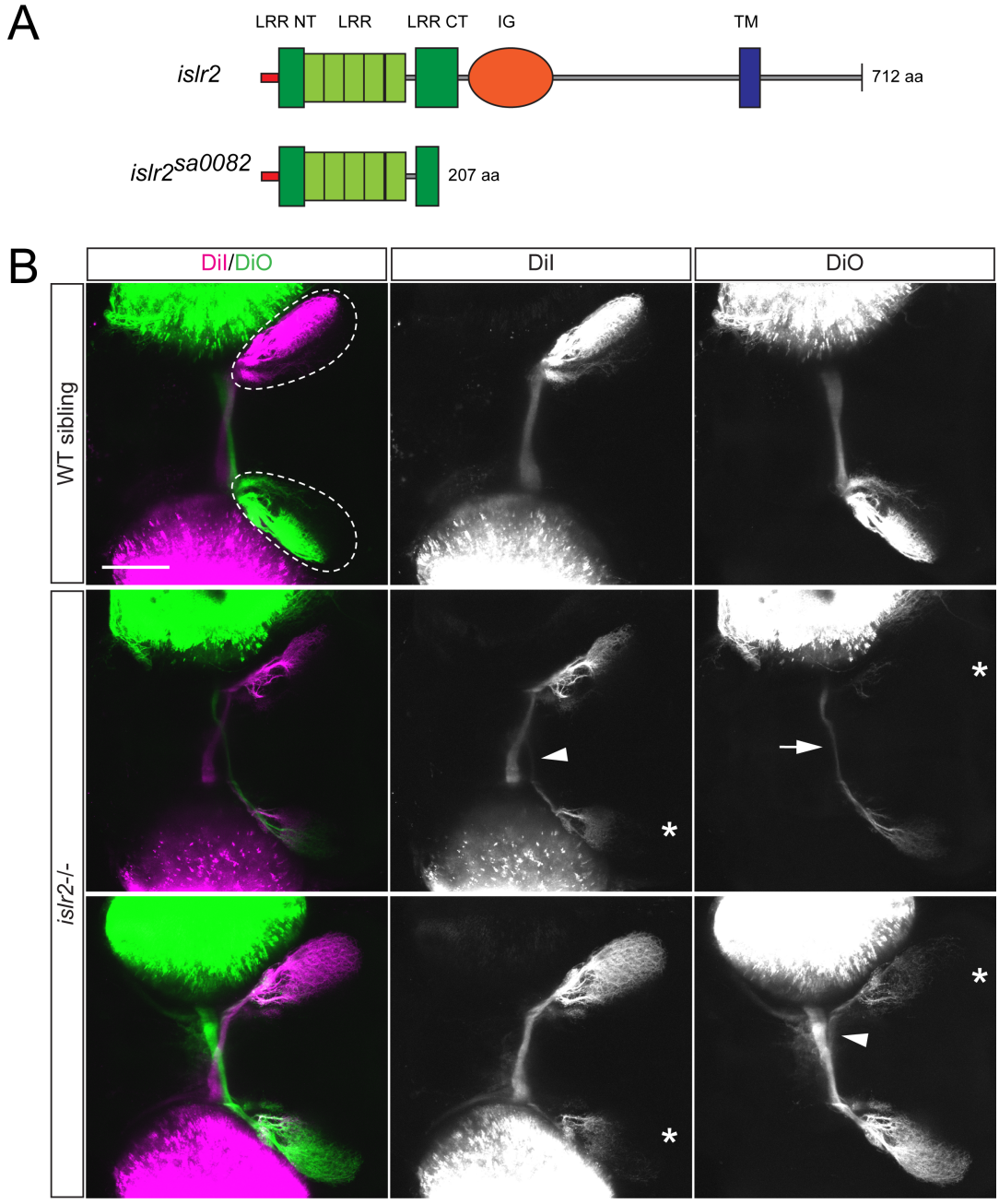

Figure 4. Retinal axon projection phenotype in *islr2*^{sa82}
(A) Schematic of the domain organization of Islr2 in its wild-type and *sa82* mutant form. *islr2*^{sa82} animals contain a C-to-T missense mutation, leading to an amino acidic substitution from Glutamine to Stop. The C-terminal LRR domain truncation, by preventing the translation of a transmembrane domain, is likely to affect protein functionality. As a consequence, the *islr2*^{sa82}allele may be functionally null. (B) Whereas wild-type zebrafish larvae display fully contralateral retinal projections (first row), *islr2* mutant optic nerves split at the diencephalic midline (arrowheads) and a subset of axons ectopically grow to innervate the ipsilateral optic tectum (asterisks). In addition, mutants may have hypoplastic optic nerves (compare second and third row), which was considered an incompletely penetrant phenotype. Dashed areas indicate the optic tecta. Z-projections of confocal datasets. Dorsal views. Anterior is to the left. Scale bar: 100 µm.

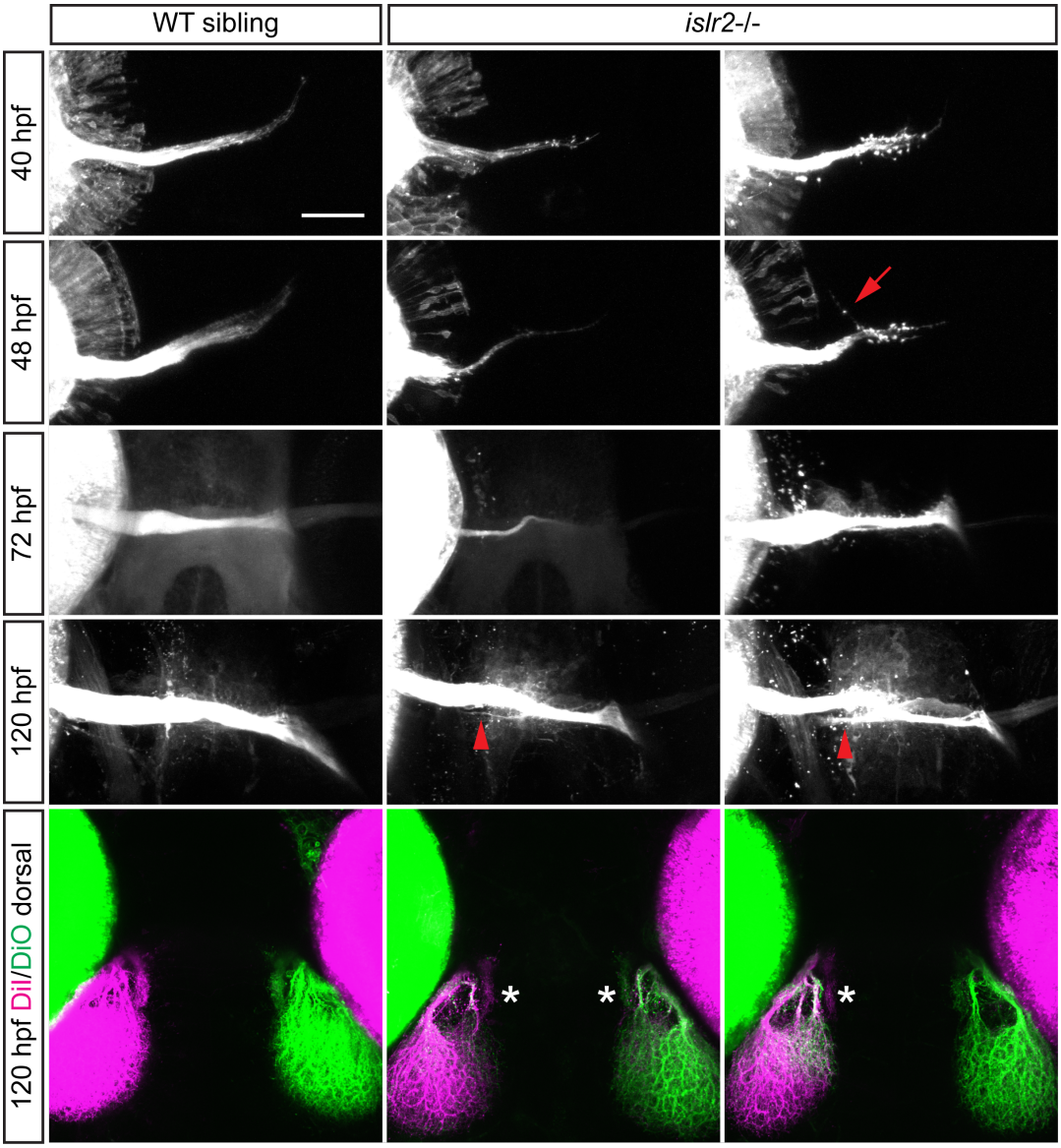

Figure 5. Chronological progression of the *islr2*^{sa82}phenotype
Lipophilic dye retinal injections highlight the appearance of outgrowth and coherence defects in the optic nerves of *islr2* mutants from 2 dpf. The arrow indicates an ectopic growth cone migrating in the ipsilateral optic tract. Arrowheads point to misprojecting retinal axons at the diencephalic midline. Asterisks show concurrent innervation of the optic tectum from the contralateral and ipsilateral retina. Z-projections of confocal datasets. Ventral views. Last row: dorsal views. Anterior is to the top. Scale bar: 50 µm.

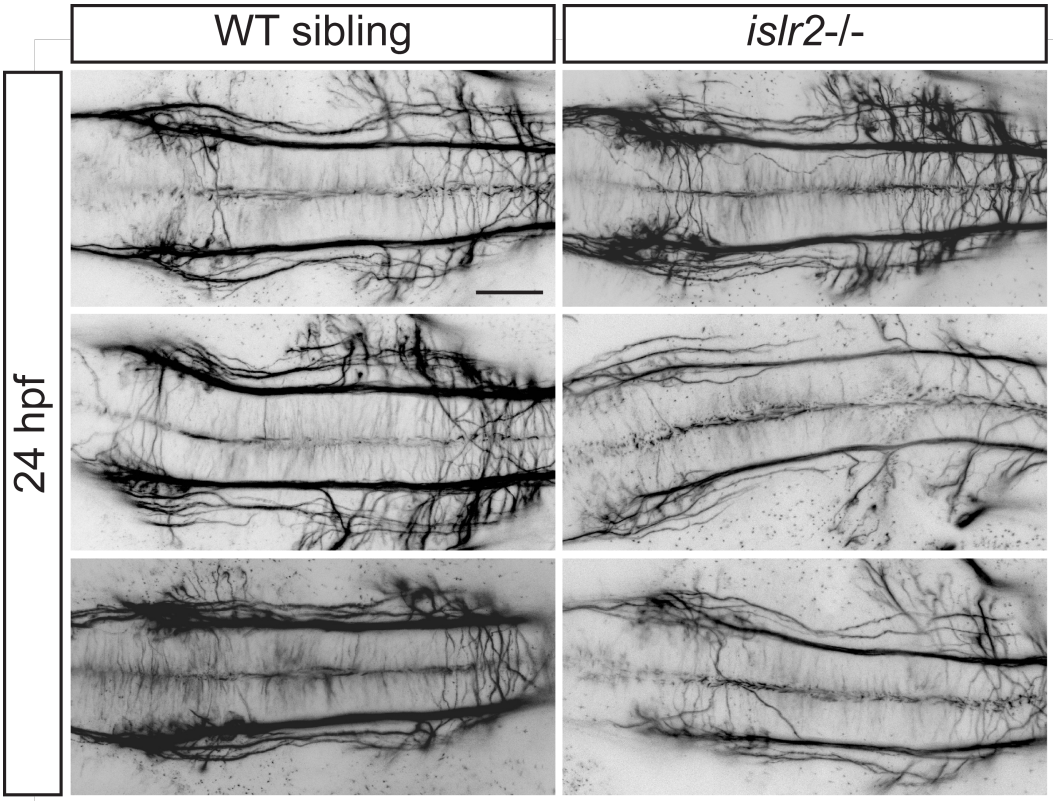

Figure 6. Embryonic axon tracts do not display overt defects in *islr2*^{sa82}mutants Acetylated Tubulin staining of 24 hpf embryos showing central axon tracts at the level of the medial longitudinal fasciculus (MLF). Thinner axon bundles were observed only in a subset of *islr2* mutant animals. The general spacing and directionality of these nerve fibers is unaltered compared to controls. Z-projections of confocal datasets. Dorsal views. Anterior is to the left. Scale bar: 50 µm.

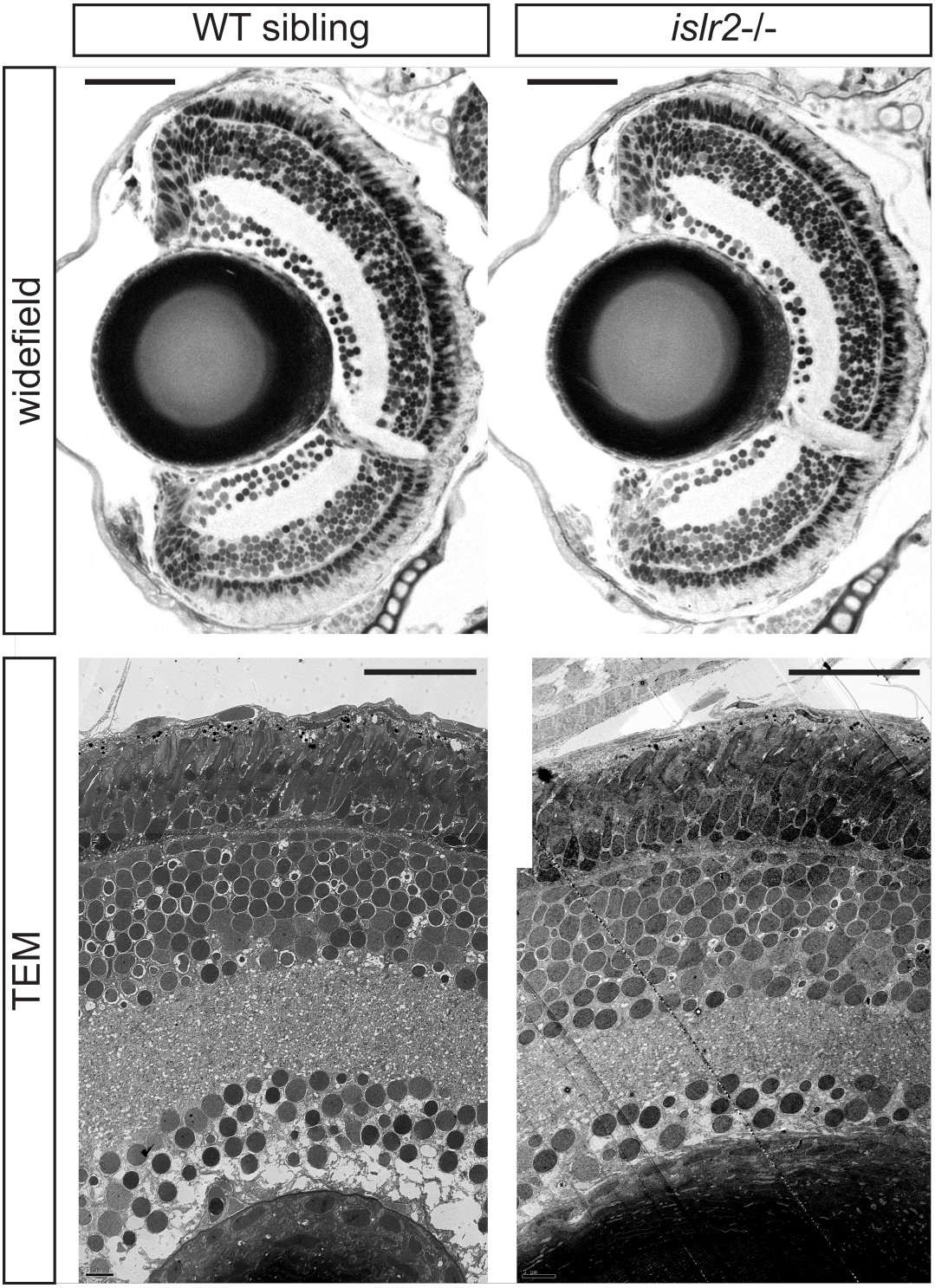

Figure 7. Unaltered retinal lamination in *islr2*^{sa82}mutants
Transverse sections through the retina of 5 dpf *islr2* mutants. Normal size, gross and ultrastructural anatomy and layering of the retina are observed in *islr2* mutants. RGCs number may be decreased in *islr2*-/- larvae. Scale bars: 50 µm (top row), 20 µm (bottom row).

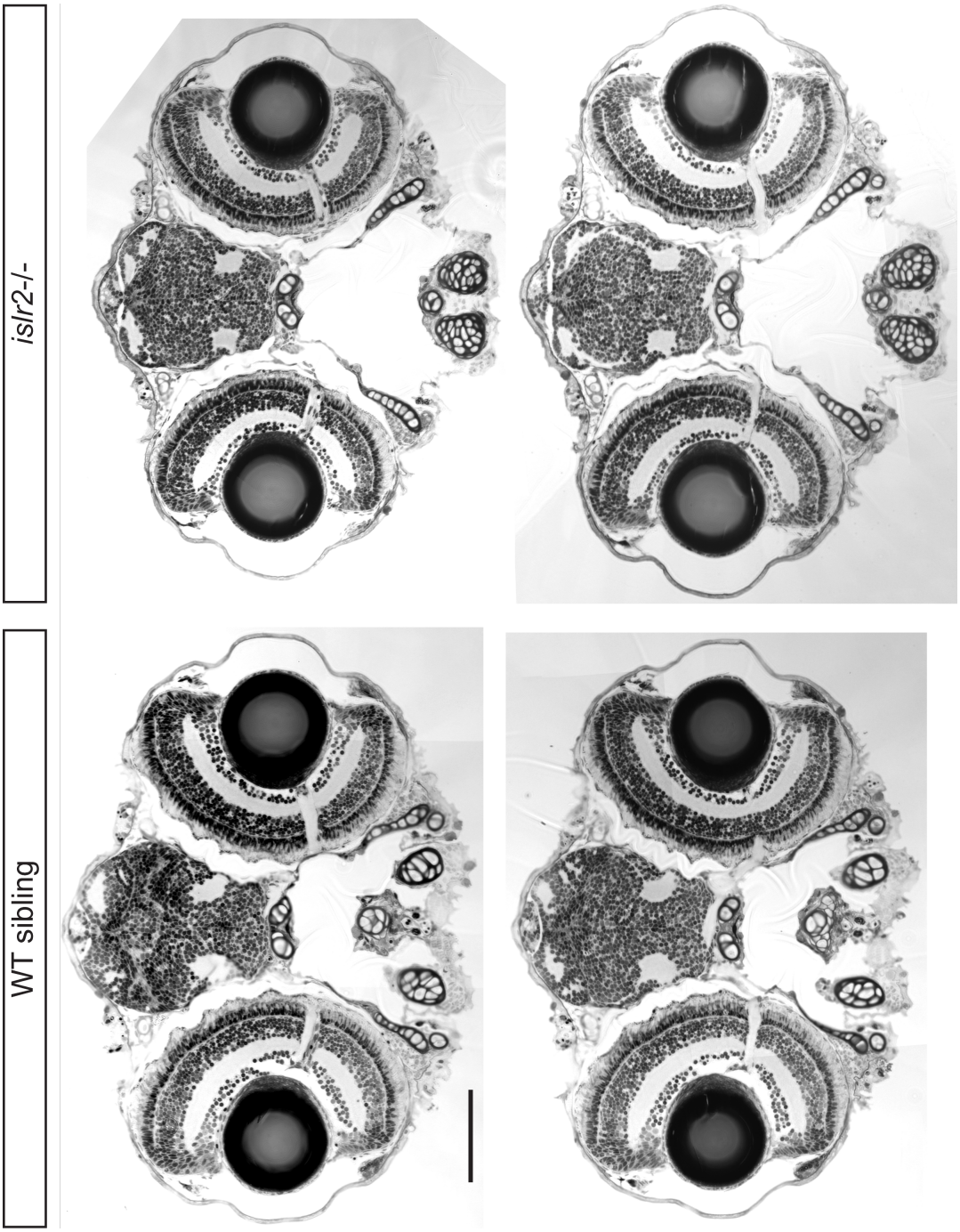

Figure 8. The diencephalic anatomy of *islr2* mutants is unaffected
Transverse sections at the level of the optic chiasm in *islr2* mutants and siblings. The chiasmatic and ventral diencephalic tissue appears normal in size and patterning, suggesting that the axon guidance phenotype of *islr2* larvae does not originate from mispatterning effects. Scale bar: 100 µm.

A second, parallel phenotype detected in *islr2* mutant visual sys-

tems is a remarkable thinning of the optic nerve. It became apparent that not all *islr2* mutants display this defect, an observation that discouraged further in-depth analysis of this phenotype. As a consequence, the characterization work described here remains preliminary. We postulated that the decreased width in selected optic nerves must derive from the reduced number or retinal fibers that fasciculate together. Based on this assumption, we considered three putative explanations for this phenotype. (1) The first implies that retinal axons are unable to exit the eye and are retained in the retina. Such case would be of primary interest, because it has been shown that specific permissive extracellular molecules are required for appropriate initial pathfinding of retinal axons and recognition of the optic nerve head (Randlett et al., 2011). Following this possibility, mutant larvae would likely display intraretinal guidance defects, possibly including ectopically-projecting axons, as already described in several mutants (Poulain et al., 2010). We addressed this possibility by crossing *islr2* mutant carriers to a fish reporter line for differentiated RGCs (*isl2b:GFP*, Pittman et al., 2008). Genotyped carriers of the reporter insertion that were heterozygotes for the $islr2^{sa82}$ allele were subsequently crossed to *islr2*+/- fish. GFP-expressing embryos were then selectively collected and fixed at consecutive time points. This method allows to recognize putative intraretinal guidance defects that would not be visible by DiI labelling, as whole-retina fills invariably make it impossible to distinguish any internal detail. Confocal micrographs from these experiments showed that thin nerves could be identified in selected mutant embryos from early timepoints, a finding confirming our staged DiI labelling experiments (Figure 5). Reduced numbers of retinal fibers persisted to late larval stages, during which it appeared that this defect may worsen over time (Figure 9). However, no erratic axons were detected inside mutant retinae, suggesting that retinal fibers correctly pathfind to the optic nerve head. A second explanation for the hypoplastic optic nerves is offered by a possible concurrent defect in RGC survival. The experimenter would in this case expect that a higher number of cells undergo apoptosis in mutant embryos. Preliminary

TUNEL stainings aiming at detecting programmed cell death in the embryonic retina, however, did not show obvious differences between mutants and control siblings. We concluded that it does not appear likely that larvae with thinner optic nerves are also affected by high cell death of RGCs or their progenitors. Nonetheless, the time course of mutant visual systems development, recorded using an RGC-specific reporter, clearly showed that *islr2* mutant embryos and larvae appear to lack a subset of differentiated RGCs, thereby giving rise to small patches where no fluorescence is detected in the respective cellular layer (Figure 9). These data, together with the negative results reported above, introduce the possibility that a subset of RGCs fail to differentiate in some *islr2* null retinae. Unfortunately we were not able to test this hypothesis. A first attempt at detecting differential apoptosis in *islr2* mutants compared to siblings did not allow the selection of putative mutant embryos for further analysis. To genetically exclude apoptosis as causative mechanism for the thinning phenotype, we crossed *islr2* carrier fish to homozygous *tp53* mutants (Berghmans et al., 2005). Trans-heterozygotes were incrossed and the progeny genotyped for both mutations after labelling of the chiasm. As shown in Figure 10, in *islr2/tp53* double mutant larvae the reduced optic nerve width is not rescued. These data exclude a major, if not the most relevant, cause of apoptosis in zebrafish embryos as causative event determining hypoplastic optic nerves in *islr2* mutants. The obtained result is in accordance to experiments on *Islr2/Linx* knockout mice, showing that thinning of limb sensory and motor projections is not eliminated in a *Bax* knockout background that reduces the level of apoptosis in pups (Mandai et al., 2009).

A more in-depth analysis was aimed at clarifying the relationship between the guidance defect and the reduced optic nerve width phenotypes. We injected tracer dyes in fixed larvae from four separate clutches. The quantification shows that most mutant larvae from two clutches analysed in Figure 11C displayed a thinner optic nerve (85%). When the extent of contralateral optic tectum innervation was evaluated, a similar number of mutant larvae showed indeed

a reduction. In parallel, very few mutants had a strong ipsilateral projection, while most of them had only few neurites labelled in the ipsilateral optic tectum. Conversely, in two different clutches (Figure 11B), most mutant larvae possessed wild-type, wide optic nerves. As a consequence, the ipsilateral projection was classified as "strong" in many mutants, and almost all of these larvae had a wild-type level of contralateral optic tectum innervation. These data suggest that, although the optic nerve thinning phenotype is specifically arising in mutant larvae, it is not fully penetrant and depends on parental contribution. In addition, a possible explanation for the apparent dominance of the thinning phenotype over the midline crossing defect would be that the two are independent. Importantly, the local site of appearance of this secondary phenotype could be indicative of the type of process regulating the number of axons in the optic nerve, through Islr2. We were not able to identify consistently a single location showing discontinuity in optic nerve width. In some cases the nerve displays normal width at the exit of the retina, while in other cases at the diencephalic entry point the number of retinal axons is already reduced. Other zebrafish mutant larvae display a similar phenotype, for example *space cadet/rb1* mutants (Gyda et al., 2012). This genetic condition is characterized by poor survival of RGC progenitors, which explains the reduced number of retinal axon fibers included in mutant optic nerves.

The lower density of RGC cell bodies in the retinae of mutant animals from incrossed *islr2*+/-;*isl2b:GFP* fish appeared to exacerbate with the age of the larvae analysed. At 7 dpf, the most striking phenotype was recorded, with only sparse RGCs present in the retinal layer. The collected data suggest that optic nerve hypoplasia may be a consequence of progressive RGC degeneration or of an arrest in differentiation. It is still not clear how much the thin nerve phenotype may be attributed to direct axon outgrowth defects in *islr2* mutant animals.

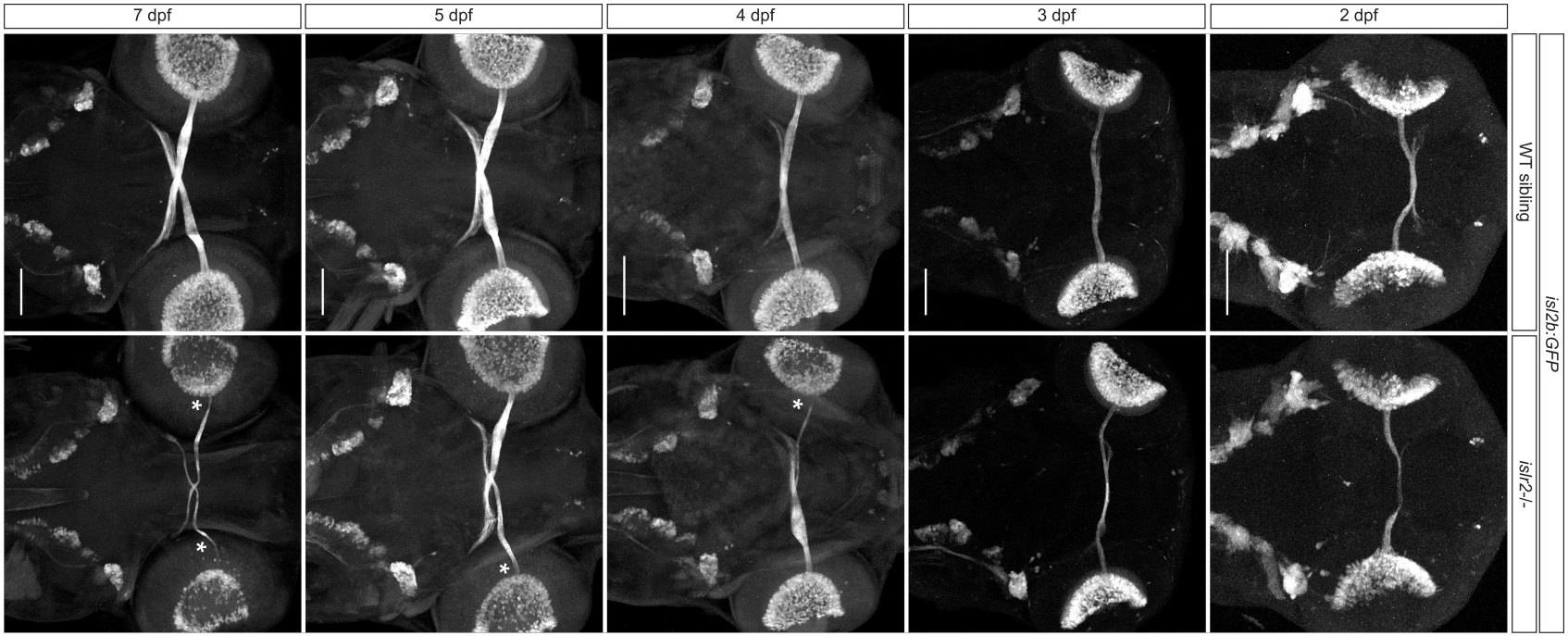

Figure 9. The number of differentiated RGCs is decreased in *islr2* mutants
In mutant larvae optic nerve hypoplasia is accompanied by the apparent loss of differentiated RGCs, marked by the *isl2b:GFP* transgene. Z-projection of confocal datasets. Dorsal views. Anterior is to the top. Scale bars: 100 µm.

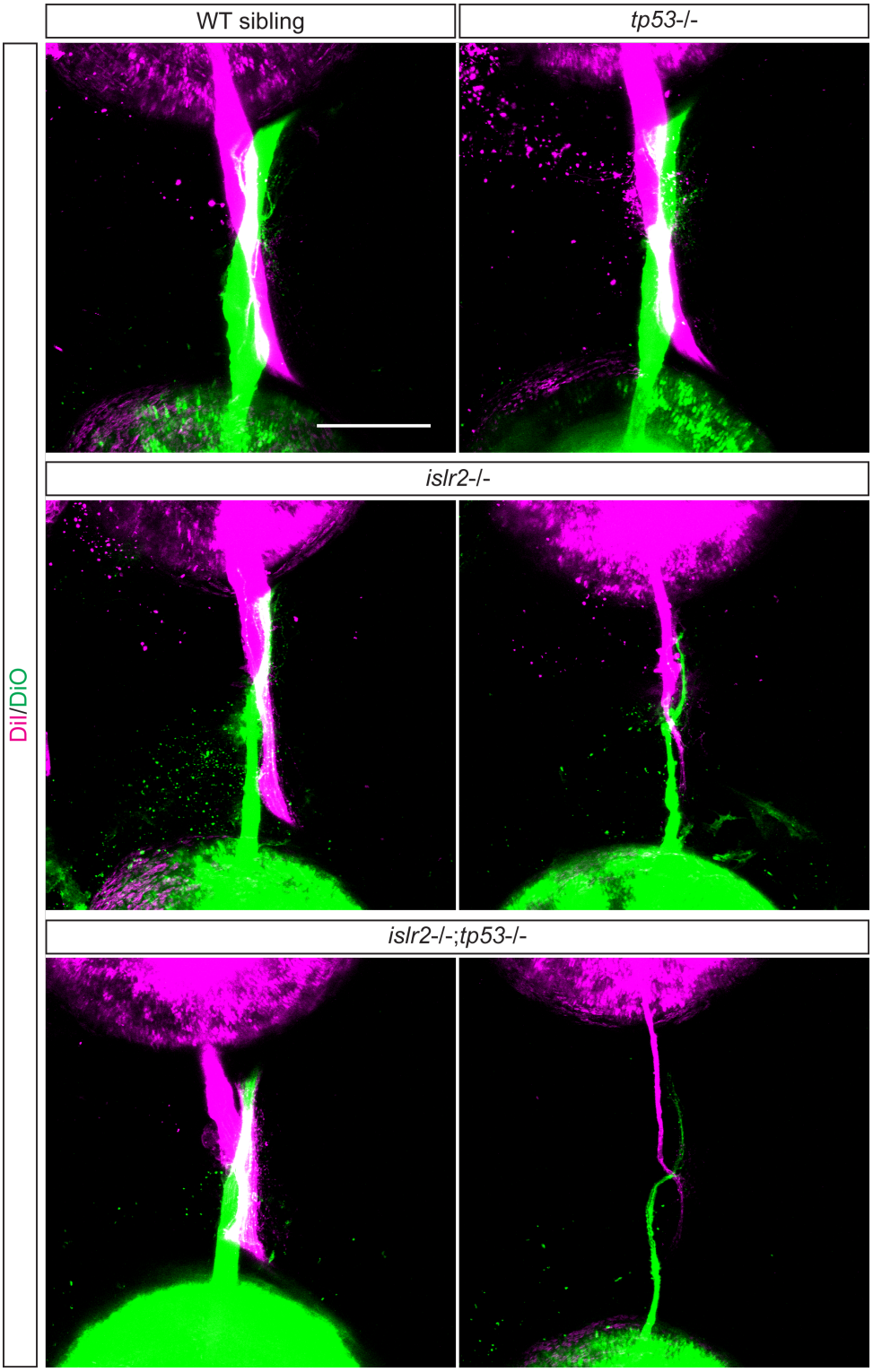

Figure 10. Null mutations in *tp53* do not rescue optic nerve hypoplasia of *islr2* mutants

DiI/DiO retinal injections show that the *islr2*/*tp53* double mutant condition cannot rescue the hypoplastic optic nerve of *islr2* single mutants, thereby ruling out Tp53-mediated apoptosis as putative causative mechanism. Z-projections of confocal datasets. Ventral views. Anterior is to the left. Scale bar: 100 µm.

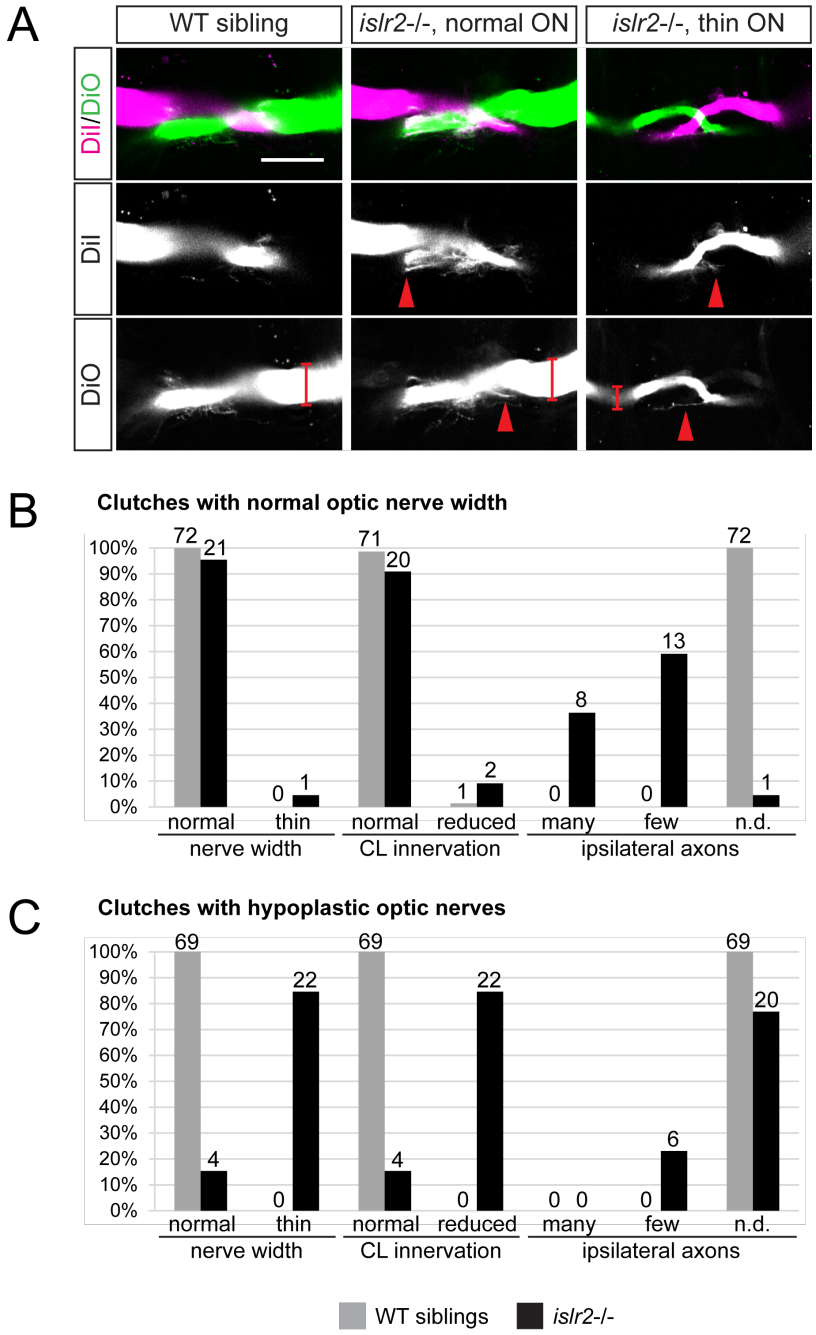

Figure 11. Optic nerve hypoplasia in *islr2* mutants
(A) The quantification of optic nerve thinning identified in *islr2* mutants was based on the injection of lipophilic dyes to label the optic nerves, which were imaged from the ventral side. Ipsilateral neurites straying from the midline (arrowheads) were often recognized in *islr2* mutants, but were never recorded in the chiasm of control siblings. Single optical sections from confocal datasets. Ventral views. Anterior is to the top. Scale bar: 50 µm. (B) Individuals from two clutches where all mutants have normal optic nerve width were more likely to display large areas of ipsilateral innervation, compared to individuals with hypoplastic optic nerves from two different clutches (C).

Islr2 and Robo2 act independently in retinal axon guidance

Analysis of *astray* mutants, identified during forward genetics screens performed in our lab, led to the identification of a critical role for the Robo2 receptor in retinal axon guidance (Fricke et al., 2001). *astray/robo2* larvae display overt axon guidance defects at multiple positions along the retinotectal pathway. The optic nerve splits in these larvae into multiple fascicles that ectopically innervate the brain. These tend to misroute after the midline, from where they shift anteriorly and posteriorly at multiple levels and tend to recross the midline at dorsal locations. This striking phenotype contributed to the characterization of the Robo2 role in containing antero-posteriorly the retinal projection, by transducing surrounding repulsion given by Slits, the prototypical axon repellents. Slits are indeed located anterior and posterior to the optic nerve route, a pathway of least-repulsion across the ventral diencephalon. The work of Hutson and Chien (2002) established that Robo2 function is required both before and after the midline. Indeed, *belladonna/lhx2b* mutants, which display a complete ipsilateral retinal projection, still require Robo2 function for proper guidance to dorsal targets. These data prompted us to investigate whether *islr2* and *robo2* are epistatic and control distinct aspects of the same developmental process, i.e. midline crossing. We raised double heterozygotes of *islr2* and *astray/robo2* mutations and incrossed positive fish to perform DiI retinal injection-based phenotyping experiments. Micrographs presented in Figure 12 show that the typical *astray/robo2* phenotype generally adds up to the *islr2* phenotype, resulting in ipsilateral projections in the background of widespread erratic guidance, typical for *astray/robo2* mutants. These results do not support a scenario where *islr2* and *robo2* control midline crossing epistatically.

Screening for Islr2-interacting partners

Recent work on the midline choice point in mouse and zebrafish highlighted the importance of local tissue architecture for proper routing of retinal axons, especially at the optic chiasm. Molecules

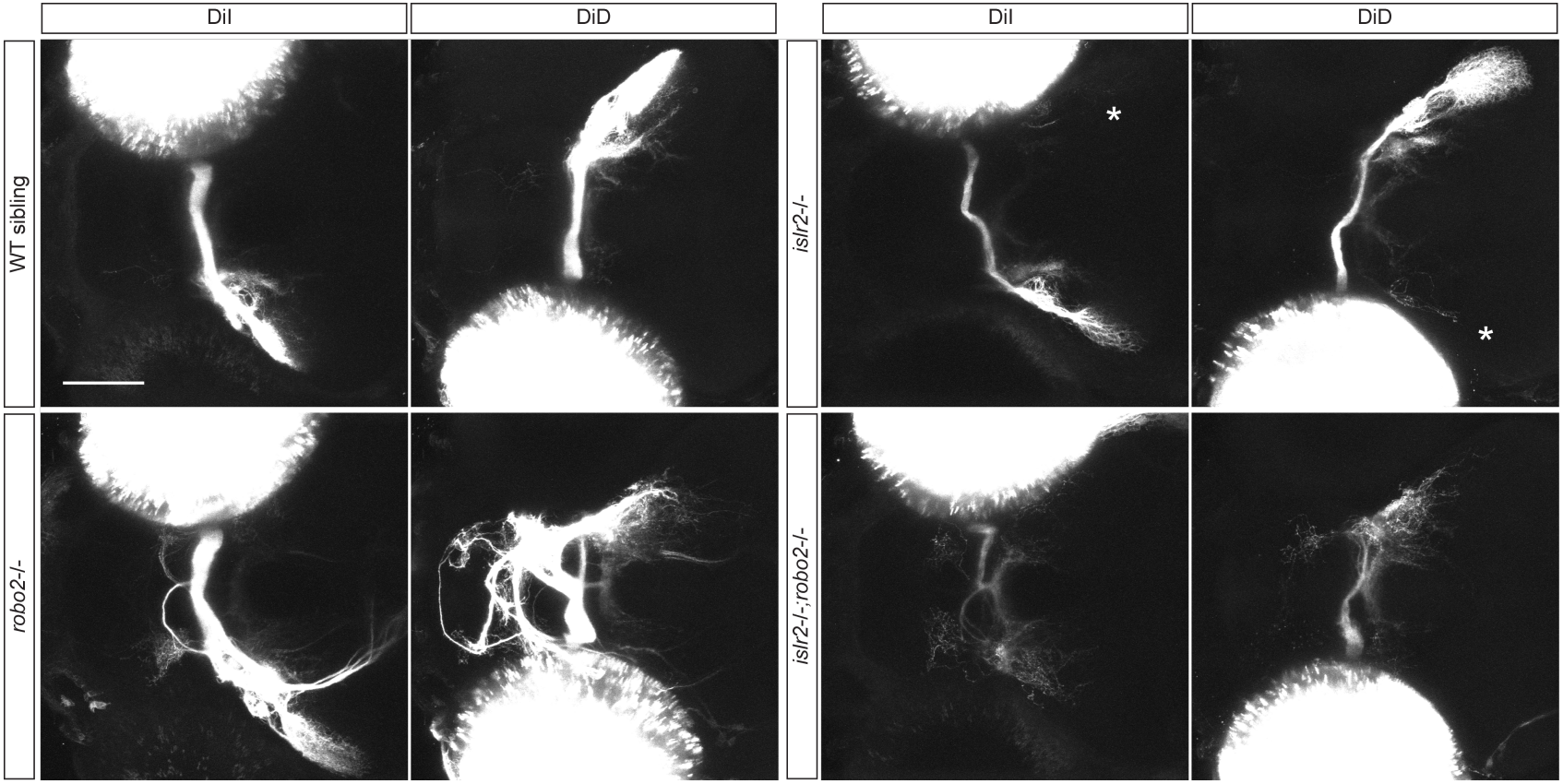

Figure 12. *islr2* and *robo2* act independently in retinal axon guidance
DiI/DiD retinal injections reveal that the phenotypes from *islr2* and *astray/robo2* mutants add up, although it is challenging to verify whether ipsilateral neurites in double mutants originate from the chiasm or from dorsal recrossing of retinal axon fibers. The collected data suggest a non-epistatic relationship between these two signalling systems. Z-projections of confocal datasets. Dorsal views. Anterior is to the left. Scale bar: 100 µm.

with known roles in axon guidance at the chiasm share strategic positioning relative to the axon course through the diencephalon. Our hypothesis envisages Islr2 acting as a signalling receptor on RGCs axons to transduce exogenous signals, positioned along the retinal axon pathway. It is therefore of critical interest to identify molecules capable of physically interacting with the ectodomain of Islr2. To screen for candidates putatively involved in Islr2 axon guidance function, we took an unbiased approach by screening a large set of cell surface and secreted molecules present in zebrafish embryos. To circumvent the common transiency in binding and the low affinity that protein interactions might display at the plasma membrane, we took advantage of a specialized assay, called AVEXIS (Bushell et al., 2008). This technique allows the identification of low affinity physical interactions between proteins and permits the systematic screening of entire protein libraries. We screened 194 zebrafish cell surface and secreted protein ectodomains, to identify the Vasorin (Vasn) paralogs as specific Islr2 interacting partners (Figure 13). In addition to confirming the published result showing the physical binding of Vasorin A to Islr2 (Söllner and Wright, 2009), these data report the detection of Islr2-Vasna and Islr2-Vasnb interactions using each binding partner in both bait or prey orientations (Figure 13A). Because in each of these cases no other hit was identified in the protein library, we conclude that the Islr2-Vasn interaction is specific.

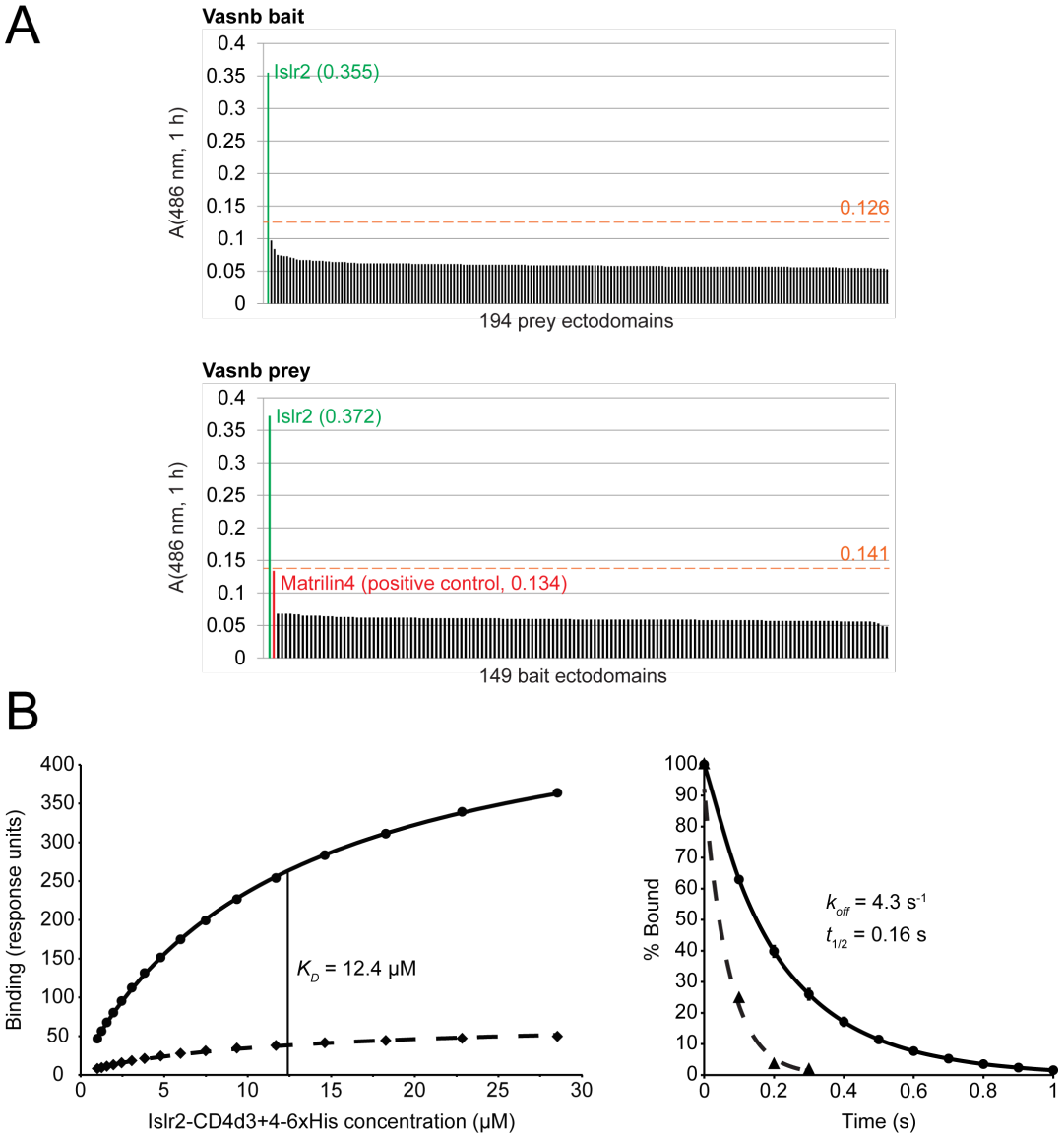

Figure 13. Vasna and Vasnb transiently bind to Islr2
(A) Results from an AVEXIS-based discovery screen for novel cell surface and secreted protein-protein interactions. Using the Vasnb ectodomain as bait or prey, we detected Islr2 as interacting partner, as shown by the elevated absorbance of the corresponding plate well (green bars) compared to the threshold (3 standard deviations over the mean, orange dashed lines). The collected data identify Vasnb-Islr2 as a novel interaction detected in both bait/prey orientations. (B, left panel) SPR data quantifying the equilibrium dissociation constant (K_D) for the interaction between Islr2 and Vasna. (B, right panel) Kinetic measurement of the dissociation rate (k_{off}) characteristic of Islr2-Vasna complexes.

Biochemical characterization of the Islr2-Vasna interaction

In order to better characterize the interaction between Islr2 and Vasn, we carried out biochemical measurements using surface plasmon resonance (SPR). This technique exploits optical phenomena and allows the quantification of protein complexes affinity and kinetics by detecting small variations in mass on a sensor chip. The equilibrium dissociation constant (K_D) is a measure of the affinity of a molecular interaction and is defined as the concentration of free ligand, at which half of the receptor population is in the bound state. To measure the K_D of our interaction of interest, we immobilized monobiotinylated Vasna ectodomains onto the streptavidin-coated sensor chip of a BIAcore instrument. Purified monomeric Islr2 ectodomain was injected at increasing concentration in the microfluidic device, leading to saturable binding. A value of 12.4 µM was then estimated. In a complementary experiment, a flow cell coated with Vasna bound to saturation to Islr2 was exposed to a constant flow of washing buffer, to determine an off-rate (k_{off}) of 4.3 s^{-1}, corresponding to an interaction half-life of 0.16 s. These values are in agreement with previously published quantifications of transient protein-protein interactions represented at the cell surface (van der Merwe and Barclay, 1994).

The extracellular portions of Islr2 and Vasn include series of protein domains typically involved in mediating protein-protein interactions. In order to isolate the amino acidic motifs required to form the binding interface between Islr2 and Vasna, we cloned deletion constructs containing one or combinations of two adjacent domains for each of the interacting partners. These constructs were then expressed and tested using a regular AVEXIS assay to narrow down the interaction to single binding domains. Data shown in Figure 14A indicate that Islr2 utilizes its LRR module to bind to the small EGF domain in Vasna (Figure 14B). During these experiments, the protein product of the *islr2*^{sa82} allele was additionally included and tested. This Islr2 protein form did not display measurable binding to Vasna in either bait or prey orientation, indicating that *islr2*^{sa82} mutants indeed carry a null allele.

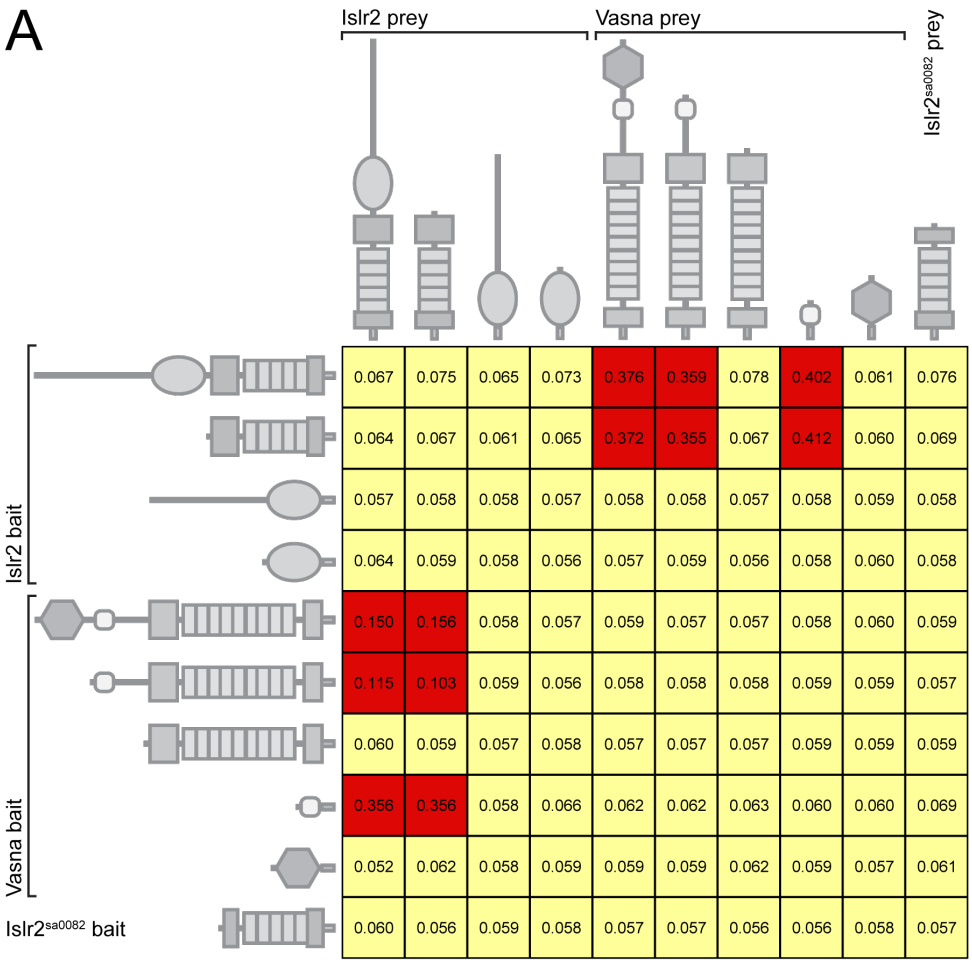
A
Islr2 prey
Vasna prey
Islr2sa0082 prey
Islr2 bait
Vasna bait
Islr2sa0082 bait
0.067 0.075 0.065 0.073 0.376 0.359 0.078 0.402 0.061 0.076
0.064 0.067 0.061 0.065 0.372 0.355 0.067 0.412 0.060 0.069
0.057 0.058 0.058 0.057 0.058 0.058 0.057 0.058 0.059 0.058
0.064 0.059 0.058 0.056 0.057 0.059 0.056 0.058 0.060 0.058
0.150 0.156 0.058 0.057 0.059 0.057 0.057 0.058 0.060 0.059
0.115 0.103 0.059 0.056 0.058 0.058 0.058 0.059 0.059 0.057
0.060 0.059 0.057 0.058 0.057 0.057 0.057 0.059 0.059 0.059
0.356 0.356 0.058 0.066 0.062 0.062 0.063 0.060 0.060 0.069
0.052 0.062 0.058 0.059 0.059 0.059 0.062 0.059 0.057 0.061
0.060 0.056 0.059 0.058 0.057 0.057 0.056 0.056 0.058 0.057
B
Islr2
TM
IG
LRR CT
LRR
LRR NT
LRR NT
LRR
LRR CT
EGF
FN3
TM
Vasorin

The Vasorin paralogs are expressed in the zebrafish visual system

With the aim of gathering clues about a putative function exerted by the Islr2-Vasorin interaction, we used mRNA expression data to identify the embryonic location where these molecules were likely to bind. Preliminary data indicated that *islr2* is expressed mostly adjacent to *vasna*-positive cells (Söllner and Wright, 2009 and Figure 2A). These results in turn suggested that the interaction might primarily occur *in trans*, in accordance to binding data. We repeated the *in situ* hybridization experiments focusing on the course of retinal axons from the embryonic eye to the dorsal midbrain. We detected vicinity of staining for *vasna* and *vasnb* in the ventralmost portion of the anterior diencephalon, corresponding to the preoptic area (Figure 15). These data suggest that *vasna*-expressing cells mark the ventral and lateral head mesenchyme in possible alignment with the course of retinal axons. The *vasnb* expression domain, on the contrary, was detected in a position encompassing the embryonic midline just anterior to *vasna*-positive cells.

Figure 14 *(preceding page)*. Mapping of the interacting domains in Islr2 and Vasna (A) Domains combinations from the extracellular portion of Islr2 and Vasna were tested pairwise using the AVEXIS assay. Islr2 uses its LRR module to bind to the small EGF domain of Vasna. Conversely, the product of the $islr2^{sa82}$ allele does not retain binding capability.

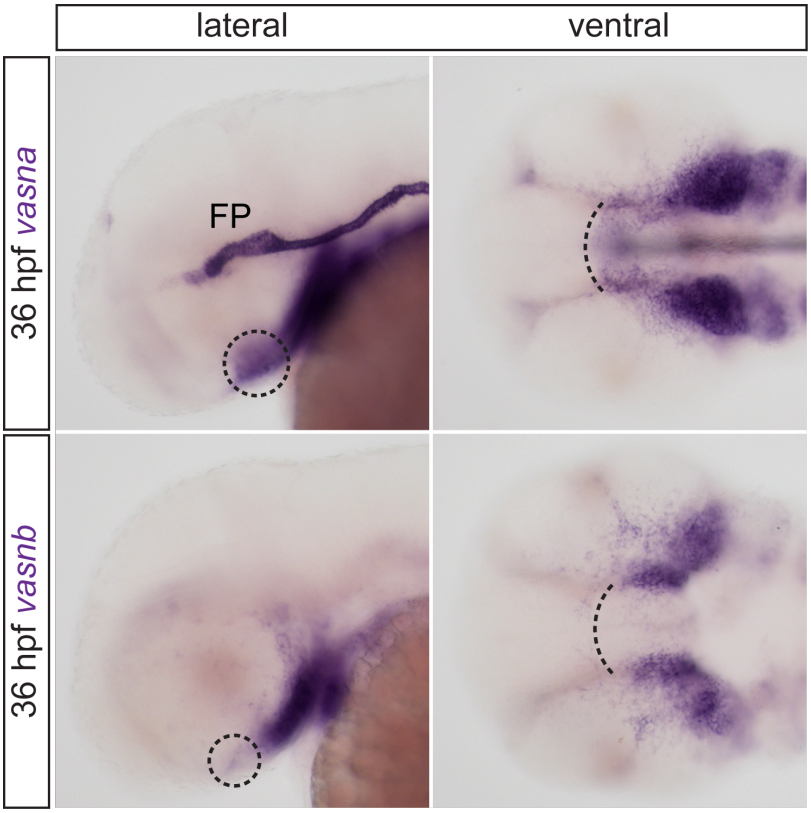

Figure 15. Detection of *vasna* and *vasnb* expression in 36 hpf zebrafish embryos Whole-mount *in situ* hybridization showing the spatial association of *vasna* and *vasnb* expression domains in the preoptic region (dashed circles) at 36 hpf. Sets of cells in the branchial arches appear to transcribe both genes. *vasna* is highly expressed by the anterior floor plate (FP), while *vasnb* transcription is undetectable in this structure. Lateral and ventral views. Anterior is to the left.

We sought to generate immunoreagents to facilitate the detection of Vasorin proteins in whole embryos. Vasna-CD4d3+4-6xHis and Vasnb-CD4d3+4-6xHis ectodomains were expressed as secreted polypeptides in HEK293-6E cells. Proteins were purified from supernatants by using HisTrap columns, and the product was injected in rabbits together with adjuvants for immunostimulation. Crude serum extracted from immunized animals was then directly tested on fixed zebrafish embryos. We performed immunostainings at two critical stages during the development of the retinal projection in zebrafish. At 36 hpf a small subset of retinal axons has reached the ventral diencephalic midline, thereby establishing the optic chiasm. 12 hours later, at 48 hpf, many axons have joined into the optic nerve

and the pioneering growth cones have reached the dorsal midbrain through the optic tract. At both these stages, Vasna was detected on the membrane of mesenchymal cells surrounding ventrally and laterally the course of the retinotectal projection (Figures 16A, 17A). This expression pattern very much resembles the mRNA expression domain detected with conventional *in situ* hybridization techniques. The anti-Vasna antibody additionally reproduces strong signal in the anterior floor plate and branchial arches. Antibody stainings using antisera recognizing Vasnb highlighted a small population of cells located between the optic recess and the optic chiasm, in the preoptic area. These cells are adjacent to Vasna-positive ventral mesenchyme and contact retinal axons along their posterior edge (Figure 16B). Such cellular domain is positioned across the ventral diencephalic midline, a location that is reminiscent of the "glial knot" (Silver, 1984; Silver et al., 1987) (Figure 16C). At 48 hpf, while the anteriormost Vasnb-positive cellular cluster is maintained, it becomes clear that other immunoreactive cells are intercalated within the chiasm and seem to support the two optic nerves across the midline. Interestingly, the retinal projections appear to be enwrapped by Vasnb-positive membranes along their ventral diencephalic course (Figure 17B).

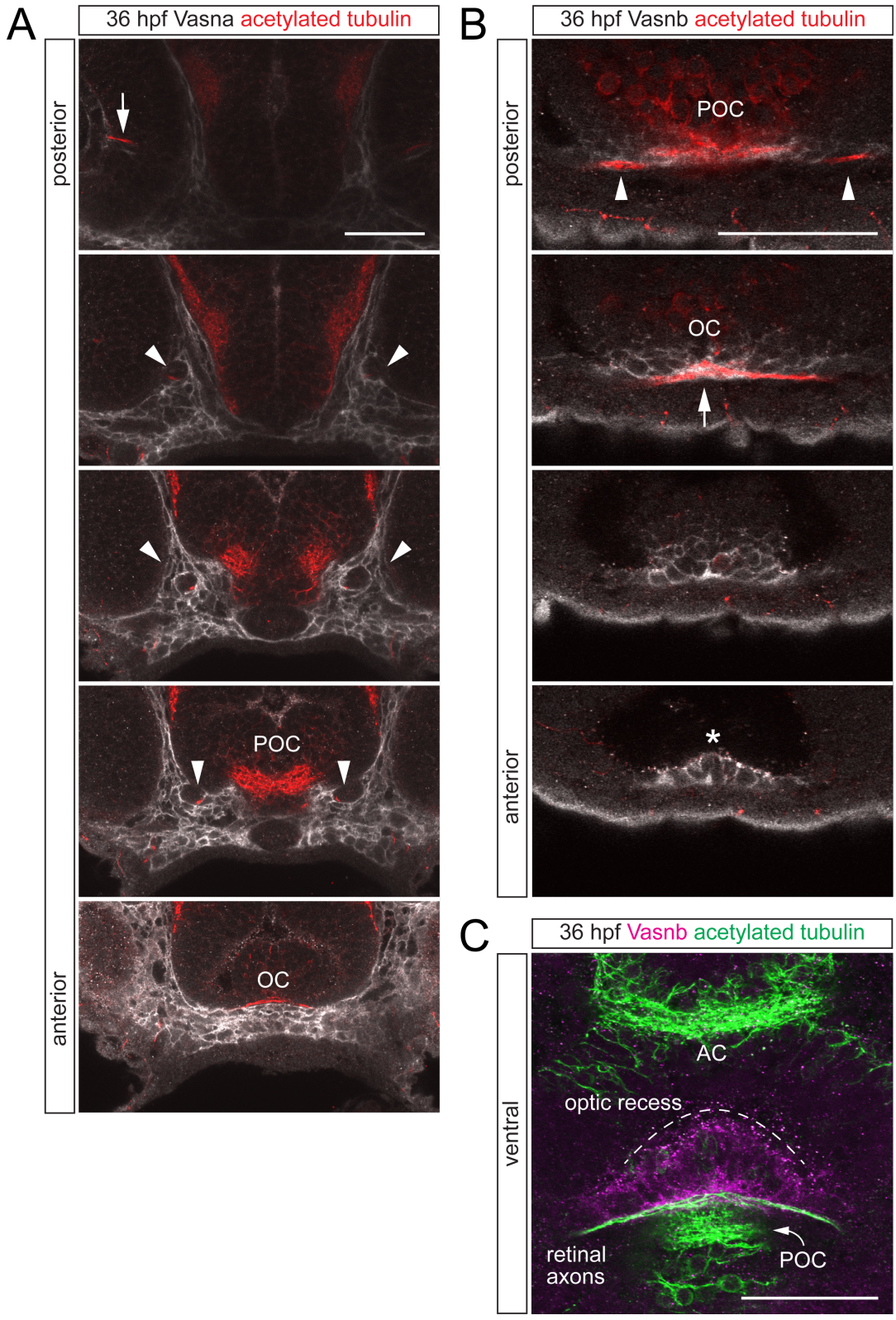
A
36 hpf Vasna acetylated tubulin
posterior
anterior
POC
OC
B
36 hpf Vasnb acetylated tubulin
posterior
anterior
POC
OC
*
C
36 hpf Vasnb acetylated tubulin
ventral
AC
optic recess
retinal axons
POC

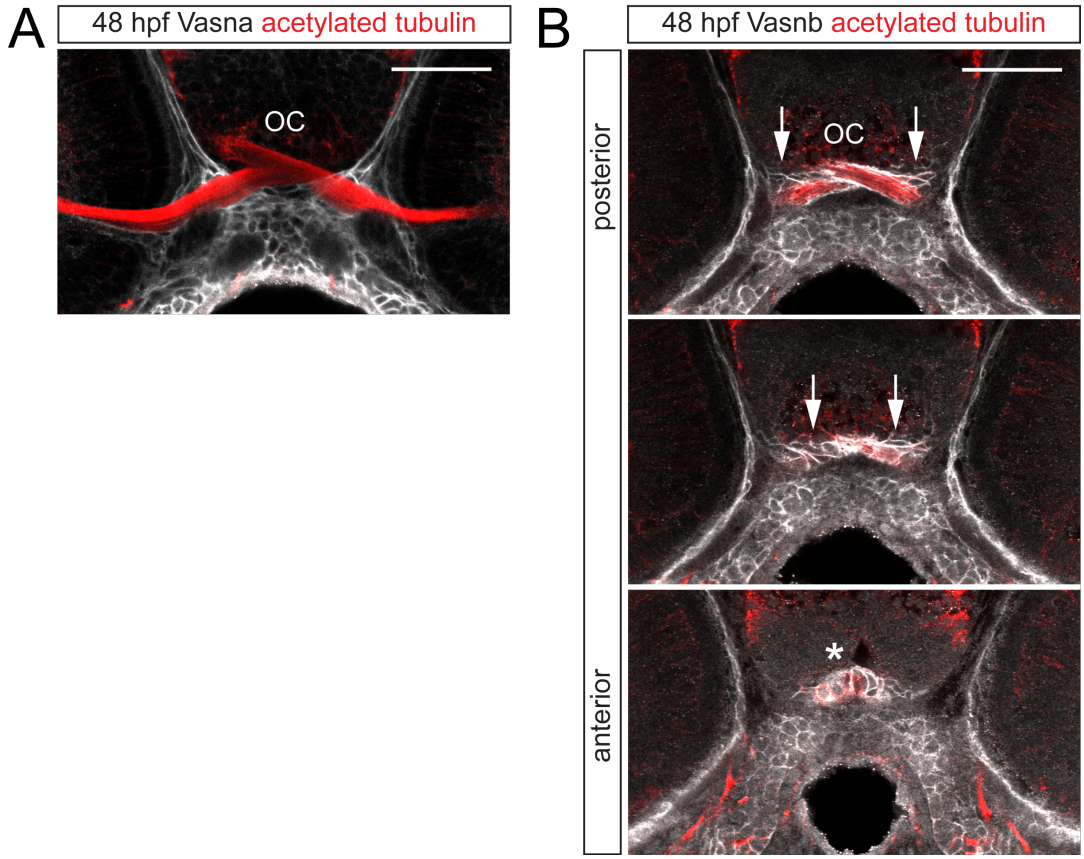

Figure 17. Vasna and Vasnb protein localization in 48 hpf embryos
(A) anti-Vasna immunolabelling highlights the head mesenchyme (white), which closely associates with the retinal axons (red). Single optical section from a confocal dataset. Anterior view. OC: optic chiasm. Scale bar: 50 µm. (B) Vasnb-expressing cells (white, arrows) surrounding the optic nerves at the chiasm. At the anterior edge of the diencephalic floor, a group of Vasnb-positive cells (asterisk) resembles the knot in shape and position. Single optical sections from a confocal dataset. Anterior views. Scale bar: 50 µm.

Figure 16 ***(preceding page).*** Vasna and Vasnb protein localization in 36 hpf embryos
(A) Staining of 36 hpf embryos using polyclonal antiserum against Vasna reveals the membrane of mesenchymal cells surrounding ventrolaterally the retinal axon pathway. Retinal axons (red) associate with Vasna-positive cells from their intraretinal differentiation site (arrow). Vasna marks the surface of a tunneling structure (arrowheads), which directs retinal axons to the optic chiasm (OC). Single optical sections from a confocal dataset. Anterior views. Scale bar: 50 µm. (B) Vasnb immunostaining in 36 hpf embryos showing direct association between retinal axons (red, arrowheads) and Vasnb-positive cells (white) at the optic chiasm (arrow). Vasnb cells also occupy the anteriormost portion of the diencephalic midline, in contact with the ventricle (the knot, asterisk). Single optical sections from a confocal dataset. Anterior views. Scale bar: 50 µm. (C) The Vasnb expression domain nested between the optic recess (anterior) and the retinal axons (posterior) at 36 hpf. AC: anterior commissure. POC: postoptic commissure. Z-projection of a confocal substack. Ventral view. Anterior is to the top. Scale bar: 50 µm.

vasna and *vasnb* mutants: generation and analysis

The paired localization of Vasna and Vasnb, as revealed by immunostaining, introduced the possibility that Islr2, expressed in RGCs, effectively transduces Vasn signals along the complete course of retinal axons. We reasoned that if Vasna and Vasnb are the exclusive functional ligands of Islr2 *in vivo*, generating null mutations in these loci would likely result in a phenotypic copy of the *islr2* mutant. We therefore set to take advantage of novel targeted mutagenesis technologies to mutate *vasna* and *vasnb*. Site-directed nucleases have emerged in the past years as the method of choice to produce deletions or insertions in a targeted fashion. We initially sought to standardize a zinc-finger nuclease (ZFN) platform for this purpose. ZFN are repeats of three zinc-finger DNA-binding domains, each recognizing three DNA base pairs. A singular ZFN protein therefore binds to a nine base pair DNA stretch with imperfect specificity (Sander et al., 2010). The introduction of Transcription activator-like effector nucleases (TALENs) and the introduction of improved methods for their custom generation allowed to target genes with increased specificity and efficiency (Cade et al., 2012; Bedell et al., 2012). We therefore used this system and successfully induced indels in the beginning of the *vasna* coding sequence. F0 individuals were incrossed and their progenies genotyped for carrying defective *vasna* sequences. These fish were subsequently outcrossed to a Tübingen wild-type strain to isolate single *vasna* mutant alleles. Although Vasna marks the tissue directly contacted by retinal axons from their site of terminal differentiation to the optic tract, we did not detect pathfinding or growth defects in *vasna* mutants. These larvae are morphologically normal and therefore indistinguishable from wild-type siblings. In addition, several alleles generated via TALEN mutagenesis could be raised to adulthood and did not highlight any morphological or reproductive defect (Figure 18A). We purchased and injected TALEN mRNA directed to the 5' segment of the *vasnb* locus. All F1 animals, however, once genotyped, were unaffected. This is not an uncommon result and could be explained in several ways, for example the poor efficiency or missing DNA recognition of

the specific TALEN pair used, a later requirement of the *vasnb* gene for metamorphosis or survival to adulthood. As a consequence, we analysed a *vasnb*^{sa6027} TILLING allele which is predicted to form a premature Stop codon before the end of the LRR domain (missense C-to-T mutation affecting amino acid 315, Arg-to-Stop). Because this allele would lack the transmembrane domain, we hypothesized that its protein product would be functionally inactive. Lipophilic dye injections in the retinae of this mutant, however, failed to highlight guidance defects of axons forming the optic nerves. This finding was surprising, because of the specific positioning of the Vasnb expression domain with respect to the retinal axon pathway. The results collected during our *vasn* mutant analysis might be explained by the fact that these alleles are not, in fact, null. Alternatively, it is possible that Vasna and Vasnb compensate for the loss of paralogous function, even though the two proteins do not appear to be extensively co-expressed. A similar condition has indeed been reported in the case of *Slit1/Slit2* mutants in the mouse optic chiasm. Slit1 and Slit2 do not appear co-expressed and their mutant phenotypes taken singularly appear negligible. *Slit1/Slit2* double mutant animals, however, show overt misguidance at the chiasm, including the formation of a supernumerary, ectopic chiasm anterior to its correct location (Plump et al., 2002). Using our antibodies against Vasna and Vasnb, we ruled out the possibility that the generated mutants retain function. Indeed, we observed the complete absence of immunoreactivity in *vasna* and *vasnb* homozygous embryos, suggesting lack of protein product and – at the same time – providing evidence for the specificity of our polyclonal sera (Figure 19). In order to investigate whether Vasna and Vasnb are functionally redundant, we generated double mutant larvae. These animals also do not display overt phenotypes in the retinal projections (Figure 18B) and are morphologically normal and viable during larval stages.

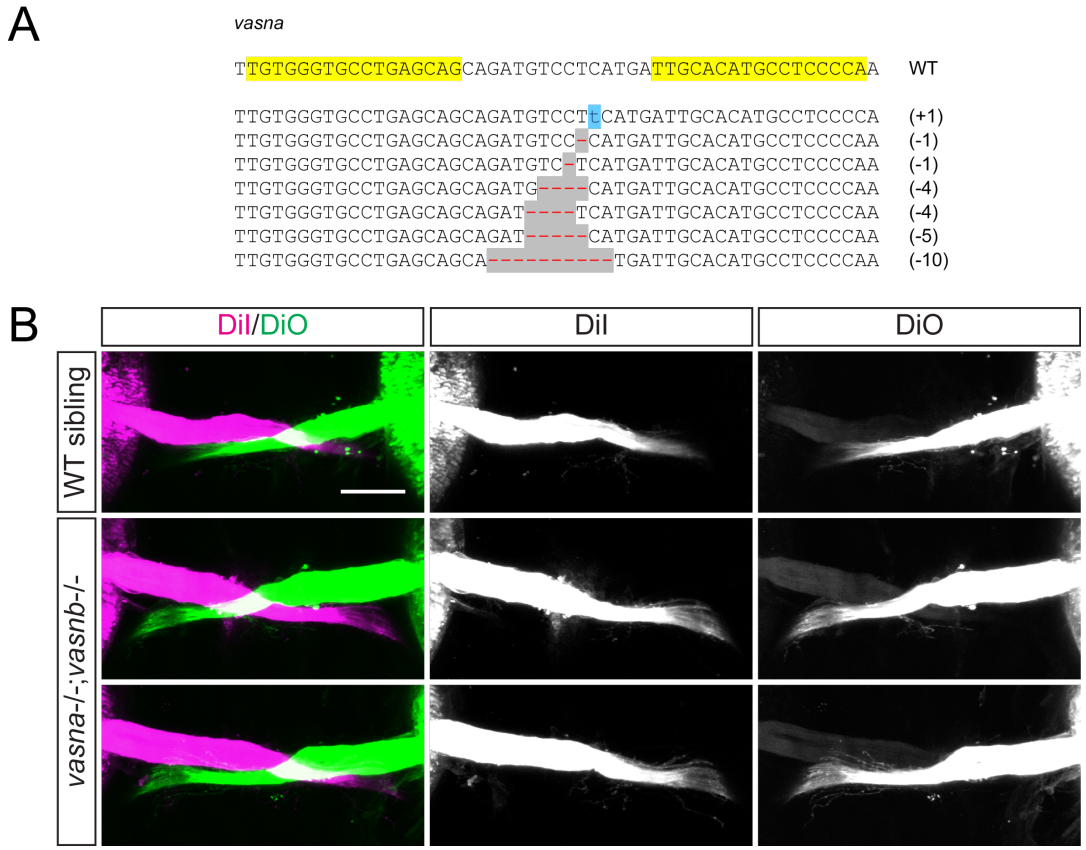

Figure 18. *vasna/vasnb* double mutants do not display overt defects in retinal axon guidance

(A) Alleles generated using TALEN mutagenesis directed to the beginning of the *vasna* locus. (B) Absence of retinal axon misprojections at the chiasm of 5 dpf *vasna/vasnb* double mutant animals. Z-projections of confocal datasets. Ventral views. Anterior is to the top. Scale bar: 50 µm.

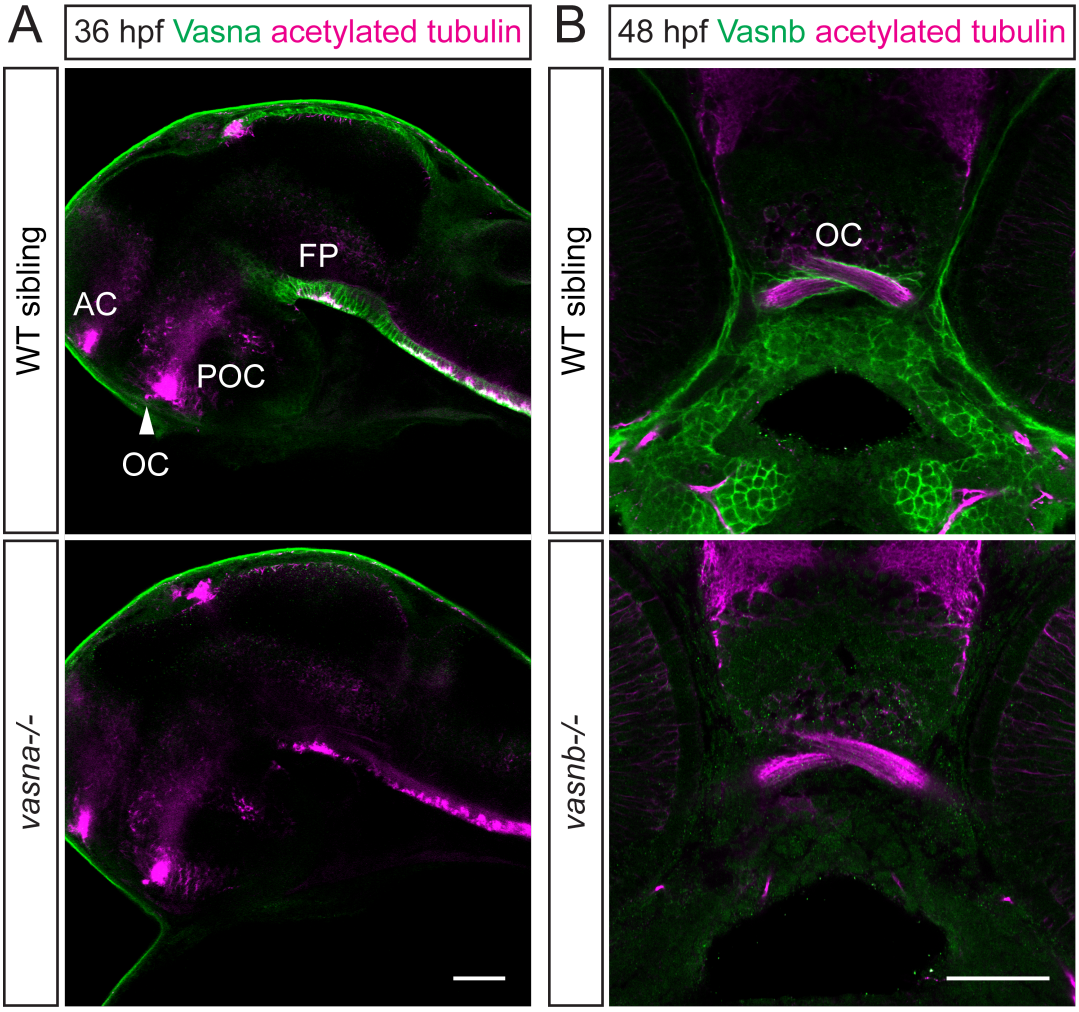

Figure 19. *vasna* and *vasnb* alleles are null mutations
(A) *vasna* alleles generated by targeted mutagenesis (TALENs) display complete loss of Vasna protein in homozygosity. AC: anterior commissure. FP: floor plate. OC: optic chiasm. POC: postoptic commissure. Single optical sections from confocal datasets. Lateral views. Anterior is to the left. Scale bar: 50 µm. (B) The *vasnb*^{sa6027} TILLING allele leads to complete loss of function, as suggested by the absence of Vasnb immunoreactivity. Single optical sections from confocal datasets. Anterior views. Scale bar: 50 µm.

In summary, considering: (1) The specific ability of Islr2 of physically binding to Vasna and Vasnb; (2) The expression of *islr2* in RGCs and that of *vasn* along the RGC axon pathway; (3) The specific presence of Vasnb in the cells forming the glial knot, which has been previously implicated in guiding retinal axons across the midline (Silver, 1984); we hypothesize that other proteins might

compensate for the loss of Vasna/Vasnb and would be expressed at the midline, because loss of Islr2 function is sufficient to induce guidance mistakes in this region. These redundant players at the chiasm might signal through Islr2 to channel growing axons to the contralateral side of the brain, and may modulate the presentation or the function of Vasn proteins. The collected expression data suggest that Vasnb is a novel marker of the glial knot in zebrafish. Anti-Vasnb antibodies highlight the cellular population primarily contacted by retinal axons along their ventral diencephalic migratory course. In order to verify that this region is morphologically intact in *islr2* mutants, we performed immunostainings on 48 hpf embryos. Retinal axons maintain correct positioning at the chiasm and the optic nerves remain associated to Vasnb-positive cells, indicating that mispatterning of this cellular population cannot account for the *islr2* mutant phenotype (Figure 20).

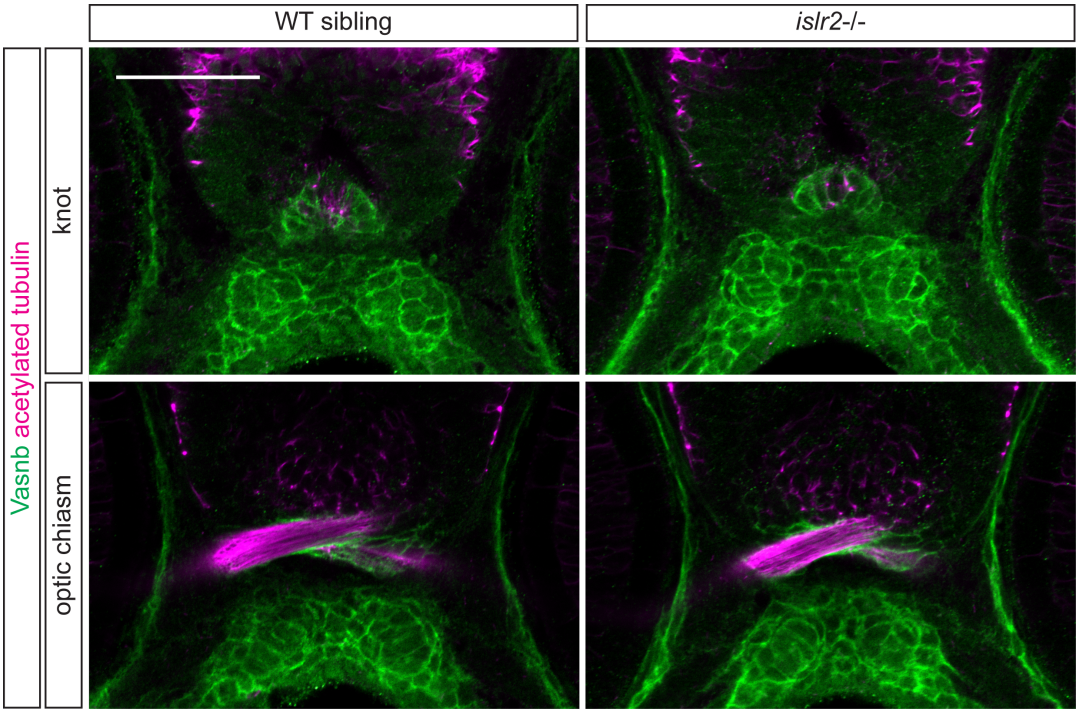

Figure 20. *islr2* mutants do not display mispatterning of cellular populations at the optic chiasm
The retinal axon misprojections identified in *islr2* mutant larvae are probably independent from mispatterning of tissue associated to the retinal axon pathway. The Vasnb-positive cellular population encompasses the course of retinal axons across the ventral diencephalon and it is unaltered in *islr2* mutants. Single optical sections from confocal datasets. Anterior views. Scale bar: 50 µm.

A first application of the chromobody technology in vertebrates

During the main work of this dissertation, related to problems in axon guidance, I became increasingly aware of how critical is the ability to detect protein localization in living and fixed animals. Through a collaboration with Prof. Dr. Ulrich Rothbauer from the Naturwissenschafliches und Medizinisches Institut der Universität Tübingen (NMI) we agreed to test and characterize chromobody constructs in living zebrafish. To investigate whether chromobodies do recognize endogenous targets in zebrafish and correctly reproduce their localization, we focused on two proteins: Actin and Proliferating Cell Nuclear Antigen (PCNA). These proteins are interesting antigens to target because they participate in fundamental

cellular housekeeping functions and display very distinct localization patterns. We hypothesized that, in case chromobodies would interfere with Actin or PCNA protein function, these antigens' fundamental roles in cellular homeostasis would be blocked, resulting in strong phenotypes during embryogenesis. Because of this possibility, we generated transgenic animals expressing chromobodies in an inducible fashion. In a first approach we paired chromobodies recognizing Actin (a tagGFP2 fusion) and PCNA (a tagRFP fusion) to a conditional heat-shock promoter (Halloran et al., 2000), thereby allowing chromobody induction at any developmental time point. Incubating transgenic embryos at 39°C for 1 h is sufficient to initiate chromobody expression as suggested by the high level of widespread fluorescence that is detectable in most embryonic tissues 4 to 6 hours after induction (Figure 21).

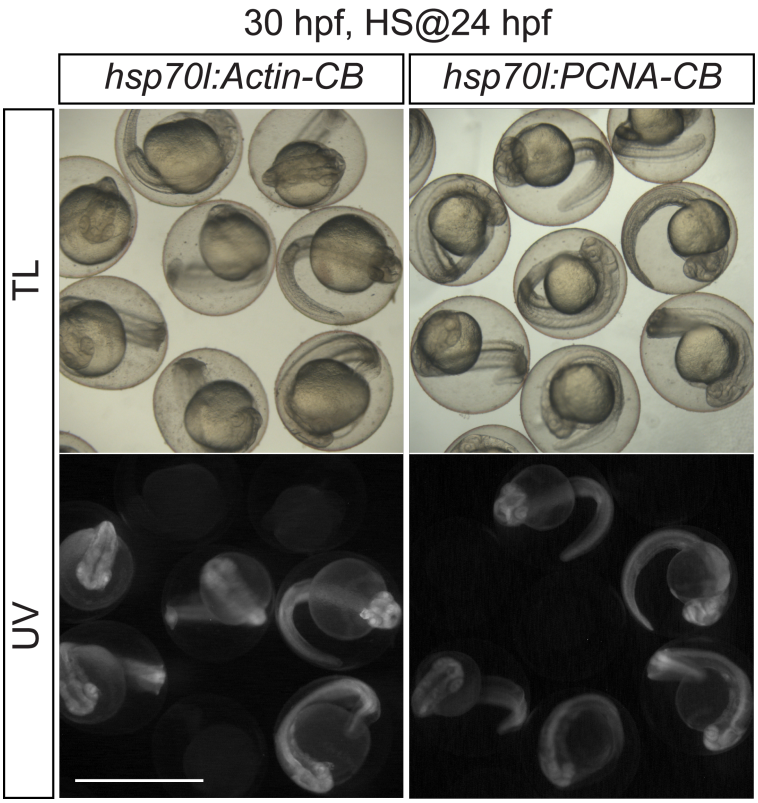

Figure 21. Wild-type morphology in embryos ubiquitously expressing chromobodies Embryos carrying either *hsp70l:Actin-CB* or *hsp70l:PCNA-CB* were heat-shocked at 39°C from 24 to 25 hpf. 6 hours later, transgenic individuals displayed robust chromobody expression, as suggested by emission of fluorescence and did not appear to suffer morphological consequences. TL: transmitted light. UV: ultraviolet light. Scale bar: 1 mm.

A closer inspection of these samples did support the idea that chromobodies can specifically trace Actin and cell cycle dynamics in living zebrafish. Heat-shocked Actin-CB embryos showed strong fluorescent signal in muscle fibers and epidermis, including their typical actinic apical ridges. In addition, the centres of rosettes located in the migrating posterior lateral line primordium (pLLP) are constituted by apically-constricted membranes and are strongly labelled by Actin-directed chromobodies. All these sites are known to be rich in cellular Actin, as confirmed by counterstaining with Phalloidin to detect polymerized F-Actin densities. Extensive co-labelling was highlighted, indicating that Actin-CB indeed recognizes endogenous Actin in zebrafish (Figure 22A, B).

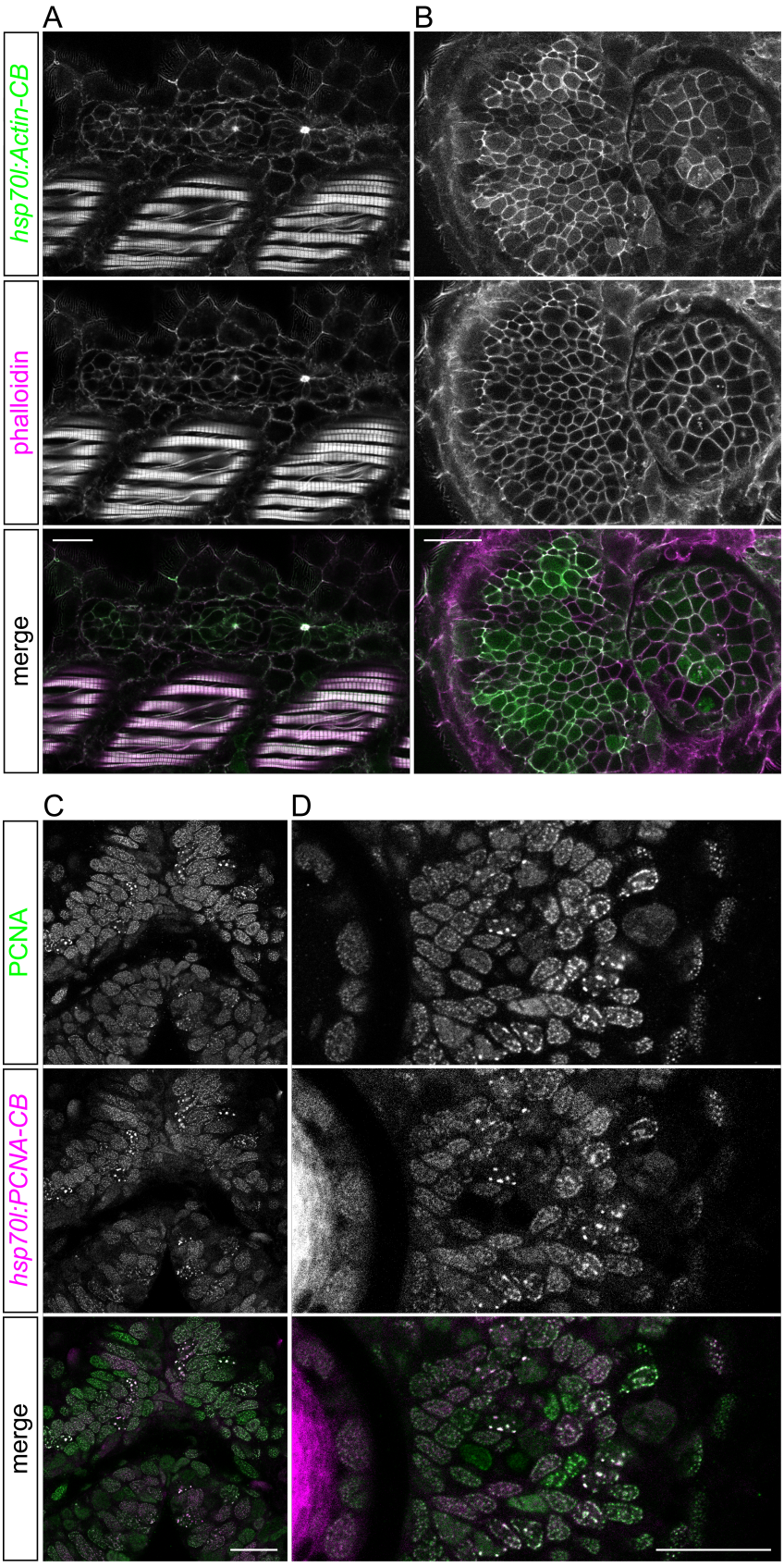
A
B
hsp70I:Actin-CB
phalloidin
merge
C
D
PCNA
hsp70I:PCNA-CB
merge

To investigate whether Actin-CB correctly reports Actin dynamics *in vivo*, we monitored the migration of the lateral line primordium, a group of cells that collectively moves along the horizontal myoseptum with anterior to posterior directionality. This cellular ganglion releases trailing groups of cells that form sensory organs, the neuromasts, on the flank of the larva. The collective migration of the lateral line primordium is a well-studied process that requires Actin dynamics at its leading edge to keep the organ moving in the correct direction (Xu et al., 2014). Using embryos ubiquitously expressing Actin-CB after heat-shock induction, we were capable of following the projection of filopodia and lamellipodia at the leading edge of the pLLP and detected no obvious defect in its migration (Figure 23A"'). These observations suggest that high levels of Actin-CB do not appear to functionally interfere with wild-type Actin (de)polymerization; this tool can therefore faithfully report dynamic Actin localization in living animals. In a parallel effort, we combined chromobody expression with the Gal4/UAS system, a widely used transcriptional control module. The *UAS:Actin-CB* transgene was tested in combination with a *csf1ra:gal4* driver line expressed in macrophages and xanthophores, two motile cell types that display fast Actin dynamics at their plasma membrane. We successfully carried out live imaging experiments documenting the projection and retraction of Actin-rich filopodia at the edge of xanthophore cellular protrusions and observed how these cytoskeletal elements form directionally toward neighbouring xanthophores, pre-

Figure 22 ***(preceding page).*** Chromobodies colocalize with target endogenous antigens

36 hpf transgenic embryos subjected to induction of Actin-CB expression at 24 hpf were counterstained for F-actin using Phalloidin. Co-labelling of similar structures, i.e. muscle fibers, epidermal cells and the apical side of pLLP rosettes (A) and the cortex of retinal cells (B), was observed. Similarly, PCNA-CB-expressing embryos were immunostained for endogenous PCNA. Nuclear densities corresponding to S phase structures associated with DNA replication were identified as sites of signal overlap, both in the dorsal midbrain (C) and retina (D). These data indicate that Actin-CB and PCNA-CB bind endogenous target structures in zebrafish. Scale bars: 20 µm.

figuring the formation of cell-cell contacts (Figure 23B).

In order to test if PCNA-directed chromobodies indeed recognize endogenous PCNA in zebrafish, we immunostained *hsp70l:PCNA-CB* embryos and detected colocalization between PCNA-CB and its endogenous target (Figure 22C,D). With the aim of further comparing PCNA-CB with state-of-the-art techniques to capture replication forks dynamics *in vivo*, we carried out time lapse analysis of heat-shocked transgenic embryos that additionally transiently expressed human PCNA-GFP from an injected DNA construct. The collected data show that PCNA-directed chromobodies and exogenously-provided human PCNA-GFP assemble in the same nuclear densities and they can both trace these structures during S phase progression (Figure 24B).

UAS:PCNA-CB transgenic carriers were crossed to *wnt1:gal4,UAS:GFP* animals, which show high levels of transactivation in the dorsal midbrain. Strong PCNA-CB expression derived from the *wnt1* promoter element and was instrumental to assess the impact of chromobodies on antigen function *in vivo*. Although GFP expression is observed from 16 hpf to adult stages (Volkmann et al., 2010), we did not detect morphological abnormalities in these animals. Embryos could be raised to adulthood and confocal time-lapse analysis of neural progenitors undergoing proliferation revealed no defect in cell cycle progression. Using these embryos we recorded dynamic localization of endogenous PCNA and could identify characteristic S phase stages. When focusing on cells displaying a finely-speckled nuclear pattern (indicative of early S phase), we observed that the densities became fewer in number and larger in size over time, reporting progression to mid and late S phase. Immediately next, the foci disappeared, leaving a uniform signal distribution in the nucleus (G2) and shortly thereafter cells underwent mitosis (Figure 25B). These data specifically reproduce the known localization dynamics of PCNA in mammalian cells (Leonhardt et al., 2000; Essers et al., 2005).

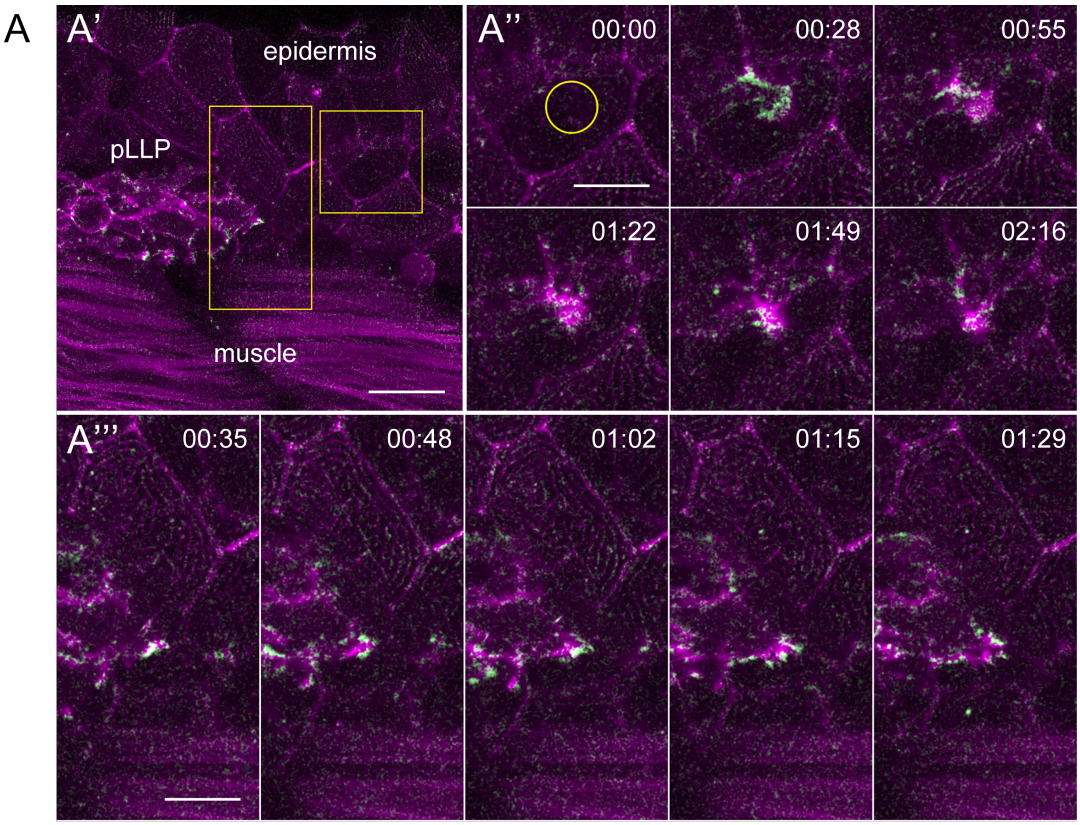
A
A'
epidermis
pLLP
muscle
A''
00:00
00:28
00:55
01:22
01:49
02:16
A'''
00:35
00:48
01:02
01:15
01:29

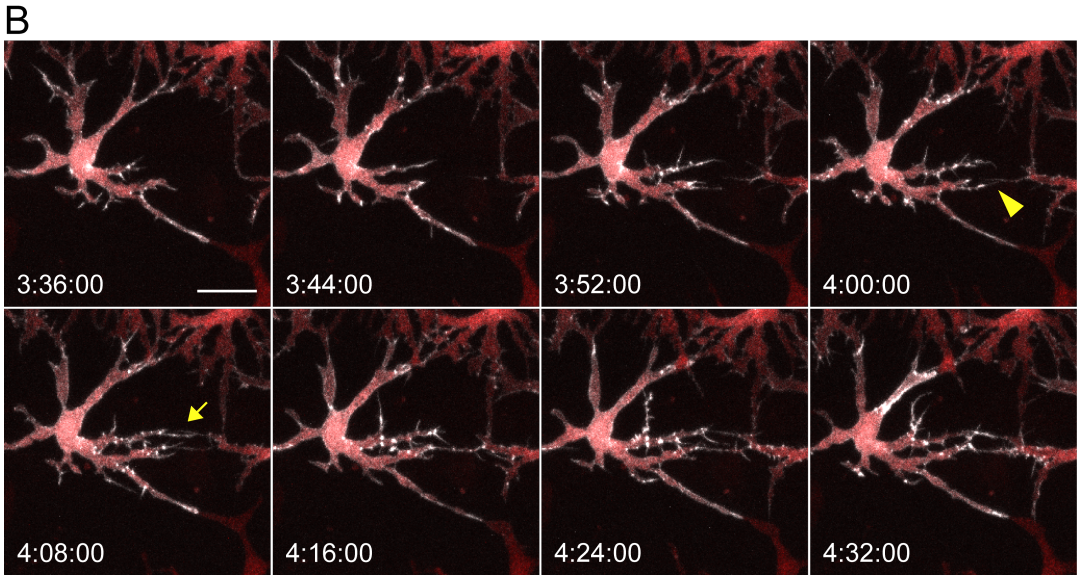
B
3:36:00
3:44:00
3:52:00
4:00:00
4:08:00
4:16:00
4:24:00
4:32:00

Figure 23 *(preceding page).* Actin-CB can trace endogenous Actin dynamics *in vivo*
(A') 36 hpf *hsp70l:Actin-CB* embryos expressing the transgene reveal chromobody localization to sites of intense cytoskeletal activity, i.e. epidermal cells with their characteristic Actin-rich apical ridges, muscle fibers and migrating pLLP cells. (A") Inducing laser damage through the epidermis of these embryos causes fast relocalization of Actin during wound closure. (A"') Live imaging of cells at the leading edge of the lateral line primordium highlights the dynamic extension of filopodia and lamellipodia. Magenta: fluorescence signal from time frame t+1. Green: signal from the subtraction of frame t from t+1, emphasizing the appearance of Actin-CB signal from frame to frame (scan interval: 7 s). Scale bars: 10 µm. Timestamps: min:s. (B) Chromobody transgenes can be coupled with the Gal4/UAS system to achieve expression in specific cellular populations. *csf1ra:gal4;UAS:NTR-mcherry* (red)*;UAS:Actin-CB* (white) xanthophores report Actin activity at the tip of their dynamic cellular protrusions. Slender cytoplasmic processes appear directionally to contact neighbouring cells (arrowhead and arrow). Scale bar: 20 µm. Timestamps: h:min:s.

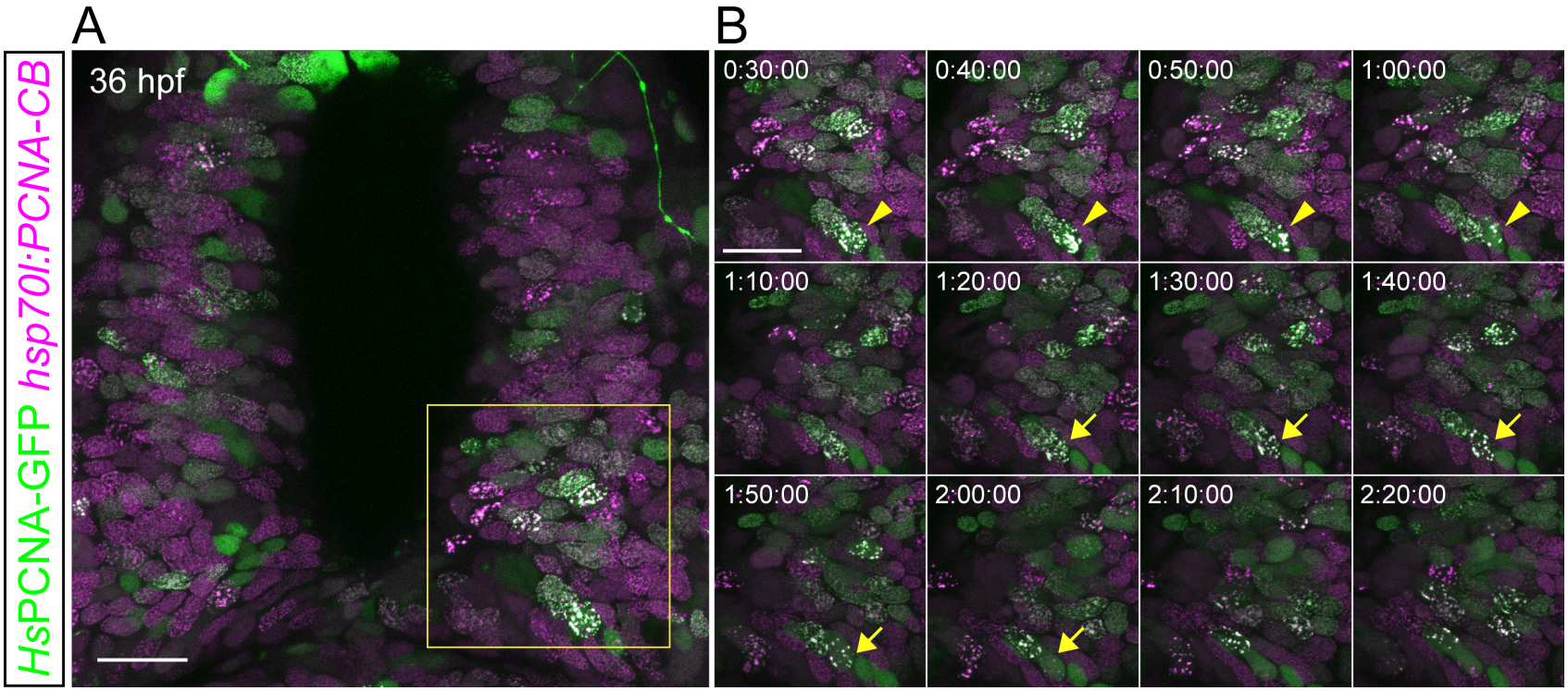

Figure 24. PCNA-CB and human PCNA-GFP trace identical structures *in vivo*
hsp70l:PCNA-CB embryos were injected at the 1-cell stage with a DNA plasmid encoding human PCNA-GFP. (A) After transgenic induction at 24 hpf, both proteins can be visualized at the same time. (B) Time lapse analysis of these embryos reveals that PCNA-CB and human PCNA-GFP mark identical structures, if co-expressed in cells proceeding through S phase (arrowhead and arrow). Scale bars: 20 µm. Timestamps: h:min:s.

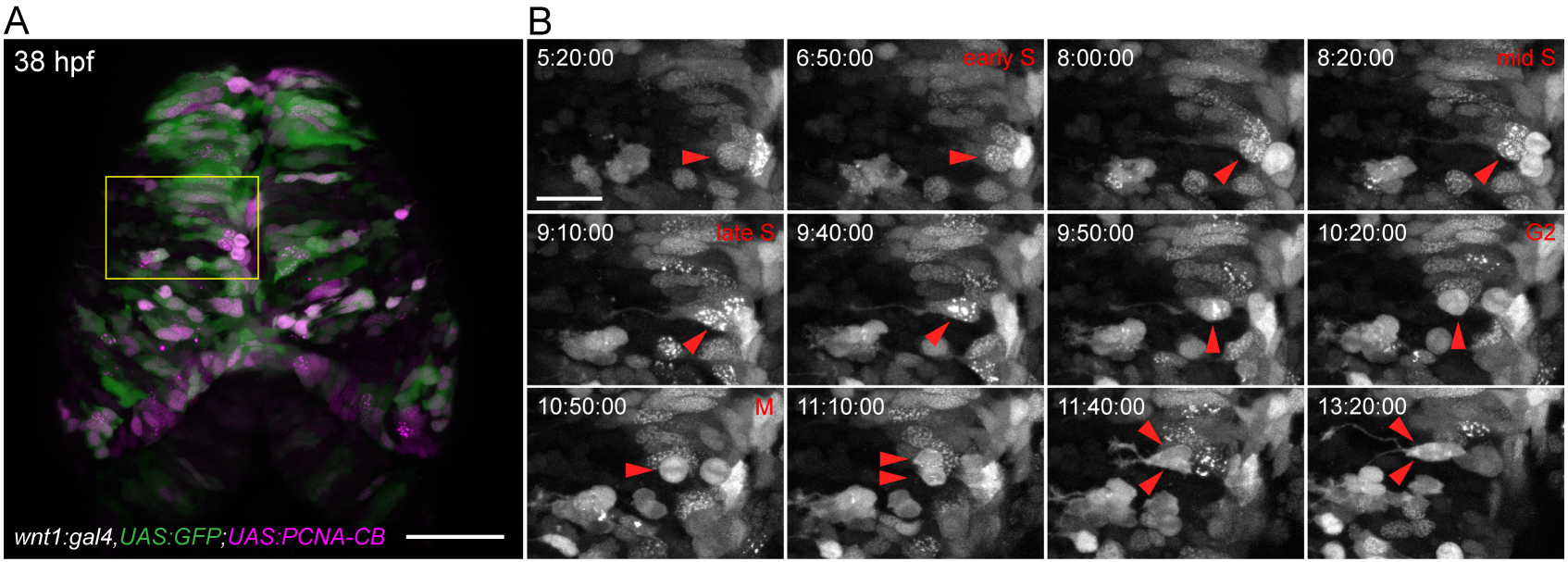

Figure 25. PCNA-CB reveals cell cycle progression in *wnt1*-positive progenitors
(A) Combining *wnt1:gal4,UAS:GFP* and *UAS:PCNA-CB* transgenes facilitates monitoring cell cycle progression in *wnt1*-positive cells of the dorsal midbrain, which are highly proliferative between 1 and 2 dpf. Scale bar: 50 µm. (B) Live imaging of chromobody-expressing cells demonstrates that the localization dynamics of PCNA, as revealed by the chromobody, faithfully reports advancement through consecutive cell cycle phases. Scale bar: 20 µm. Timestamps: h:min:s.

Discussion

Identification of new players in retinal axon guidance

The identification of proteins involved in axon guidance has traditionally relied on the serial purification of tissue extracts and the isolation of progressively less complex protein fractions capable of perturbing an *in vitro* axon guidance readout. This methodology has been practically abandoned because of its limited sensitivity (i.e. only very strong guidance cues can be reproducibly isolated). Another problem majorly contributing to the difficulty of carrying out these experiments is the fact that the functional integration of guidance cues takes place at the growth cone membrane. The biochemical characterization of axon guidance regulators is therefore greatly complicated by the fact that the majority of these proteins are inserted into membranes. Additionally, any *in vitro* readout system is likely not to faithfully reproduce the *in vivo* condition, because it automatically abstracts from the endogenous tissue patterning. As an alternative, forward genetics screens have been employed for the same purpose of identifying guidance cues. During this process, phenotypic classes are selected from a population of animals harbouring randomly-introduced point mutations. The genes involved in the developmental process of interest are then identified by genetic mapping. This system provides an unbiased entry-point into the description of biological processes, limited only by the magnitude of the selected phenotypes. In zebrafish, forward genetics screens have been successfully applied to dissect axon guidance problems (Baier et al., 1996; Karlstrom et al., 1996; Trowe et al., 1996; Xiao et al., 2005), however, only a handful of factors turned out to be cell-autonomous to misguided neurons. The joint analysis

of mutants involved in retinal axon behaviour in zebrafish led to the identification of a strong role for Hedgehog signalling in patterning the ventral diencephalic tissue. It is however possible that more subtle cell-autonomous phenotypes are additionally displayed by these mutants, although these defects are masked by overt brain mispatterning effects. These data are not surprising when considering axon guidance as a highly redundant process, tightly dependent on the appropriate presentation of multiple non-cell-autonomous cues. The combination of these factors largely contributes to the difficulty in carrying out genetic dissections of axon guidance processes and to the stereotypy of these cellular decisions. As a consequence, deeper analyses of axon guidance events might perhaps require the use of sensitized genetic backgrounds. For these reasons, we adopted a candidate approach which combines the isolation of type-I transmembrane eLRR proteins with relevant spatiotemporal expression, and the isolation of interacting partners using an unbiased assay that is optimized to detect low affinity binding events. The obtained results demonstrate the utility of such approach, as shown by: (1) The isolation of *islr2* as candidate gene for retinal axon guidance decisions. Indeed *islr2* mutants display misprojecting axons at the optic chiasm. (2) The identification of the Vasorin paralogs as physical binding partners of Islr2. Their expression in zebrafish embryos shows intimate association to the retinal axon pathway, which is indicative of complex axon-environment signalling events.

Redundancy at the optic chiasm

The characterization of molecular pathways controlling retinal axon midline crossing in rodents contributed to create a picture of the chiasm as a highly redundant environment. Slits are well-known, prototypical axon repellents and thus very likely to exhibit guidance defects in their knockout condition. In the mouse retinal pathway, however, removing *Slit1* or *Slit2* does not lead to overt axon misprojections, which is surprising, given the fact that these genes do not spatially overlap in expression. Despite these data, double knockout animals display an ectopic, supernumerary anterior chiasm, an obvi-

ous phenotype which indicates functional redundancy (Plump et al., 2002). Another example refers to the main receptor class transducing cell-autonomously the effect of the midline repellent Ephrin-B2 on RGCs. *EphB1* knockouts show a decussation phenotype where a subset of retinal axons – normally contributing to the ipsilateral projection – are instead crossing the midline in association with the rest of the optic nerve. *EphB1* is expressed specifically in ventrotemporal RGCs, the group of neurons that are programmed to give rise to the ipsilateral projection. However, other *EphB* family members are expressed in the same region of the retina and are therefore good candidates to have similar roles. A triple knockout condition in which *EphB1*, *EphB2* and *EphB3* are all eliminated, however, indicates that these receptors are not redundant, as shown by the similarity to the single *EphB1* mutant phenotype. At the same time, the complete elimination of Ephrin-B/EphB signalling does not lead to total absence of ipsilateral retinal axons, suggesting the existence of parallel strategies to redirect axons at the chiasm (Williams et al., 2003). Conversely, knocking-out *VEGF164*, a recently identified axon attractant at the midline, determines the redirection of a subset of axons from a contralateral to ipsilateral course (Erskine et al., 2011). These observations are not qualitatively dissimilar to the ones reported previously, and highlight the chiasm as a truly binary decision territory for retinal axons, integrating multiple signalling systems, in other words, the real definition of a "choice point". In agreement with this interpretation, Nr-CAM and Plexin-A1 have been recently described to sense a midline molecule, Sema-6D. This guidance cue is quite unconventional, because the sign of its effect on retinal axons can change upon differences in the molecular context this protein is presented in (Kuwajima et al., 2012). Nr-CAM has been identified as a permissive factor in midline crossing at the chiasm thanks to semi-intact explant experiments, in which blocking its function leads to an increase in the ipsilateral component of the retinal projection. However, mutant animals do not show any phenotype, suggesting that other molecules compensate for Nr-CAM loss (Williams et al., 2006). Recent work found

that Nr-CAM and Plexin-A1 are independently required for Sema-6D signal transduction and are in parallel used at the midline to transform Sema6D from an axonal repellent to a growth-promoting cue. A similar picture of genetic redundancy emerges from analyses of retinal axon midline crossing in zebrafish. *sema3d* and *nrp1a* morphant embryos display the presence of ipsilaterally-projecting retinal axons (Sakai and Halloran, 2006; Dell et al., 2013). However, it is not known whether these larvae also exhibit concurrent morphological defects and it is difficult to estimate the aspecific impact of morpholinos in general (Kok et al., 2015). Although the zebrafish *nrp1a* knockdown phenotype is similar to the *Nrp1* mouse knockout condition (Erskine et al., 2011), it fails to be recapitulated by a *nrp1a* zebrafish mutant allele (Dell et al., 2013). In addition, only 23% of *sema3d* zebrafish mutants display ipsilateral axons found in 80% of morphants. The *space cadet/rb1* mutation was identified in zebrafish presenting motor defects and ipsilateral retinal projections (Granato et al., 1996; Lorent et al., 2001). These mutants do not present overt morphological defects, however, only 17% of these larvae display ipsilateral projections. *Space cadet/rb1* mutant larvae display a series of defects consistent with its non-spatially-restricted expression in the retina. These individuals have intraretinal guidance defects, axonal deficits in exiting the retina, hypoplastic optic nerves and stalling at the midline, in addition to ipsilateral axons. In contrast to all zebrafish mutants displaying phenotypes that are not fully penetrant, we isolated in our work *islr2*-deficient larvae that present fully penetrant ipsilateral projections when optic nerve thickness is normal. These data show the importance of Islr2 in guiding retinal axons at the midline. We report the identification of Vasna and Vasnb as Islr2-binding partners. Mutants in *vasna* and *vasnb*, even combined, did not display defects at the level of retinal axon projection. However, given the regulatory mechanisms at work in the chiasmatic tissue, explained above, it is not surprising that other factors could compensate for the loss of Vasorins, probably by acting through Islr2.

Function of Islr2-Vasorin signalling

Vasorin was first identified as a TGF-beta-binding protein regulating the response to vascular lesions (Ikeda et al., 2004). It is known from *in vitro* experiments that Vasorin may be processed by ADAM17 to act as a secreted inhibitor, thereby controlling TGF-beta-induced epithelial-to-mesenchymal transition (EMT) (Malapeira et al., 2011). Whereas the expression of *vasna* in zebrafish was thought to be indicative of functions in central nervous system and vascular morphogenesis (Chen et al., 2005), knockin mice harbouring LacZ in the *Vasorin* locus rather show expression associated to the skeletal system (Krautzberger et al., 2012).

The discovery that Islr2 and Vasorins physically interact, and that their expression spatiotemporally overlaps with the process of chiasm establishment, made it likely that these proteins indeed constitute an active signalling mechanism *in vivo*. However, if one could deduce Islr2 involvement in retinal axon midline crossing in the light of the mutant phenotype, the absence of a phenocopy from the *vasna* and *vasnb* knockout efforts, leaves this conclusion unverified. To investigate whether these molecules exert a similar type of function in other organisms, we initiated a collaboration with Prof. Carol Ann Mason (Columbia University, New York, USA) and Prof. Kenji Mandai (Kobe University, Kobe, Japan). We carried out a double blind analysis of *Islr2/Linx* knockout mice, specifically aimed at detecting phenotypes in the visual system. *Islr2* mutants display a dual phenotype: first, a substantial number of retinal axons appear to be misrouted at the chiasm and follow the opposite optic nerve retinopetally; second, axons stray from the main optic tract at few, precise locations (Figure 26). These data suggest that Islr2 might more generally control axon routing at the chiasm, rather than specifically control ipsilateral versus contralateral guidance in mouse.

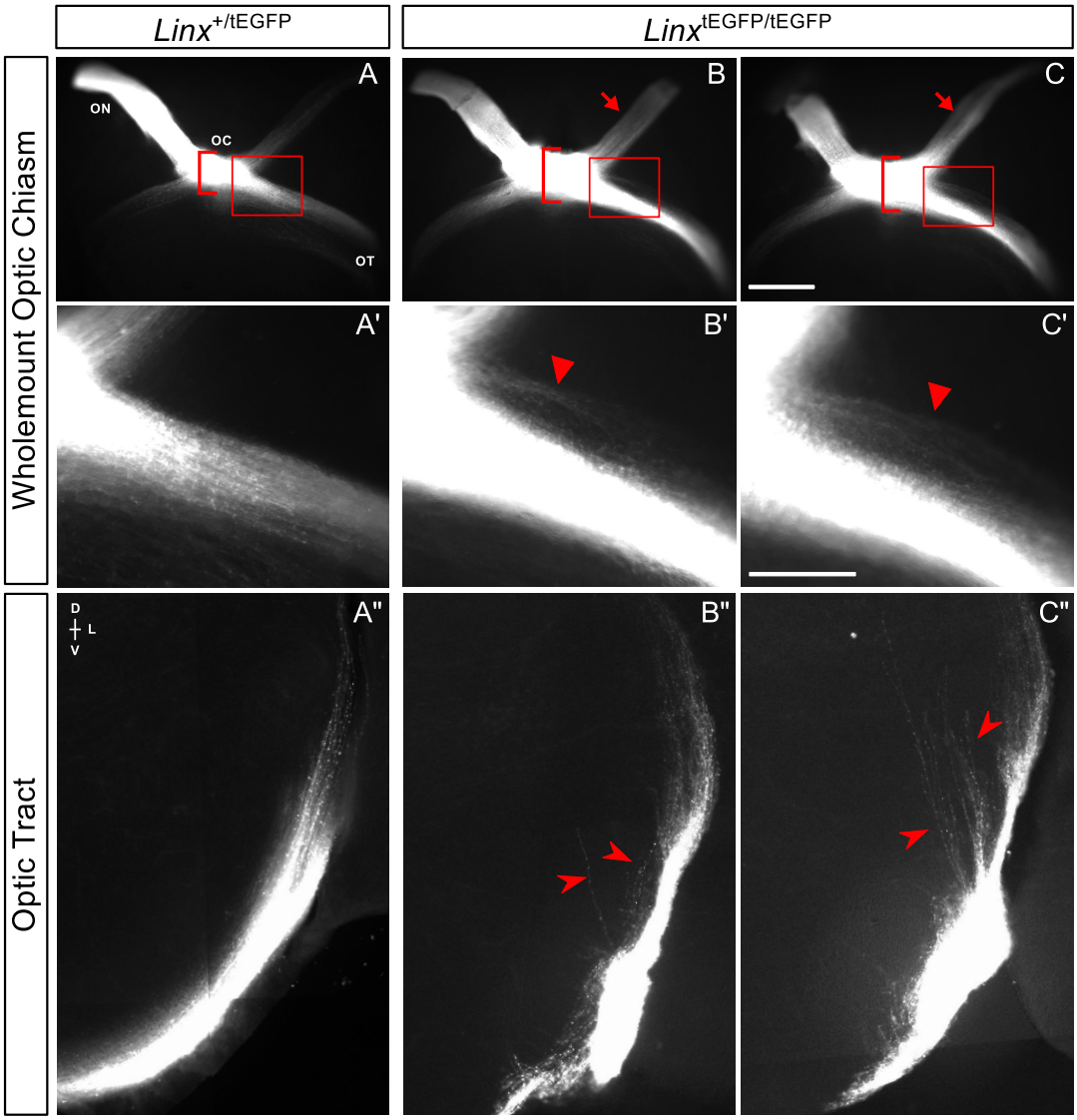

Figure 26. The *Islr2/Linx* knockout mouse phenotype
E16.5 mutant *Islr2* mice display expanded chiasms along the anteroposterior axis (brackets in B and C, compared to A). In addition, a higher number of axons enters the opposite optic nerve with retinopetal directionality (arrows in B and C). Although no clear increase in the number of ipsilaterally-projecting fibers relative to the contralateral projection can be observed, other defects were identified along the postcrossing route of retinal axons. Defasciculation effects in the optic tract were observed both at ventral (B' and C') and dorsal locations (B" and C"), where many axons stray from their normal course (arrowheads). Arrowheads in B' and C' indicate axons departing rostrally from the chiasm, a common phenotype observed in situations when guidance through the chiasm is impaired. ON: optic nerve. OC: optic chiasm. OT: optic tract. Scale bars: 500 µm (A-C), 200 µm (A'-C' and A"-C").

A reinterpretation of the zebrafish phenotype would consequently

assume that coherence among retinal fibers is somewhat perturbed in the mutant condition, such that a subset of axons is directed to the ipsilateral optic tract, which is a known permissive territory for axon growth (Burrill and Easter Jr, 1995). Interestingly, the mouse knockout phenotype partly resembles guidance errors described in *Slit1/Slit2* double mutants, where axons enter the opposite optic nerve, too. *Slit1* and *Slit2* are expressed by cells along the retinal axon pathway and in an anterior-medial location consistent with the position of the glial knot (Plump et al., 2002; Niclou et al., 2000; Erskine et al., 2000). These molecules cooperate to exert short range axon repulsion and fasciculate retinal fibers inside the tract. *In vitro*, Slit2 not only repels axons, but also inhibits their outgrowth. In a very similar way, Vasorins are expressed adjacent to the retinal projection: they outline the pathway followed by axons from the site of RGC differentiation up to the optic tract. Vasnb is expressed at the anterior midline, in cells that separate axons from the optic recess and later on marks cells and processes that appear to specifically enwrap optic nerves at the chiasm. This spatial distribution of Islr2-interacting proteins is highly suggestive of functions ensuring containment of the retinal projection, similarly to what has been described for Slits. The major difference between Slits and Vasorins (alias Slit-like2) is that the latter do not show phenotypes associated to the retinal projection. In contrast, our data collectively suggest that other molecules might also signal through Islr2, such that even in a *vasna/vasnb* null condition normal axon pathfinding would be restored.

A class of multifunctional candidate molecules that may modulate Islr2/Vasorin signalling are proteoglycans (Lee et al., 2004; Silver and Silver, 2014). Heparan sulfate proteoglycans (HSPGs) and chondroitin sulfate proteoglycans (CSPGs) share expression domains in the murine retina, optic chiasm midline and optic tract (Chung et al., 2001, 2000a), showing intimate association with the retinal axon pathway. Both HSPGs and CSPGs are expressed by SSEA-1-positive neurons bordering the optic chiasm at caudal positions. While a mutant allele of *Exostosin glycosyltransferase 1*

(*EXT1*) is lethal in mouse, as result of gastrulation defects, conditional *EXT1* knockout in neural progenitors gives rise to brain patterning defects reminiscent of defective morphogen signalling and commissural axon errors at the midline. Specifically, *EXT1* genetically interacts with *Slit2* to ensure proper routing of retinal fibers at the optic chiasm and to avoid misprojections to the contralateral optic nerve (Inatani et al., 2003). Mouse mutants for Heparan sulfotransferases *Hs2st* and *Hs6st1*, key enzymes mediating suphation of HSPG side chains, also display phenotypes similar to those of *Slit1* or *Slit2* null animals and genetically interact with Slit/Robo signalling (Pratt et al., 2006; Conway et al., 2011). Contrarily to the situation in mouse, *dackel/ext2* and *boxer/extl3* zebrafish mutants have normal brain patterning, probably because of maternal gene contribution, and are rather characterized by their role in controlling coherence and sorting of retinal axons in the optic tract. Combined *dackel/boxer* mutants, however, have stronger phenotypes compared to each mutation considered singularly. These larvae display ipsilateral projections that do not originate from the ventral midline, but are caused by ectopic dorsal crossing of fibers that leave the optic tract. Additionally, retinopetal innervation from the opposite eye and lack of coherence in the optic nerve at the chiasm were observed, a combination of phenotypes that reminds of *astray/robo2* mutants and had been obtained by morpholino knockdown of *slit1a* (Lee et al., 2004). Finally, HSPGs were found to be required non-cell-autonomously to correct topographic sorting errors in the optic tract (Poulain and Chien, 2013). Because CSPGs, like HSPGs, also appear to be involved in pretarget axon pathfinding along the *Xenopus* optic tract (Walz et al., 2002) and maintenance of optic nerve coherence in mouse (Chung et al., 2000b) they are both prime candidates to interact with Islr2/Vasorin signalling. In particular, the phenotypes of HS- or CS-deficient animals in part resemble the defects displayed by *Islr2/Linx* knockout mice. Moreover, the expression of HSPGs in zebrafish embryos, as shown by staining with a monoclonal antibody, is tightly associated to the complete retinal axon pathway (Lee et al., 2004), in striking analogy to the patterns

of Vasna and Vasnb immunostaining. Compensatory regulation introduced by third molecules is likely to prevent the assignment of specific functions to the molecules we analysed. It is possible that these functions are to a certain extent conserved in different organisms, however we rather think that certain anatomical features with distinctive signalling capabilities might be shared in different vertebrates, as exposed next.

The glial knot, an anatomical feature required for retinal axon midline crossing?

Beginning in the 1980s, research intensified on the anatomical structures that appeared to control axon fibre directionality. Silver and others recognized that the callosal commissure is prefigured by the formation of a cellular bridge which comes in association with commissural axons, dictating their course. This cellular population was named "glial sling" and was found to be required for callosal development (Silver et al., 1982), although the majority of cells forming the sling have been now recognized as migrating neurons (Shu et al., 2003a). Another cell population, the "glial wedge" was described to mediate cortical axon guidance of callosal axons. These cells, contrarily to the midline sling, do express glial markers and are located in the ventricular zone. The glial wedge precisely colocalizes with domains of *Slit2* expression (Shu and Richards, 2001; Shu et al., 2003b), which critically mediates pre- and postcrossing axon guidance, thereby contributing to correct guidance at the midline (Shu et al., 2003b). Reminiscent of the sling/wedge system, a glial bridge-like formation was described in the zebrafish to precede and provide a substrate for POC axon crossing (Barresi et al., 2005). Commissural glial bridges in zebrafish embryos are largely devoid of *slit2* and *slit3* expression, supporting the role of these molecules as axon repellants. The work of Barresi et al. (2005) established that Hedgehog signalling controls commissure formation by influencing brain patterning and not by acting directly as an axon guidance molecule. *you-too/gli2a* mutant embryos are therefore devoid of axons approaching the midline, because of erroneous

patterning and consequent *slit* misexpression. In addition, *slit2* and *slit3* knockdown causes defects in glial cell positioning, suggesting a parallel, direct function of Slit/Robo signalling in axon guidance and extra-axonal environment patterning. Silver and Rutishauser (1984) described the histology of the midline diencephalic tissue bordering the retinal axon projection in the mouse. These surprising data show that ventronasal (contralateral) and ventrotemporal (ipsilateral) axons associate to radically different tissue types in E13.5 mice. The axonal population that will be redirected from the midline to the ipsilateral optic tract invades a territory made by radial glia, characterized by large extracellular spaces separating thin cellular processes that contact the pial surface with large endfeet. This pathway appeared to be permissive in nature to axon growth. In sharp contrast, contralaterally-projecting axons were found in proximity to an anterior knot-like cellular formation. Cells forming this "glial knot" possess short protrusions, directed centripetally and compose a dense cellular barrier, largely devoid of extracellular spaces. The immunohistochemical analysis of the chiasmatic region in zebrafish, by highlighting Vasna- and Vasnb-positive cells, revealed that Vasnb expression is localized just anteriorly to the chiasm, as soon as it forms (36 hpf, Figure 16B). This population is nested between retinal axons and the optic recess and the cells appear to be stacked in a dense formation, similarly to the description of the knot. At later stages the Vasnb-positive cell group appears to have expanded to new locations. Whereas the cells at the anteriormost diencephalic midline are still present, they appear to be positioned at a distance from the chiasm. Many other VasnB positive cells are instead neighbouring the retinal axons at the chiasm and appear to shape their course and maintain the two optic nerves separated in the correct dorso-ventral orientation. The most striking feature of the chiasm at 48 hpf is that the optic nerves are not only selectively embedded in Vasnb-positive tissue, but they are also wrapped by Vasnb-positive membranes specifically along their ventral diencephalic path (Figure 17B). Niclou et al. (2000) reports that the cells positioned anteriorly to the optic chiasm in mouse express *Slit2*. It is not clear

whether these cells are corresponding to the glial knot, although their location would be compatible. Data from Barresi et al. (2005), however, show that the expression of the axon repellant is not shared by similarly positioned cells in zebrafish. This population in fish instead appears to be characterized by the transcription of *slit1a*. Loss-of-function analyses indicate that *slit1a* does not appear to behave as expected from an axon repellant (phenotypes obtained in the *slit2* and *slit3* knockdown condition). Instead, Barresi et al. postulate that Slit1a might indeed rather function as an adhesion factor, a very unconventional role for Slit proteins. Although this conclusion is based on unreported results, it would be in agreement with a hypothetical role of the glial knot in promoting retinal axon midline crossing. Supporting this scenario is the documented involvement of Sema3d in guiding retinal growth cones at the midline, as suggested both by knockdown and ectopic expression conditions (Sakai and Halloran, 2006). *sema3d* indeed appears to be expressed by a subset of cells at the anterior diencephalic midline (Barresi et al., 2005), cells that likely co-express *slit1a* and *vasnb*. Glial scaffolds that are associated to early embryonic commissures share the character of "substrate", helping axons to correctly navigate a complex environment. In his description of the glial knot, Silver (1984) proposed that the reorientation induced on retinal axons by these cells could derive from a combination of attraction and repulsion at the molecular level. In the same way, cellular barricades described in other work all are associated with dramatic changes in the directionality of axonal fibers (Navascués et al., 1987). From this point of view, we observe that Vasna and Vasnb mark specific regions of the retinal axon pathway where axons turn with respect to the body axes. In conclusion, we find that our data highlight a putative role for the glial knot in retinal axon midline crossing, based on the fact that the tissue primarily contacted by retinal axons at the zebrafish midline is made of Vasnb-positive cells.

Divergence in midline crossing strategies of zebrafish and rodent retinal axons

Although the genetic programs to generate RGCs and ventral diencephalic cellular fates are mostly unaltered between zebrafish and rodents, the most striking difference in these animals is the type of connectivity displayed by the retinal projection. This can be seen as the consequence of molecular and/or cellular diversification, although the functional drive to generate such variability has not been clearly investigated. When considering the genetic program controlling ipsilaterality in the rodent visual system, its critical components are not found expressed during the development of the zebrafish retinal projection. This is the case for example of Zic2, the master transcription factor that both directly and indirectly induces EphB1 expression in a subset of RGCs. Whereas in mouse Zic2 controls the levels of Islet-2, eliminating it in ventrotemporal RGCs, Islet-2 (*isl2b*) is uniformly expressed in all differentiated RGCs in zebrafish, indicating the absence of dedicated guidance programs. Similarly, Ephrin-B molecules – the main mediator of ipsilateral axons repulsion from the rodent midline – are not expressed by zebrafish chiasm cells (Nakagawa et al., 2000). Sema3d and Sema3e are the only midline factors identified so far to have a role in controlling midline crossing of zebrafish retinal axons (Sakai and Halloran, 2006; Dell et al., 2013). One striking feature of *sema3d* is that phenotypes deriving from its depletion and ectopic expression are similar. For this reason, it has been difficult to attribute the character of attractive or repulsive cue to it. It is to note that the role of orthologous molecules in rodents appears quite different: class 3 Semaphorins have been subject to analysis and found not to be expressed at the murine midline (Erskine et al., 2011). Instead, Sema6d repels retinal axons at the mouse chiasm. Exposure to local Nr-CAM and Plexin-A1 cues, however, inverts the sign of Sema6D function, transforming it into a growth-promoting factor (Kuwajima et al., 2012). This evidence clarifies the dynamic role of Sema6D at the midline and may provide a similar explanation for the controversial role of Sema3d in zebrafish. Erskine et al. found that *Nrp1* mouse mutants show an

increase in the ipsilateral component of the retinal projection, suggesting that Nrp1 functions as receptor for signals controlling midline crossing. Nrp1 canonical ligands are class 3 Semaphorins and VEGF164, but only the latter was found to signal through Nrp1 as part of a chemoattractive system (Erskine et al., 2011). Later work from Jonathan Raper and colleagues indicated that Nrp1a may function as receptor for Sema3d/Sema3e in zebrafish. This conclusion is based on knockdown experiments detecting ectopic ipsilateral neurites, similarly to phenotypes produced by *sema3d* or *sema3e* morpholinos. However, a *nrp1a* mutant allele fails to recapitulate the knockdown condition for this gene (Dell et al., 2013). A potential involvement of Nrp1a in transducing midline-derived VEGF signals has not been investigated. In conclusion, numerous pieces of evidence indicate the presence of different midline crossing signalling systems in zebrafish and mouse. If molecules are certainly the direct driver of guidance, however, the cellular architecture of axon pathways constitutes the blueprint along which molecules are distributed and therefore contributes a great deal to stereotypical axon migration. In this respect, we report data suggestive of a conserved structure (the glial knot identified in chick and mouse thus far) which correlates with the development of the contralateral retinal projection in different animals. In contrast to the knot, a radial glia territory, characterized by wide-bore extracellular spaces, appears to be selectively associated with the early ipsilateral projection in mouse (Silver, 1984). In addition, a specific subset of midline radial glia is responsible for the redirection of EphB1-positive axons to the ipsilateral optic tract (Petros et al., 2008). Similarly, pioneer retinal growth cones grow in apposition to endfeet of neuroepithelial cells in the chicken visual system. This pathway is marked by NCAM and has been therefore thought to constitute a preformed adhesive pathway for axon growth (Silver and Rutishauser, 1984). Extracellular spaces formed by neuroepithelial processes arranged perpendicularly to the pial surface undergo variations in organization during early embryonic development of the chick. Initially they appear regularly distributed, to then become wider and irregular,

before shrinking and disappearing, being replaced by primitive interfascicular laminar glia (Navascués et al., 1987). Analyses of the zebrafish diencephalic floor did not highlight the presence of radial glia at the stage of optic chiasm formation. GFAP-positive processes appear to remain associated to POC axons and form the interface between retinal and POC axons at 48 hpf, 12 hours after chiasm establishment (Marcus and Easter, 1995). We attempted at recording signal from a *nestin:GFP* reporter in the 36 hpf and 48 hpf zebrafish chiasm, but could not observe positive cells. Collectively these data indicate that the presence of cells belonging to midline radial glia populations might correlate with the appearance of ipsilateral projections in different animals. Whereas rodents display permanent ipsilateral retinal projections, in chick ipsilateral neurites are transient and are completely removed by day 15 of incubation (Thanos and Bonhoeffer, 1984), raising the possibility that their development relates to the temporary existence of extracellular spaces permissive for growth. Interestingly, such palisade of radial neuroepithelial processes has not yet been described in zebrafish, where all retinal axons cross the midline.

Chromobodies as a complementary method to investigate endogenous protein dynamics

In a parallel project carried out, we examined whether chromobodies are reagents that could be transposed for future use in living animal models. The chromobody technique is very attractive for adaptation to developmental biology, because it promises very limited interference with the system in analysis, together with the possibility of tracing endogenous proteins in an intact, developing organism. Chromobodies are selected for live imaging applications, implying that (1) their expression must be tolerated in cultured cells, to allow for long-term data collection; (2) the interaction to the antigen must be rapid and reversible, which is empirically considered the reason why no adverse effects are detected as a consequence of chromobody expression (Rothbauer et al., 2006; Kaiser et al., 2014). In order to characterize the antigen binding rates displayed

by Actin-CB and PCNA-CB, we performed fluorescence recovery after photobleaching (FRAP) experiments. These data show that, not only chromobody fluorescence recovers faster than in the case of GFP-tagged Beta-actin or PCNA, but also that the localization of chromobodies to target structures (as shown in the prebleaching condition), is immediately recapitulated after bleaching (Figure 27). A simple explanation for these observations is that chromobodies are highly diffusible molecules and their on- and off-rate, when considering their interaction to antigens, are both extremely elevated (Panza et al., accepted). As a consequence, no background can be detected in our cell culture experiments. Interestingly, the dynamics of Actin and PCNA appear to be slower, further contributing to the ability of chromobodies to recapitulate the localization shifts of these structures with high fidelity. The absence of functional interference exerted by these molecules, although they bind to antigens with critical roles in maintaining cellular homeostasis, is also suggested by our ability to follow detailed cytoskeletal remodelling after treatment of chromobody-expressing HeLa cells with drugs inhibiting F-Actin polymerization (Figure 28A). In addition, we could visualize PCNA localization dynamics during cell cycle progression (Figure 28B). These data are in agreement with previously published studies using the two chromobodies (Burgess et al., 2012; Rocchetti et al., 2014; Akopyan et al., 2014; Kaiser et al., 2014).

Live imaging data collected using both heat-shock and *UAS* transgenes indicate that Actin- and PCNA-directed chromobodies are advantageous in zebrafish. First, counterstains for F-Actin (using Phalloidin) and endogenous PCNA (with anti-PCNA antibodies) show that Actin-CB and PCNA-CB correctly recognize their antigens' orthologs, although they have been selected to trace human proteins. PCNA-CB performed similarly when compared to the current state-of-the-art of PCNA tracing in zebrafish, which relies on the exogenous expression of human PCNA-GFP (Leung et al., 2011). Second, we successfully followed Actin dynamics in migrating cells (pLLP) and dendritic xanthophores, and could describe the appearance and reorganization of nuclear granules associated with DNA

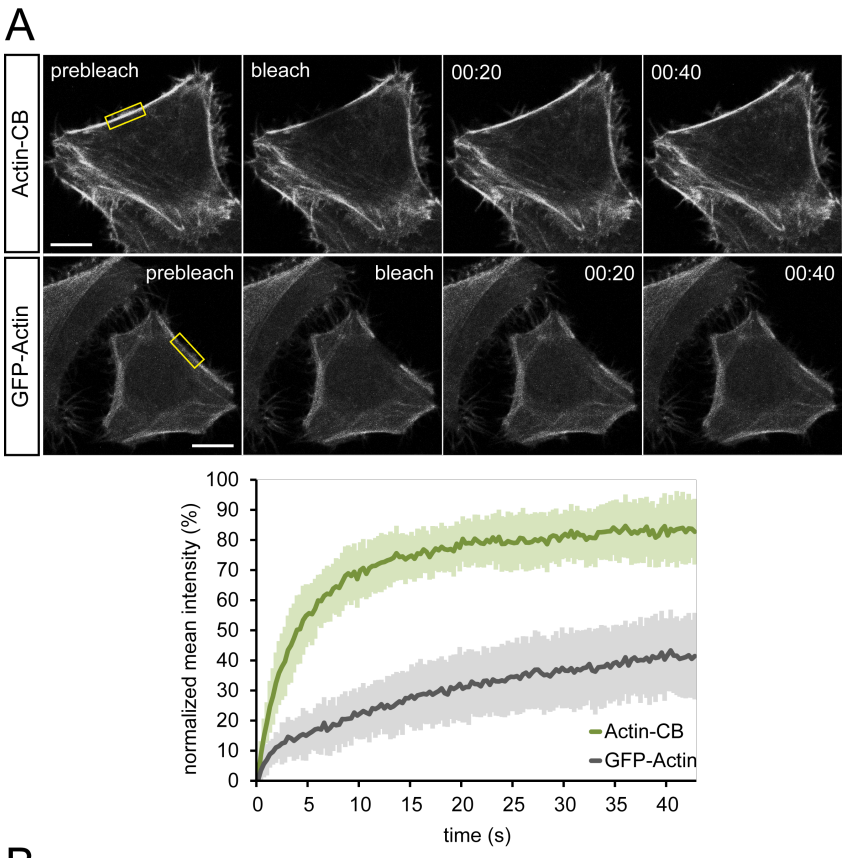
A
Actin-CB
GFP-Actin
prebleach
bleach
00:20
00:40
normalized mean intensity (%)
time (s)
Actin-CB
GFP-Actin
B
PCNA-CB
GFP-PCNA
PCNA-CB
GFP-PCNA

replication forks in neural progenitors during S phase. Collectively, these results indicate that the generated visualization tools can be applied to different tissues and different developmental stages of the zebrafish. Third, building on our FRAP data, indicating rapid dissociation rates, we report multiple lines of evidence supporting our statement of negligible functional interference: (1) Embryos from at least eight independent transgenic integration events, heat-shocked or crossed to three different *gal4* driver lines do not display morphological defects or overt phenotypes in cell proliferation or survival. All these animals could be raised to adulthood. (2) The directionality of migrating pLLP cells is unaffected after ubiquitous chromobody expression, despite any interference with Actin dynamics in leader cells determines clear defects during the advancement of the primordium (Xu et al., 2014). (3) Despite the elevated transactivation level in the dorsal midbrain region of *wnt1:gal4;UAS:PCNA-CB* embryos from 16 hpf, throughout embryonic development, and possibly persisting to adult stages (Volkmann et al., 2010), we did not observe morphological abnormalities. Specifically, we could observe that cell cycle progression was unaffected. During the past two years, targeted genome editing methods have reached widespread use and efficiencies that render them popular. Knock-in of fluorescent tags, however, remains a specialized application still in need of optimization in many model organisms, although it has already been demonstrated (Dickinson et al., 2013). Despite the ease of using modern

Figure 27 ***(preceding page).*** The interaction between chromobodies and their antigens is transient

(A) FRAP experiments on cells transiently expressing either Actin-CB (top row) or GFP-Actin (bottom row) shows faster recovery of the fluorescent signal in chromobody-expressing HeLa cells ($t_{1/2}$= 3.83 s, graph). Scale bars: 10 µm. Timestamps: min:s. Graph: quantitation of FRAP data showing mean curves, n = 10. Error bars: s.d. (B) HeLa cells transiently expressing PCNA-CB (top row) show faster recovery of the fluorescent signal ($t_{1/2}$= 1.81 s, graph), compared to GFP-PCNA (bottom row). Scale bars: 10 µm. Timestamps: min:s. Graph: mean curves of FRAP measurements, n = 10. Error bars: s.d.

In both cases, the quantification indicates transient binding between chromobodies and their target antigens.

gene editing tools, however, analyses of tagged or overexpressed proteins often fail to recapitulate endogenous protein localization and dynamics (Huh et al., 2003; Swulius and Jensen, 2012; Khmelinskii et al., 2012). Large tags frequently contribute to mask functional epitopes or interaction surfaces and introduce a tendency to multimerize. In addition, expression of tagged proteins from additional gene copies is likely to perturb the level at which these proteins are present, thereby introducing artifactual behaviours. Guidelines to conduct protein localization studies encourage the collection and comparison of multiple datasets obtained using different techniques, including end-point immunostainings and live imaging of tagged proteins (Schnell et al., 2012). We introduce new reagents addressed primarily to live imaging applications, allowing the tracing of specific endogenous proteins in living, intact vertebrates. This technique is complementary to standard methods of protein detection in animal tissues. However, our data show that chromobodies are promising tools for their reversible binding to target antigens, which determines limited functional interference with cellular processes, even when central for cell proliferation and survival.

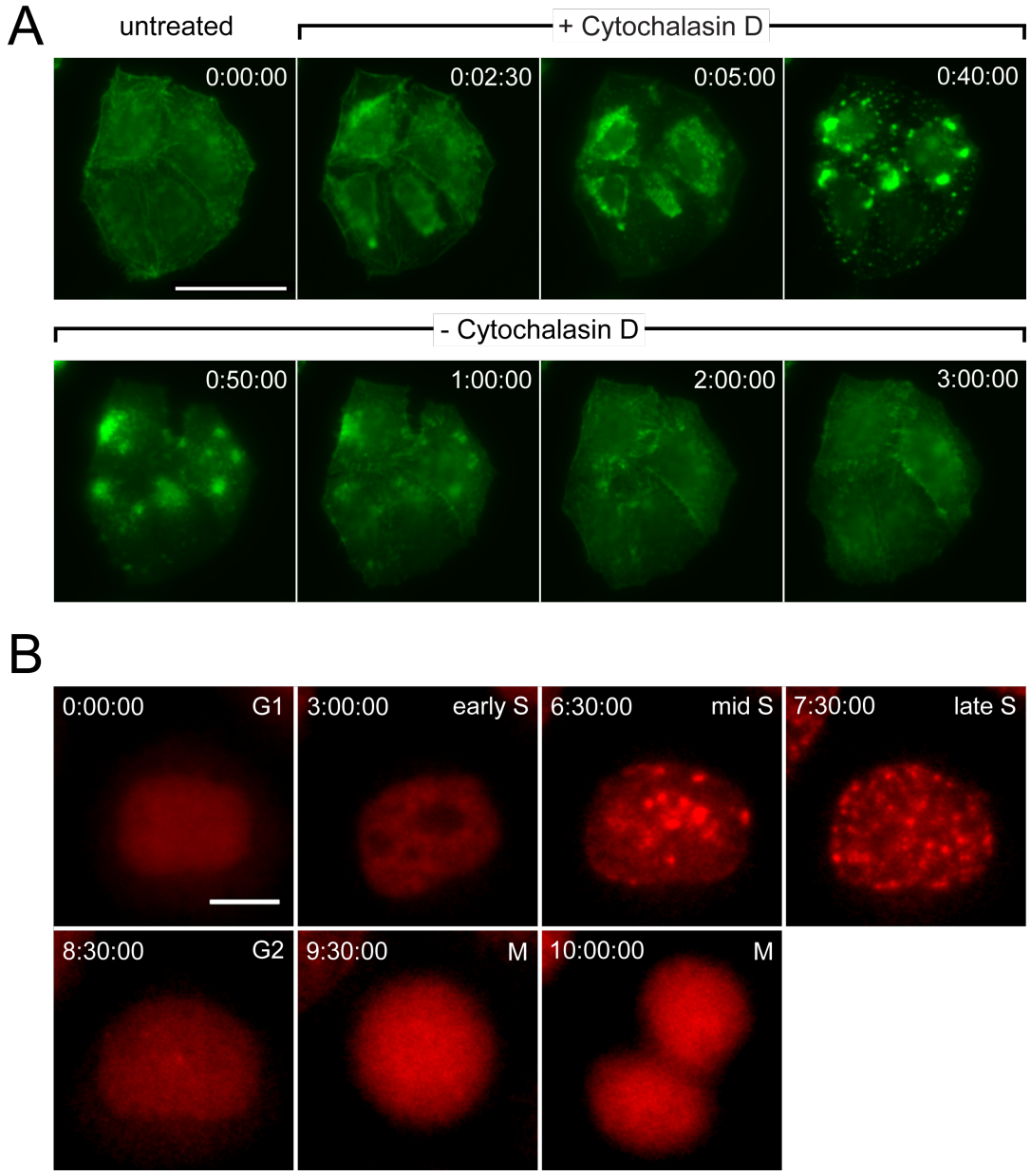

Figure 28. Actin-CB and PCNA-CB trace dynamic behaviours of intracellular structures

(A) HeLa cells stably expressing Actin-CB were incubated for 40 min in medium containing 2 µM Cytochalasin D, a compound that inhibits Actin polymerization. During treatment and recovery (180 min), the cells were imaged to record drug-induced reorganization of cellular Actin. Scale bar: 50 µm. Timestamps: h:min:s. (B) PCNA-CB localization, as revealed by PCNA-CB stably expressed by HeLa cells, is shown as evenly distributed throughout the nucleus in G1. Over time, fluorescent foci redistribute to sites of DNA replication (S phase) and disappear in G2, before the cell undergoes mitosis. Scale bar: 10 µm. Timestamps: h:min:s.

Materials and methods

Zebrafish animal maintenance

All zebrafish experiments were performed in accordance with the guidelines of the Max Planck Society and approved by the Regierungspräsidium Tübingen, Baden-Württemberg, Germany (Aktenzeichen: 35/9185.46). Zebrafish were bred and reared as described in Nüsslein-Volhard and Dahm (2002). Briefly, embryos were raised in E3 medium (5 mM NaCl, 0.17 mM KCl, 0.33 mM $CaCl_2$, 0.33 mM $MgSO_4$, 10^{-5}% methylene blue in ddH_2O) at 28.5°C at a density of 60 individuals per petri dish (about 30 ml) for the first 5 days of development. Larvae and fish were maintained on a 14-hour light/10-hour dark cycle. The following zebrafish strains were used: wild-type Tübingen, *islr2*^{sa82}and *vasnb*^{sa6027} (Zebrafish Mutation Project, Wellcome Trust Sanger Institute, Hinxton, UK), Tg(*-17.6isl2b:GFP*)^{zc7} (Pittman et al., 2008), *Tg(gfap:GFP)*^{mi2001} (Bernardos and Raymond, 2006), *TgBAC(gfap:gfap-GFP)* and *Tg(-3.9nes:GFP)*^{zf168} (Lam et al., 2009), *Tg(hsp70l:Actin-CB,cmlc2:GFP)*, *Tg(hsp70l:PCNA-CB,cmlc2:GFP)*, *Tg(UAS:Actin-CB,crybb:eCFP)*, *Tg(UAS:PCNA-CB,crybb:eCFP)* (this work), *TgBAC(csf1ra:Gal4-VP16)*^{i186} and *Tg(UAS-E1b:NTR-mCherry)*^{i149} (Gray et al., 2011), *Tg(-6.6wnt1:Gal4-VP16-6.7wnt1,14xUAS-E1b:EGFP)*^{tg2229} (Volkmann et al., 2010).

Embryological techniques

In order to ensure the transparency of the embryos and larvae analysed, the E3 medium was supplemented with 0.003% 1-phenyl 2-thiourea (PTU, Sigma-Aldrich P7629), a chemical inhibitor of Tyrosinase, from about 8 hpf.
Embryos destined to be raised to adulthood or sent to other labs

were disinfected by submersion for 5 min in bleaching solution (380 µl/L 12% NaClO in tap water, Carl Roth 9062.3), followed by 5 min in washing solution (tap water) and repeated twice. After bleaching, 10 µl Pronase (30 mg/ml in E2, Roche 11459643001) were added to each petri dish to facilitate hatching. The bleaching treatment was performed during the second day of development.
Embryos and larvae were anesthetized using dilutions of 0.4% ethyl 3-aminobenzoate methanesulfonate salt (MESAB, Sigma-Aldrich A5040). Prior to fixation, embryos were dechorionated manually using forceps or by Pronase treatment (100 µl per petri dish) for about 1-1.5 h. Embryos and larvae were fixed in 4% formaldehyde (Thermo Scientific 28908) in PBS overnight at 4°C, unless specified otherwise.
Heat-shock induction of transgenic expression was performed by transferring embryos in E3 medium pre-heated to 39 °C. Petri dishes were then let float on water in a bath set to 39°C for 1 h. Subsequently, embryos were transferred to 28.5°C medium and let recover in an air incubator at the same temperature. Animals were sorted by normal morphology and transgenic expression (fluorescence level) prior to analysis.

Genotyping of zebrafish individuals

Preparation of genomic DNA, from both tailclips and fixed embryos or larvae, was performed according to Meeker et al. (2007).
Genotyping of embryos or fish was performed by PCR-amplification from genomic DNA using the JumpStart REDTaq DNA polymerase (Sigma-Aldrich P1107):

Genomic DNA	10x	1 µl
Forward primer	10 µM	0.3 µl
Reverse primer	10 µM	0.3 µl
REDTaq ReadyMix		5 µl
ddH_2O		3.4 µl
Total volume		10 µl

Amplification program		
(1)	94°C	3 min
(2)	94°C	30 s
(3)	60°C (-0.5°C/s)	30 s
(4)	72°C	30 s
(5)	go to (2)	x9
(6)	94°C	30 s
(7)	56°C	30 s
(8)	72 °C	30 s
(9)	go to (6)	x31
(10)	72°C	1 min

cDNA preparation

Total RNA from embryos was isolated following the TRIzol Reagent manual (Invitrogen 15596-018). cDNA was synthesized using Cloned AMV Reverse Transcriptase (Invitrogen 12328-019) according to the manufacturer's instructions.

Amplification from cDNA

Selected expressed genes were amplified and cloned from cDNA, especially to generate expression plasmids for the AVEXIS screen. For this purpose, a forward primer including a NotI site and a Kozak sequence, and a reverse primer containing an AscI restriction site were used. Upon restriction, amplicons encompassing proteins' extracellular domain were ligated into CD4d3+4-bio (`http://www.addgene.org/32402/`) or CD4d3+4-blac (`http://www.addgene.org/32403/`) plasmids . PCR-amplifications were carried out using the KOD Hot Start DNA Polymerase (Merck Millipore 71086-3) as follows:

cDNA		1 µl
Forward primer	10 µM	1.5 µl
Reverse primer	10 µM	1.5 µl
10x KOD buffer		5 µl
dNTPs	2 mM	5 µl
$MgSO_4$	25 mM	3 µl
KOD polymerase		1 µl
ddH_2O		32 µl
Total volume		50 µl

Amplification program

(1)	95°C	2 min
(2)	95°C	30 s
(3)	70°C	30 s
(4)	go to (2)	x5
(5)	95°C	30 s
(6)	66°C	30 s
(7)	70°C	20 s/kb
(8)	go to (5)	x5
(9)	95°C	30 s
(10)	59 °C	30 s
(11)	70°C	20 s/kb
(12)	go to (9)	x30
(13)	70°C	10 min

Cloning

DNA fragments were purified by gel elution or column filtering using either Wizard SV Gel and PCR Clean-Up System (Promega A9282) or QIAquick PCR Purification Kit (QIAGEN 28106). Cloning reactions were performed by using the Dual Promoter TOPO TA Cloning Kit (Invitrogen 45-0640), the Zero Blunt TOPO PCR Cloning Kit (Invitrogen 45-0245) or the pGEM-T Easy Vector System (Promega A1360) according to the manufacturer's instructions. DNA restrictions and ligations were performed using NEB or Thermo Scientific enzymes and the NEB Quick Ligation Kit (NEB M2200S), following the manifacturer's instructions.

Transformation

Chemically competent One-Shot TOP10 *E. coli* cells (Invitrogen C4040-03) were thawed on ice for few minutes. 1-4 µl of plasmid solution were added and gently shaken. The bacteria were incubated on ice for 30 min in order to allow the plasmid to associate to the cell wall. Vials were then heat-shocked for 1 min at 42°C and immediately transferred to ice for few minutes. After the addition

of 250 µl SOC medium, the bacteria were incubated at 37°C on a thermoshaker (600 rpm) for 30 min to 1 h. Generally 1:10 dilutions were plated on LB-agar additioned with the appropriate antibiotics. Colonies were picked after overnight growth in a 37°C air incubator and inoculated in LB medium with antibiotics.

Plasmid preparation

Plasmids were harvested from bacterial cultures and purified using the QIAprep Spin Miniprep Kit (QIAGEN 27106), QIAGEN Plasmid *Plus* Midi Kit (QIAGEN 12945) or QIAGEN Plasmid Maxi Kit (QIAGEN 12165) following the manifacturer's instructions.

Sequencing

Sequencing reactions were set up as follows, using the BigDye Terminator Sequencing Kit v3.1 (Applied Biosystems). The sequencing buffer composition is: 400 mM Tris HCl pH 9, 10 mM $MgCl_2$.

DNA	200 ng/µl	1 µl
Sequencing primer	3 µM	1 µl
Sequencing buffer	5x	1.9 µl
BigDye Terminator		0.5 µl
ddH_2O		5.6 µl
Total volume		10 µl

Thermocycler program

(1)	96°C	20 s
(2)	50°C	10 s
(3)	60°C	4 min
(4)	go to (1)	x30

RNA preparation

mRNA for injections was synthesized using the mMESSAGE mMACHINE Kit (Ambion AM1340 or AM1344). RNA for *in situ* hybridization probes was transcribed using the MEGAscript Kit (Ambion AM1330 or AM1334). RNA molecules were column-purified following the instructions of the MEGAclear Kit (Ambion 1908).

In situ hybridization

Single mRNA detection by whole-mount *in situ* hybridization was carried out according to Filippi et al. (2007). The two-colour flu-

orescent *in situ* hybridization protocol has been described in Clay and Ramakrishnan (2005).

Immunohistochemistry

Staged animals were manually freed from chorions if necessary and fixed in 4% formaldehyde overnight at 4°C. The samples were washed in PBS and dehydrated through a methanol series. The embryos were stored in 100% methanol at -20°C until used. All embryos were permeabilized in cold acetone at -20°C and washed again in 100% methanol. After rehydration by scalar washes in methanol dilutions, embryos were digested using Proteinase K (10 µg/ml, Merck 1245680100) and subsequently fixed in 4% formaldehyde for 20 min at room temperature. A blocking step with 10% normal goat serum (NGS, Gibco PCN5000) was carried out for 5-6 h at room temperature. Primary antibodies were added at a 1:1000 dilution in 10% NGS overnight at 4°C. The samples were then washed in PBST (PBS, 0.1% Triton X-100, Sigma-Aldrich T8787) and incubated with secondary antibodies (1:250 in 1% NGS) overnight at 4°C, protected from light. After several PBST washes, the samples were post-fixed and brought in glycerol through scalar washes.

Whole-eye fills by lipophilic dye injection

5 dpf larvae were fixed in 4% formaldehyde for two days at 4°C on a turning wheel. Larvae were extensively washed in ddH_2O at room temperature and injected on a standard agarose injection plate, with larvae fitted in the grooves (Nüsslein-Volhard and Dahm, 2002). DiI, DiO or DiD (Molecular Probes V-22885, V-22886, V-22887) were pressure-injected in the RGC layer until filled. Injected samples were kept in water at 22°C or RT, overnight in the dark to let the dyes diffuse. Jaws were surgically removed and larvae were mounted in 3% methylcellulose (Sigma-Aldrich M0387) in E2, between two coverslips. Then the retinal projection was imaged at 25x magnification from both the dorsal and the ventral side. For earlier time points, embryos and larvae were fixed in 4% formaldehyde at room

temperature for 1 h and then overnight at 4°C (Hutson and Chien, 2002).

AVEXIS

Protein interaction screening was performed according to Bushell et al. (2008).

Rabbit antisera production

Vasna and Vasnb ectodomains cloned in CD4d3+4-His vectors were expressed in HEK293-6E cells as secreted proteins. Supernatants were collected and purified using HisTrap HP columns (GE Healthcare 17-5247-01). Rabbits were first immunized by injection of a mixture containing 1 ml antigen (0.5 mg/ml) and 1 ml complete Freund's adjuvant (Sigma-Aldrich F5881). At 14 days intervals, boost injections were performed. 1 ml antigen (0.2 mg/ml) mixed with 1 ml incomplete Freund's adjuvant (Sigma-Aldrich F5506) was used for the first boost. Two additional boosts using 1 ml antigen (0.1 mg/ml) mixed with 1 ml incomplete Freund's adjuvant were performed. All injections were directed subcutaneously and intramuscularly. 50 ml bleeds were drawn starting from 1 week after the last boost. These antibodies were used as crude antisera on fixed zebrafish embryos.

Generation of targeted knockout lines

TALENs constructs were purchased from Cellectis Bioresearch. mRNA was prepared as indicated and injected in one-cell stage embryos at different dilutions averaging 100-150 ng/µl for each left or right TALEN. Injected embryos were grown to adulthood. Progenies of incrosses were genotyped to isolate founder animal pairs, from which single alleles were subsequently obtained by outcrossing.

Generation of transgenic fish lines

Actin-CB and PCNA-CB were cloned into pDONR221 (Invitrogen) to generate Gateway-compatible Middle Entry (pME) plas-

mids. Chromobody pME clones were combined with Tol2kit plasmids (Kwan et al., 2007) p5E-hsp70 (#222), p3E-polyA (#302) and pDEST-Tol2CG2 (#395) to generate *hsp70l:Actin-CB* and *hsp70l:PCNA-CB* constructs. Actin-CB and PCNA-CB pME clones were also combined with p5E-UAS (#327), p3E-polyA (#302) and pDEST-Tol2-crybb:eCFP (a gift from Darren Gilmour, EMBL Heidelberg) to generate *UAS:Actin-CB* and *UAS:PCNA-CB* constructs. Gateway recombinations were performed according to the Tol2kit instructions (`http://tol2kit.genetics.utah.edu/`). The final constructs were coinjected at 10 ng/µl together with 30 ng/µl Tol2 transposase mRNA. 1-2 nl of nucleic acid solution was injected into one-cell stage embryos. Injected embryos sorted for the expression of the transgenesis marker (green heart for heat-shock transgenes and blue lens for *UAS* transgenes) were raised. Adult founders were identified during outcrosses and their transgenic progenies were raised independently.

Imaging

Images were acquired on a Zeiss LSM 510 Meta confocal microscope using a 25x glycerol-immersed objective. Injected larvae were mounted in 3% methylcellulose, jaws were surgically removed. Collected scans were processed using Fiji (Schindelin et al., 2012), by generating a maximum intensity projection of the stacks, unless specified otherwise. Chromobody-transgenic embryos at different stages were manually dechorionated and mounted on glass-bottom petri dishes (MatTek P35G-1.5-14-C) using 0.8% low-melting point agarose (NuSieve GTG Agarose, Lonza 50080). During imaging sessions, they were submerged in E2 medium supplemented with PTU (0.003%) to inhibit melanogenesis and anesthetic solution. A Zeiss LSM 780 NLO inverted confocal microscope was used to acquire scans. For wound induction, an 800 nm wavelength MaiTai laser was used at 100% intensity with a 0.41 µs pixel dwell time. Data processing and analysis were carried out using Fiji and ZEN 2010 (Zeiss) software.

Histological methods

Fish larvae were fixed in 100 mM PO_4 buffer pH 7.2 containing 4% formaldehyde and 2.5% glutaraldehyde at room temperature for 2 hours. Further fixation was carried out overnight at 4°C. The samples were post-fixed with 0.1% osmium tetroxide on ice for one hour and then stained with 1% aqueous uranyl acetate at 4°C for one hour in the dark. The samples were dehydrated in a graded series of ethanol/water concentrations; subsequently, a graded series of epon/araldite resin (EMS Araldite 502/Embed 812 Kit) in propylene oxide was used for embedding.
3 µm semi thin transverse sections were stained with Toluidine Blue and embedded in Epon before imaging at 16x magnification on a Zeiss Axioplan widefield microscope equipped with a F-View camera (Soft Imaging Systems).
50-70 nm ultra thin sections were taken along the transverse axis of the fish larva using a Leica Ultracut UCT microtome. Specimens were examined in a FEI Tecnai G2 Spirit transmission electron microscope operating at 120 kV. Images were taken with a Gatan Ultrascan 4000 camera at maximum resolution using the manufacturer's software.

Antibodies

Primary antibodies	Source	Working dilution
rabbit polyclonal anti-Vasna, crude serum	this work	1:1000
rabbit polyclonal anti-Vasnb, crude serum	this work	1:1000
rabbit polyclonal anti-PCNA	GeneTex GTX124496	1:200
mouse monoclonal anti-acetylated Tubulin	Sigma-Aldrich T6793	1:1000

Secondary antibodies	Source	Working dilution
goat polyclonal anti-rabbit IgG Alexa488	Molecular Probes A-11008	1:250-1:400
goat polyclonal anti-rabbit IgG Cy3	Jackson ImmunoResearch 111-165-003	1:250
goat polyclonal anti-rabbit IgG Cy5	Jackson ImmunoResearch 111-175-144	1:250
goat polyclonal anti-mouse IgG Alexa 488	Molecular Probes A-11029	1:250
goat polyclonal anti-mouse IgG Alexa 647	Molecular Probes A-21236	1:250

Others	Source	Working dilution
Rhodamine Phalloidin	Molecular Probes R415	1:500

Table 1. List of immunoreagents used in this study

Appendix

Table 2. Type-I transmembrane LRR proteins in zebrafish

Mm gene	**Dr gene**	**RGC expression**	**First stage of expression**	**% Identity to query gene**	**Orthology [0 low, 1 high]**
Ntrk1	*ntrk1*	n		51	1
Ntrk2	*ntrk2b*	y	2 dpf	61	1
	ntrk2a	y	6 dpf	62	1
Ntrk3	*ntrk3a*	y	3 dpf	64	1
	ntrk3b	y	6 dpf	58	1
Lrrn1	*lrrn1*	n		80	1
	sc:d0413	y	2 dpf		
Lrrn2	*lrrn2*			53	1
Lrrn3	*lrrn3*	y	2 dpf	57	1
Lingo1	*lingo1a*	y	5 dpf	81	1
	lingo1b	y	2 dpf	73	1
Lingo2	*lingo2a*	n		63	1
	lingo2b			51	1
Lingo3	*lingo3a*	n		63	1
	lingo3b			64	1
Lingo4	*lingo4a*			41	1
	lingo4b			42	1
Lrrc4	*lrrc4.1*	y	2 dpf	72	1
	lrrc4.2			71	1
Lrrc4b	*lrrc4ba*	n		67	1
	lrrc4bb			66	1
Lrrc4c	*lrrc4c*	n		72	1
Lrig1	*lrig1*	n		57	1
Lrig2	*lrig2*	n		58	1

Lrig3	*lrig3*	n		50	1
Islr2	*islr2*	y	36 hpf	45	0
Lrit1	*lrit1b*	n		46	1
	lrit1a			48	1
Lrit2	*lrit2*	n		43	1
Lrit3	*lrit3b*	n		28	1
	lrit3a			44	1
Lrrc24	*lrrc24*	n		53	0
	lrrc24(2)			53	0
Amigo1	*amigo1*	y	5 dpf	54	1
Amigo2					
Amigo3	*CR385022.1*			31	1
	amigo3			38	1
Lrfn1	*lrfn1/mb21d2b*	n		54	1
Lrfn2	*lrfn2b*			64	1
	lrfn2a	n		67	1
Lrfn3	*lrfn3*			54	0
Lrfn4	*lrfn4b*			59	0
	lrfn4a			58	0
Lrfn5	*lrfn5b*	y	2 dpf	60	1
	lrfn5a	n		71	1
Flrt1	*flrt1b*	n		59	1
	flrt1a	y	2 dpf	60	1
Flrt2	*flrt2*	n		63	1
	flrt2(2)			61	1
Flrt3	*flrt3*	n		73	1
Elfn1	*elfn1b*	n		59	1
	elfn1a			60	1
Elfn2	*elfn2a*	n		60	1
	elfn2b			58	1
Lrrn4	*FP245511.1*			9	1
	CU984579.1			9	1
Lrrtm1	*lrrtm1*	y	4 dpf	66	1
Lrrtm2	*lrrtm2*	y	4 dpf	65	1
	lrrtm2(2?)			65	1

Lrrtm3					
Lrrtm4	*lrrtm4l1*	y	2 dpf	49	1
	lrrtm4			58	1
	lrrtm4(2)			60	1
	lrrtm4l2	y	4 dpf	49	1
Lrtm1	*lrtm1*			40	1
Lrtm2	*lrtm2*	y	2 dpf	57	1
Slitrk1	*slitrk1*	y	3 dpf	70	1
Slitrk2	*slitrk2*	y	3 dpf	73	1
Slitrk3	*slitrk3b*	y	3 dpf	60	1
	slitrk3a	n		68	1
Slitrk4	*slitrk4*	n		73	1
Slitrk5	*slitrk5*	y	3 dpf	63	0
	slitrk5b	n		51	0
Slitrk6	*slitrk6*	y	3 dpf	53	1
Tpbg	*tpbgb*	n		38	0
	tpbga	n			
	tpbgl				
Gm4980	*waif2*			33	1
Lrrc3	*lrrc3*	n		56	1
Lrrc3b	*lrrc3b*	n		65	1
Tlr1	*tlr1*	n		35	1
Tlr2	*tlr2*	n		40	1
Tlr3	*tlr3*	n		47	1
Tlr4	*tlr4ba*	n		35	1
	tlr4al			37	1
	tlr4bb	n		35	1
Tlr5	*tlr5a*	n		38	1
	tlr5b	n		39	1
Tlr6	*tlr1*	n		34	1
Tlr7	*tlr7*	n		54	1
Tlr8	*tlr8(3)*			41	1
	tlr8b	n		30	1
	tlr8a	n		41	1
Tlr9	*tlr9*	n		36	0

Tlr11	*si:dkey-193n17.5*		7	1
	tlr19	n	18	1
	tlr20a	n	7	1
	si:dkey-100n23.2		16	1
	si:dkey-193n17.7		7	1
	tlr20f	n	7	1
	tlr19(2?)		16	1
	tlr20al		14	1
Tlr12	*si:dkey-193n17.5*		8	1
	tlr19	n	20	1
	tlr20a	n	8	1
	si:dkey-100n23.2		18	1
	si:dkey-193n17.7		7	1
	tlr20f	n	8	1
	tlr19(2?)		19	1
	tlr20al		15	1
Tlr13	*tlr21*	n	31	0
Cd180	*cd180(2)*		37	1
	cd180		37	1
Gp5	*gp5*		27	1
Lrrc15	*lrrc15*	n	33	1
Tril				
Lrrc32	*lrrc32*		38	1
Nrros	*nrros*	n	35	1
Vasn	*vasna*	n	39	1
	vasnb	n	39	1
Gp1ba	*CU896563.2*		12	0
Gp1bb	*gp1bb*		37	0
Gp9	*gp9*		30	0

Lrrc19				
Lrrc25				
Lrrc26				
Lrrc38	*lrrc38*	n	48	1
	lrrc38(2)		51	1
Lrrc52	*lrrc52*		36	0
	lrrc52(2)		32	0
Lrrc55				
Lrrc66	*lrrc66*		5	1

Contributions

TILLING mutant fish strains were kindly provided by the Zebrafish Mutation Project (Wellcome Trust Sanger Institute, Cambridge, UK). AVEXIS interaction data and protein domain screen data were obtained by Dr. Christian Söllner. The identification and preliminary analysis of *islr2* mutant zebrafish larvae was carried out by Dr. Christian Söllner with technical assistance from Hans-Martin Maischein. SPR data were provided by Dr. Gavin Wright (Cell Surface Signalling Laboratory, Wellcome Trust Sanger Institute, Cambridge, UK). Histological sections and electron microscopy on *islr2* mutant larvae were performed by Iris Koch and Dr. Matthias Flötenmeyer (Elektronenmikroskopie, Max-Planck-Institut für Entwicklungsbiologie). *Islr2* knockout mice were provided by Prof. Kenji Mandai (Kobe University, Kobe, Japan) and analysed by Austen Sitko, under the supervision of Prof. Carol Ann Mason (Columbia University, New York, USA). FRAP results on expressed chromobodies and live imaging of HeLa cells were carried out by Julia Maier, in a collaboration with Prof. Dr. Ulrich Rothbauer (NMI and Eberhard Karls Universität Tübingen). All sequencing reactions were finalized by Andrea Belkacemi at the Genomcenter, Max-Planck-Institut für Entwicklungsbiologie, headed by Dr. Christa Lanz. Antibodies were produced following instructions given by Dr. Wolfram Antonin, with the technical assistance of Edith Haug. All imaging sessions were carried out using equipment provided by the Lichtmikroskopie Einrichtung, Max-Planck-Institut für Entwicklungsbiologie, headed by Dr. Christian Liebig. Fish larvae were raised and adult fish were maintained by Mario Pezzuti and Salvatore Giarmana. Transgenic fish lines were shared by Dr. Leanne Godinho

(Technische Universität München), Prof. Dr. Uwe Strähle (Karlsruher Institut für Technologie), Dr. Aristides Arrenberg and Prof. Dr. Wolfgang Driever (Albert-Ludwigs-Universität Freiburg). Plasmids were provided by ChromoTek GmbH, Dr. Darren Gilmour (EMBL Heidelberg) and Dr. Caren Norden (Max-Planck-Institut für molekulare Zellbiologie und Genetik, Dresden). Tol2kit reagents were kindly provided by Prof. Kristen Kwan (University of Utah, Salt Lake City, USA). This work has been carried out thanks to support from Prof. Dr. Christiane Nüsslein-Volhard and was funded by the Max-Planck-Gesellschaft zur Förderung der Wissenschaften and by a ZF-HEALTH grant (project number 242048).

Acknowledgements

I would like to thank Dr. Christian Söllner for the opportunity to work on a challenging project in his research group. I am grateful for his helpfulness and support at all times. I thank Prof. Dr. Christiane Nüsslein-Volhard, who supported me in her Department, and the members of my PhD Advisory Committee: Dr. Gáspár Jékely, Dr. Andrea Wizenmann and Prof. Dr. Ralf J. Sommer. I wish a lot of success to Xuefan Gao, with whom I shared the highs and lows of research during our PhD. I am much indebted to past and present members of the Nüsslein-Volhard lab, who helped me getting started during the initial phases of my work. I am really grateful to anyone who contributed and helped making this work something worth remembering (see Contributions). Finally, my thoughts go to my family, they keep me strong, and to Daniela, she keeps me (in)sane.

Bibliography

Akopyan, K., Silva Cascales, H., Hukasova, E., Saurin, A. T., Müllers, E., Jaiswal, H., Hollman, D. A. A., Kops, G. J. P. L., Medema, R. H., and Lindqvist, A. (2014). Assessing Kinetics from Fixed Cells Reveals Activation of the Mitotic Entry Network at the S/G2 Transition. *Molecular Cell*, 53(5):843–853.

Baier, H., Klostermann, S., Trowe, T., Karlstrom, R., Nusslein-Volhard, C., and Bonhoeffer, F. (1996). Genetic dissection of the retinotectal projection. *Development*, 123(1):415–425.

Bak, M. and Fraser, S. E. (2003). Axon fasciculation and differences in midline kinetics between pioneer and follower axons within commissural fascicles. *Development*, 130(20):4999–5008.

Barresi, M., Hutson, L., Chien, C., and Karlstrom, R. (2005). Hedgehog regulated Slit expression determines commissure and glial cell position in the zebrafish forebrain. *Development*, 132(16):3643–3656.

Bedell, V. M., Wang, Y., Campbell, J. M., Poshusta, T. L., Starker, C. G., Krug Ii, R. G., Tan, W., Penheiter, S. G., Ma, A. C., Leung, A. Y. H., Fahrenkrug, S. C., Carlson, D. F., Voytas, D. F., Clark, K. J., Essner, J. J., and Ekker, S. C. (2012). In vivo genome editing using a high-efficiency TALEN system. *Nature*, 491(7422):114–118.

Berghmans, S., Murphey, R. D., Wienholds, E., Neuberg, D., Kutok, J. L., Fletcher, C. D. M., Morris, J. P., Liu, T. X., Schulte-Merker, S., Kanki, J. P., Plasterk, R., Zon, L. I., and Look, A. T. (2005). tp53 mutant zebrafish develop malignant peripheral nerve sheath tumors. *Proceedings of the National Academy of Sciences of the United States of America*, 102(2):407–412.

Bernardos, R. L. and Raymond, P. A. (2006). GFAP transgenic zebrafish. *Gene Expression Patterns*, 6(8):1007–1013.

Blackshaw, S., Harpavat, S., Trimarchi, J., Cai, L., Huang, H., Kuo, W. P., Weber, G., Lee, K., Fraioli, R. E., Cho, S.-H., Yung, R., Asch, E., Ohno-Machado, L., Wong, W. H., and Cepko, C. L. (2004). Genomic Analysis of Mouse Retinal Development. *PLoS Biol*, 2(9):e247.

Bradford, Y., Conlin, T., Dunn, N., Fashena, D., Frazer, K., Howe, D. G., Knight, J., Mani, P., Martin, R., Moxon, S. A. T., Paddock, H., Pich, C., Ramachandran, S.,

Ruef, B. J., Ruzicka, L., Schaper, H. B., Schaper, K., Shao, X., Singer, A., Sprague, J., Sprunger, B., Slyke, C. V., and Westerfield, M. (2011). ZFIN: enhancements and updates to the zebrafish model organism database. *Nucleic Acids Research*, 39(suppl 1):D822–D829.

Burgess, A., Lorca, T., and Castro, A. (2012). Quantitative Live Imaging of Endogenous DNA Replication in Mammalian Cells. *PLoS ONE*, 7(9):e45726.

Burrill, J. and Easter Jr, S. (1994). Development of the retinofugal projections in the embryonic and larval zebrafish (Brachydanio rerio). *The Journal of comparative neurology*, 346(4):583–600.

Burrill, J. and Easter Jr, S. (1995). The first retinal axons and their microenvironment in zebrafish: cryptic pioneers and the pretract. *The Journal of neuroscience*, 15(4):2935–2947.

Bushell, K. M., Sollner, C., Schuster-Boeckler, B., Bateman, A., and Wright, G. J. (2008). Large-scale screening for novel low-affinity extracellular protein interactions. *Genome Research*, 18(4):622–630.

Cade, L., Reyon, D., Hwang, W. Y., Tsai, S. Q., Patel, S., Khayter, C., Joung, J. K., Sander, J. D., Peterson, R. T., and Yeh, J.-R. J. (2012). Highly efficient generation of heritable zebrafish gene mutations using homo- and heterodimeric TALENs. *Nucleic Acids Research*, 40(16):8001–8010.

Charron, F., Stein, E., Jeong, J., McMahon, A. P., and Tessier-Lavigne, M. (2003). The Morphogen Sonic Hedgehog Is an Axonal Chemoattractant that Collaborates with Netrin-1 in Midline Axon Guidance. *Cell*, 113(1):11–23.

Chédotal, A. (2011). Further tales of the midline. *Current Opinion in Neurobiology*, 21(1):68–75.

Chen, L., Yao, J.-h., Zhang, S.-h., Wang, L., Song, H.-d., and Xue, J.-l. (2005). Slit-like 2, a novel zebrafish slit homologue that might involve in zebrafish central neural and vascular morphogenesis. *Biochemical and Biophysical Research Communications*, 336(1):364–371.

Chen, Z., Gore, B. B., Long, H., Ma, L., and Tessier-Lavigne, M. (2008). Alternative Splicing of the Robo3 Axon Guidance Receptor Governs the Midline Switch from Attraction to Repulsion. *Neuron*, 58(3):325–332.

Chiang, C., Litingtung, Y., Lee, E., Young, K. E., Corden, J. L., Westphal, H., and Beachy, P. A. (1996). Cyclopia and defective axial patterning in mice lacking Sonic hedgehog gene function. *Nature*, 383(6599):407–413.

Chitnis, A. B. and Kuwada, J. Y. (1991). Elimination of a brain tract increases errors in pathfinding by follower growth cones in the zebrafish embryo. *Neuron*, 7(2):277–285.

Chung, K.-Y., Leung, K.-M., Lin, L., and Chan, S.-O. (2001). Heparan sulfate proteoglycan expression in the optic chiasm of mouse embryos. *The Journal of Comparative Neurology*, 436(2):236–247.

Chung, K.-Y., Shum, D. K.-Y., and Chan, S.-O. (2000a). Expression of chondroitin sulfate proteoglycans in the chiasm of mouse embryos. *The Journal of Comparative Neurology*, 417(2):153–163.

Chung, K. Y., Taylor, J. S., Shum, D. K., and Chan, S. O. (2000b). Axon routing at the optic chiasm after enzymatic removal of chondroitin sulfate in mouse embryos. *Development*, 127(12):2673–2683.

Clay, H. and Ramakrishnan, L. (2005). Multiplex Fluorescent In Situ Hybridization in Zebrafish Embryos Using Tyramide Signal Amplification. *Zebrafish*, 2(2):105–111.

Conway, C. D., Howe, K. M., Nettleton, N. K., Price, D. J., Mason, J. O., and Pratt, T. (2011). Heparan Sulfate Sugar Modifications Mediate the Functions of Slits and Other Factors Needed for Mouse Forebrain Commissure Development. *The Journal of Neuroscience*, 31(6):1955–1970.

de Wit, J., Hong, W., Luo, L., and Ghosh, A. (2011). Role of Leucine-Rich Repeat Proteins in the Development and Function of Neural Circuits. *Annual Review of Cell and Developmental Biology*, 27(1):697–729.

Dell, A. L., Fried-Cassorla, E., Xu, H., and Raper, J. A. (2013). cAMP-Induced Expression of Neuropilin1 Promotes Retinal Axon Crossing in the Zebrafish Optic Chiasm. *The Journal of Neuroscience*, 33(27):11076–11088.

Dickinson, D. J., Ward, J. D., Reiner, D. J., and Goldstein, B. (2013). Engineering the Caenorhabditis elegans genome using Cas9-triggered homologous recombination. *Nature Methods*, 10(10):1028–1034.

Dolan, J., Walshe, K., Alsbury, S., Hokamp, K., O'Keeffe, S., Okafuji, T., Miller, S. F., Tear, G., and Mitchell, K. J. (2007). The extracellular Leucine-Rich Repeat superfamily; a comparative survey and analysis of evolutionary relationships and expression patterns. *BMC Genomics*, 8(1):320.

D'Souza, J., Hendricks, M., Le Guyader, S., Subburaju, S., Grunewald, B., Scholich, K., and Jesuthasan, S. (2005). Formation of the retinotectal projection requires Esrom, an ortholog of PAM (protein associated with Myc). *Development*, 132(2):247–256.

Erskine, L. and Herrera, E. (2014). Connecting the Retina to the Brain. *ASN Neuro*, 6(6):1759091414562107.

Erskine, L., Reijntjes, S., Pratt, T., Denti, L., Schwarz, Q., Vieira, J. M., Alakakone, B., Shewan, D., and Ruhrberg, C. (2011). VEGF Signaling through Neuropilin 1 Guides Commissural Axon Crossing at the Optic Chiasm. *Neuron*, 70(5):951–965.

Erskine, L., Williams, S. E., Brose, K., Kidd, T., Rachel, R. A., Goodman, C. S., Tessier-Lavigne, M., and Mason, C. A. (2000). Retinal Ganglion Cell Axon Guidance in the Mouse Optic Chiasm: Expression and Function of Robos and Slits. *The Journal of Neuroscience*, 20(13):4975–4982.

Essers, J., Theil, A. F., Baldeyron, C., Cappellen, W. A. v., Houtsmuller, A. B., Kanaar, R., and Vermeulen, W. (2005). Nuclear Dynamics of PCNA in DNA Replication and Repair. *Molecular and Cellular Biology*, 25(21):9350–9359.

Evans, T. A. and Bashaw, G. J. (2010). Axon guidance at the midline: of mice and flies. *Current Opinion in Neurobiology*, 20(1):79–85.

Fadool, J. and Dowling, J. (2008). Zebrafish: A model system for the study of eye genetics. *Progress in Retinal and Eye Research*, 27(1):89–110.

Feldheim, D. A. and O'Leary, D. D. M. (2010). Visual Map Development: Bidirectional Signaling, Bifunctional Guidance Molecules, and Competition. *Cold Spring Harbor Perspectives in Biology*, 2(11):a001768–a001768.

Filippi, A., Durr, K., Ryu, S., Willaredt, M., Holzschuh, J., and Driever, W. (2007). Expression and function of nr4a2, lmx1b, and pitx3 in zebrafish dopaminergic and noradrenergic neuronal development. *BMC Developmental Biology*, 7:135.

Fricke, C., Lee, J.-S., Geiger-Rudolph, S., Bonhoeffer, F., and Chien, C.-B. (2001). astray, a Zebrafish roundabout Homolog Required for Retinal Axon Guidance. *Science*, 292(5516):507–510.

Gejima, R., Okafuji, T., and Tanaka, H. (2006). The LRR and Ig domain-containing membrane protein SST273 is expressed on motoneurons. *Gene Expression Patterns*, 6(3):235–240.

Godement, P., Salaün, J., and Mason, C. A. (1990). Retinal axon pathfinding in the optic chiasm: Divergence of crossed and uncrossed fibers. *Neuron*, 5(2):173–186.

Godement, P., Vanselow, J., Thanos, S., and Bonhoeffer, F. (1987). A study in developing visual systems with a new method of staining neurones and their processes in fixed tissue. *Development*, 101(4):697–713.

Godement, P., Wang, L. C., and Mason, C. A. (1994). Retinal axon divergence in the optic chiasm: dynamics of growth cone behavior at the midline [published erratum appears in J Neurosci 1995 Mar;15(3):following table of contents]. *The Journal of Neuroscience*, 14(11):7024–7039.

Granato, M., Eeden, F. J. v., Schach, U., Trowe, T., Brand, M., Furutani-Seiki, M., Haffter, P., Hammerschmidt, M., Heisenberg, C. P., Jiang, Y. J., Kane, D. A., Kelsh, R. N., Mullins, M. C., Odenthal, J., and Nusslein-Volhard, C. (1996). Genes controlling and mediating locomotion behavior of the zebrafish embryo and larva. *Development*, 123(1):399–413.

Gray, C., Loynes, C. A., Whyte, M. K. B., Crossman, D. C., Renshaw, S. A., and Chico, T. J. A. (2011). Simultaneous intravital imaging of macrophage and neutrophil behaviour during inflammation using a novel transgenic zebrafish:. *Thrombosis and Haemostasis*, 105(5):811–819.

Gyda, M., Wolman, M., Lorent, K., and Granato, M. (2012). The Tumor Suppressor Gene Retinoblastoma-1 Is Required for Retinotectal Development and Visual Function in Zebrafish. *PLoS Genet*, 8(11):e1003106.

Halloran, M. C., Sato-Maeda, M., Warren, J. T., Su, F., Lele, Z., Krone, P. H., Kuwada, J. Y., and Shoji, W. (2000). Laser-induced gene expression in specific cells of transgenic zebrafish. *Development*, 127(9):1953–1960.

Hamers-Casterman, C., Atarhouch, T., Muyldermans, S., Robinson, G., Hammers, C., Songa, E. B., Bendahman, N., and Hammers, R. (1993). Naturally occurring antibodies devoid of light chains. *Nature*, 363(6428):446–448.

Hendricks, M. and Jesuthasan, S. (2009). PHR Regulates Growth Cone Pausing at Intermediate Targets through Microtubule Disassembly. *The Journal of Neuroscience*, 29(20):6593–6598.

Herrera, E., Brown, L., Aruga, J., Rachel, R. A., Dolen, G., Mikoshiba, K., Brown, S., and Mason, C. A. (2003). Zic2 Patterns Binocular Vision by Specifying the Uncrossed Retinal Projection. *Cell*, 114(5):545–557.

Holt, C. E. and Schuman, E. M. (2013). The Central Dogma Decentralized: New Perspectives on RNA Function and Local Translation in Neurons. *Neuron*, 80(3):648–657.

Homma, S., Shimada, T., Hikake, T., and Yaginuma, H. (2009). Expression pattern of LRR and Ig domain-containing protein (LRRIG protein) in the early mouse embryo. *Gene Expression Patterns*, 9(1):1–26.

Huh, W.-K., Falvo, J. V., Gerke, L. C., Carroll, A. S., Howson, R. W., Weissman, J. S., and O'Shea, E. K. (2003). Global analysis of protein localization in budding yeast. *Nature*, 425(6959):686–691.

Hutson, L. D., Campbell, D. S., and Chien, C.-B. (2004). Analyzing axon guidance in the zebrafish retinotectal system. *Methods in cell biology*, 76:13–35.

Hutson, L. D. and Chien, C.-B. (2002). Pathfinding and Error Correction by Retinal Axons: The Role of astray/robo2. *Neuron*, 33(2):205–217.

Ikeda, Y., Imai, Y., Kumagai, H., Nosaka, T., Morikawa, Y., Hisaoka, T., Manabe, I., Maemura, K., Nakaoka, T., Imamura, T., Miyazono, K., Komuro, I., Nagai, R., and Kitamura, T. (2004). Vasorin, a transforming growth factor β-binding protein expressed in vascular smooth muscle cells, modulates the arterial response to injury in vivo. *Proceedings of the National Academy of Sciences of the United States of America*, 101(29):10732–10737.

Inatani, M., Irie, F., Plump, A. S., Tessier-Lavigne, M., and Yamaguchi, Y. (2003). Mammalian Brain Morphogenesis and Midline Axon Guidance Require Heparan Sulfate. *Science*, 302(5647):1044–1046.

Jeffery, G. and Erskine, L. (2005). Variations in the architecture and development of the vertebrate optic chiasm. *Progress in Retinal and Eye Research*, 24(6):721–753.

Jung, H., Yoon, B. C., and Holt, C. E. (2012). Axonal mRNA localization and local protein synthesis in nervous system assembly, maintenance and repair. *Nature Reviews Neuroscience*, 13(5):308–324.

Jusuf, P. R., Albadri, S., Paolini, A., Currie, P. D., Argenton, F., Higashijima, S.-i., Harris, W. A., and Poggi, L. (2012). Biasing Amacrine Subtypes in the Atoh7 Lineage through Expression of Barhl2. *The Journal of Neuroscience*, 32(40):13929–13944.

Kaiser, P. D., Maier, J., Traenkle, B., Emele, F., and Rothbauer, U. (2014). Recent progress in generating intracellular functional antibody fragments to target and trace cellular components in living cells. *Biochimica et Biophysica Acta (BBA) - Proteins and Proteomics*, 1844(11):1933–1942.

Karlstrom, R., Trowe, T., and Bonhoeffer, F. (1997). Genetic analysis of axon guidance and mapping in the zebrafish. *Trends in neurosciences*, 20(1):3–8.

Karlstrom, R., Trowe, T., Klostermann, S., Baier, H., Brand, M., Crawford, A., Grunewald, B., Haffter, P., Hoffmann, H., Meyer, S., et al. (1996). Zebrafish mutations affecting retinotectal axon pathfinding. *Development*, 123(1):427–438.

Keleman, K., Rajagopalan, S., Cleppien, D., Teis, D., Paiha, K., Huber, L. A., Technau, G. M., and Dickson, B. J. (2002). Comm Sorts Robo to Control Axon Guidance at the Drosophila Midline. *Cell*, 110(4):415–427.

Keleman, K., Ribeiro, C., and Dickson, B. J. (2005). Comm function in commissural axon guidance: cell-autonomous sorting of Robo in vivo. *Nature Neuroscience*, 8(2):156–163.

Khmelinskii, A., Keller, P. J., Bartosik, A., Meurer, M., Barry, J. D., Mardin, B. R., Kaufmann, A., Trautmann, S., Wachsmuth, M., Pereira, G., Huber, W., Schiebel, E., and Knop, M. (2012). Tandem fluorescent protein timers for in vivo analysis of protein dynamics. *Nature Biotechnology*, 30(7):708–714.

Kok, F. O., Shin, M., Ni, C.-W., Gupta, A., Grosse, A. S., van Impel, A., Kirchmaier, B. C., Peterson-Maduro, J., Kourkoulis, G., Male, I., DeSantis, D. F., Sheppard-Tindell, S., Ebarasi, L., Betsholtz, C., Schulte-Merker, S., Wolfe, S. A., and Lawson, N. D. (2015). Reverse Genetic Screening Reveals Poor Correlation between Morpholino-Induced and Mutant Phenotypes in Zebrafish. *Developmental Cell*, 32(1):97–108.

Krautzberger, A. M., Kosiol, B., Scholze, M., and Schrewe, H. (2012). Expression of vasorin (Vasn) during embryonic development of the mouse. *Gene Expression Patterns*, 12(5–6):167–171.

Kuwajima, T., Yoshida, Y., Takegahara, N., Petros, T. J., Kumanogoh, A., Jessell, T. M., Sakurai, T., and Mason, C. (2012). Optic Chiasm Presentation of Semaphorin6d in the Context of Plexin-A1 and Nr-CAM Promotes Retinal Axon Midline Crossing. *Neuron*, 74(4):676–690.

Kwan, K. M., Fujimoto, E., Grabher, C., Mangum, B. D., Hardy, M. E., Campbell, D. S., Parant, J. M., Yost, H. J., Kanki, J. P., and Chien, C.-B. (2007). The Tol2kit: A multisite gateway-based construction kit for Tol2 transposon transgenesis constructs. *Developmental Dynamics*, 236(11):3088–3099.

Lam, C. S., März, M., and Strähle, U. (2009). gfap and nestin reporter lines reveal characteristics of neural progenitors in the adult zebrafish brain. *Developmental Dynamics*, 238(2):475–486.

Lee, J.-S., von der Hardt, S., Rusch, M. A., Stringer, S. E., Stickney, H. L., Talbot, W. S., Geisler, R., Nüsslein-Volhard, C., Selleck, S. B., Chien, C.-B., and Roehl, H. (2004). Axon Sorting in the Optic Tract Requires HSPG Synthesis by ext2 (dackel) and extl3 (boxer). *Neuron*, 44(6):947–960.

Lee, R., Petros, T. J., and Mason, C. A. (2008). Zic2 Regulates Retinal Ganglion Cell Axon Avoidance of ephrinB2 through Inducing Expression of the Guidance Receptor EphB1. *The Journal of Neuroscience*, 28(23):5910–5919.

Leonhardt, H., Rahn, H.-P., Weinzierl, P., Sporbert, A., Cremer, T., Zink, D., and Cardoso, M. C. (2000). Dynamics of DNA Replication Factories in Living Cells. *The Journal of Cell Biology*, 149(2):271–280.

Leung, L., Klopper, A. V., Grill, S. W., Harris, W. A., and Norden, C. (2011). Apical migration of nuclei during G2 is a prerequisite for all nuclear motion in zebrafish neuroepithelia. *Development*, 138(22):5003–5013.

Lindwall, C., Fothergill, T., and Richards, L. J. (2007). Commissure formation in the mammalian forebrain. *Current Opinion in Neurobiology*, 17(1):3–14.

Lorent, K., Liu, K., Fetcho, J., and Granato, M. (2001). The zebrafish space cadet gene controls axonal pathfinding of neurons that modulate fast turning movements. *Development*, 128(11):2131–2142.

Lowery, L. A. and Van Vactor, D. (2009). The trip of the tip: understanding the growth cone machinery. *Nature Reviews Molecular Cell Biology*, 10(5):332–343.

Malapeira, J., Esselens, C., Bech-Serra, J. J., Canals, F., and Arribas, J. (2011). ADAM17 (TACE) regulates TGFβ signaling through the cleavage of vasorin. *Oncogene*, 30(16):1912–1922.

Mandai, K., Guo, T., St. Hillaire, C., Meabon, J. S., Kanning, K. C., Bothwell, M., and Ginty, D. D. (2009). LIG Family Receptor Tyrosine Kinase-Associated Proteins Modulate Growth Factor Signals during Neural Development. *Neuron*, 63(5):614–627.

Mandai, K., Reimert, D. V., and Ginty, D. D. (2014). Linx Mediates Interaxonal Interactions and Formation of the Internal Capsule. *Neuron*, 83(1):93–103.

Marcus, R. C., Blazeski, R., Godement, P., and Mason, C. A. (1995). Retinal axon divergence in the optic chiasm: uncrossed axons diverge from crossed axons within a midline glial specialization. *The Journal of Neuroscience*, 15(5):3716–3729.

Marcus, R. C. and Easter, S. S. (1995). Expression of glial fibrillary acidic protein and its relation to tract formation in embryonic zebrafish (Danio rerio). *The Journal of Comparative Neurology*, 359(3):365–381.

Marcus, R. C. and Mason, C. A. (1995). The first retinal axon growth in the mouse optic chiasm: axon patterning and the cellular environment. *The Journal of Neuroscience*, 15(10):6389–6402.

Mason, C. A. and Sretavan, D. W. (1997). Glia, neurons, and axon pathfinding during optic chiasm development. *Current Opinion in Neurobiology*, 7(5):647–653.

Mason, C. A. and Wang, L.-C. (1997). Growth Cone Form Is Behavior-Specific and, Consequently, Position-Specific along the Retinal Axon Pathway. *The Journal of Neuroscience*, 17(3):1086–1100.

Meeker, N. D., Hutchinson, S. A., Ho, L., and Trede, N. S. (2007). Method for isolation of PCR-ready genomic DNA from zebrafish tissues. *BioTechniques*, 43(5):610, 612, 614.

Muyldermans, S. (2013). Nanobodies: Natural Single-Domain Antibodies. *Annual Review of Biochemistry*, 82(1):775–797.

Nakagawa, S., Brennan, C., Johnson, K. G., Shewan, D., Harris, W. A., and Holt, C. E. (2000). Ephrin-B Regulates the Ipsilateral Routing of Retinal Axons at the Optic Chiasm. *Neuron*, 25(3):599–610.

Navascués, J., Rodríguez-Gallardo, L., García-Martínez, V., Alvarez, I. S., and Martín-Partido, G. (1987). Extra-axonal environment and fibre directionality in the early development of the chick embryo optic chiasm: A light and scanning electron microscopic study. *Journal of Neurocytology*, 16(3):299–310.

Niclou, S. P., Jia, L., and Raper, J. A. (2000). Slit2 Is a Repellent for Retinal Ganglion Cell Axons. *The Journal of Neuroscience*, 20(13):4962–4974.

Nüsslein-Volhard, C. and Dahm, R., editors (2002). *Zebrafish: a practical approach*. Number no. 261 in The practical approach series. Oxford University Press, Oxford, 1st ed edition.

Oster, S. F., Deiner, M., Birgbauer, E., and Sretavan, D. W. (2004). Ganglion cell axon pathfinding in the retina and optic nerve. *Seminars in Cell & Developmental Biology*, 15(1):125–136.

Pak, W., Hindges, R., Lim, Y.-S., Pfaff, S. L., and O'Leary, D. D. M. (2004). Magnitude of Binocular Vision Controlled by Islet-2 Repression of a Genetic Program that Specifies Laterality of Retinal Axon Pathfinding. *Cell*, 119(4):567–578.

Petros, T., Rebsam, A., and Mason, C. (2008). Retinal axon growth at the optic chiasm: to cross or not to cross. *Annu. Rev. Neurosci.*, 31:295–315.

Pittman, A. J., Law, M.-Y., and Chien, C.-B. (2008). Pathfinding in a large vertebrate axon tract: isotypic interactions guide retinotectal axons at multiple choice points. *Development*, 135(17):2865–2871.

Plump, A. S., Erskine, L., Sabatier, C., Brose, K., Epstein, C. J., Goodman, C. S., Mason, C. A., and Tessier-Lavigne, M. (2002). Slit1 and Slit2 Cooperate to Prevent Premature Midline Crossing of Retinal Axons in the Mouse Visual System. *Neuron*, 33(2):219–232.

Po, M. D., Hwang, C., and Zhen, M. (2010). PHRs: bridging axon guidance, outgrowth and synapse development. *Current Opinion in Neurobiology*, 20(1):100–107.

Poulain, F. E. and Chien, C.-B. (2013). Proteoglycan-Mediated Axon Degeneration Corrects Pretarget Topographic Sorting Errors. *Neuron*, 78(1):49–56.

Poulain, F. E., Gaynes, J. A., Hörndli, C. S., Law, M.-Y., and Chien, C.-B. (2010). Analyzing Retinal Axon Guidance in Zebrafish. In H. William Detrich, M. W. a. L. I. Z., editor, *Methods in Cell Biology*, volume 100 of *The Zebrafish: Cellular and Developmental Biology, Part A*, pages 2–26. Academic Press.

Pratt, T., Conway, C. D., Tian, N. M. M.-L., Price, D. J., and Mason, J. O. (2006). Heparan Sulphation Patterns Generated by Specific Heparan Sulfotransferase Enzymes Direct Distinct Aspects of Retinal Axon Guidance at the Optic Chiasm. *The Journal of Neuroscience*, 26(26):6911–6923.

Randlett, O., Poggi, L., Zolessi, F. R., and Harris, W. A. (2011). The Oriented Emergence of Axons from Retinal Ganglion Cells Is Directed by Laminin Contact In Vivo. *Neuron*, 70(2):266–280.

Raper, J. and Mason, C. (2010). Cellular Strategies of Axonal Pathfinding. *Cold Spring Harbor Perspectives in Biology*, 2(9):a001933.

Rocchetti, A., Hawes, C., and Kriechbaumer, V. (2014). Fluorescent labelling of the actin cytoskeleton in plants using a cameloid antibody. *Plant Methods*, 10(1):12.

Rothbauer, U., Zolghadr, K., Tillib, S., Nowak, D., Schermelleh, L., Gahl, A., Backmann, N., Conrath, K., Muyldermans, S., Cardoso, M. C., and Leonhardt, H. (2006). Targeting and tracing antigens in live cells with fluorescent nanobodies. *Nature Methods*, 3(11):887–889.

Sakai, J. A. and Halloran, M. C. (2006). Semaphorin 3d guides laterality of retinal ganglion cell projections in zebrafish. *Development*, 133(6):1035–1044.

Sander, J. D., Dahlborg, E. J., Goodwin, M. J., Cade, L., Zhang, F., Cifuentes, D., Curtin, S. J., Blackburn, J. S., Thibodeau-Beganny, S., Qi, Y., Pierick, C. J., Hoffman, E., Maeder, M. L., Khayter, C., Reyon, D., Dobbs, D., Langenau, D. M., Stupar, R. M., Giraldez, A. J., Voytas, D. F., Peterson, R. T., Yeh, J.-R. J., and Joung, J. K. (2010). Selection-free zinc-finger-nuclease engineering by context-dependent assembly (CoDA). *Nature Methods*, 8(1):67–69.

Schindelin, J., Arganda-Carreras, I., Frise, E., Kaynig, V., Longair, M., Pietzsch, T., Preibisch, S., Rueden, C., Saalfeld, S., Schmid, B., Tinevez, J.-Y., White, D. J., Hartenstein, V., Eliceiri, K., Tomancak, P., and Cardona, A. (2012). Fiji: an open-source platform for biological-image analysis. *Nature Methods*, 9(7):676–682.

Schnell, U., Dijk, F., Sjollema, K. A., and Giepmans, B. N. G. (2012). Immunolabeling artifacts and the need for live-cell imaging. *Nature Methods*, 9(2):152–158.

Shu, T., Li, Y., Keller, A., and Richards, L. J. (2003a). The glial sling is a migratory population of developing neurons. *Development*, 130(13):2929–2937.

Shu, T. and Richards, L. J. (2001). Cortical Axon Guidance by the Glial Wedge during the Development of the Corpus Callosum. *The Journal of Neuroscience*, 21(8):2749–2758.

Shu, T., Sundaresan, V., McCarthy, M. M., and Richards, L. J. (2003b). Slit2 Guides Both Precrossing and Postcrossing Callosal Axons at the Midline In Vivo. *The Journal of Neuroscience*, 23(22):8176–8184.

Silver, D. J. and Silver, J. (2014). Contributions of chondroitin sulfate proteoglycans to neurodevelopment, injury, and cancer. *Current Opinion in Neurobiology*, 27:171–178.

Silver, J. (1984). Studies on the factors that govern directionality of axonal growth in the embryonic optic nerve and at the chiasm of mice. *The Journal of Comparative Neurology*, 223(2):238–251.

Silver, J., Lorenz, S. E., Wahlsten, D., and Coughlin, J. (1982). Axonal guidance during development of the great cerebral commissures: Descriptive and experimental studies, in vivo, on the role of preformed glial pathways. *The Journal of Comparative Neurology*, 210(1):10–29.

Silver, J., Poston, M., and Rutishauser, U. (1987). Axon pathway boundaries in the developing brain. I. Cellular and molecular determinants that separate the optic and olfactory projections. *The Journal of Neuroscience*, 7(7):2264–2272.

Silver, J. and Rutishauser, U. (1984). Guidance of optic axons in vivo by a preformed adhesive pathway on neuroepithelial endfeet. *Developmental Biology*, 106(2):485–499.

Söllner, C. and Wright, G. J. (2009). A cell surface interaction network of neural leucine-rich repeat receptors. *Genome Biology*, 10(9):R99.

Sperry, R. W. (1943). Effect of 180 degree rotation of the retinal field on visuomotor coordination. *Journal of Experimental Zoology*, 92(3):263–279.

Sretavan, D. W. (1990). Specific routing of retinal ganglion cell axons at the mammalian optic chiasm during embryonic development. *The Journal of Neuroscience*, 10(6):1995–2007.

Sretavan, D. W., Feng, L., Puré, E., and Reichardt, L. F. (1994). Embryonic neurons of the developing optic chiasm express L1 and CD44, cell surface molecules with opposing effects on retinal axon growth. *Neuron*, 12(5):957–975.

Sretavan, D. W., Puré, E., Siegel, M. W., and Reichardt, L. F. (1995). Disruption of retinal axon ingrowth by ablation of embryonic mouse optic chiasm neurons. *Science (New York, N.Y.)*, 269(5220):98–101.

Stoeckli, E. T. (2006). Longitudinal axon guidance. *Current Opinion in Neurobiology*, 16(1):35–39.

Stuermer, C. and Bastmeyer, M. (2000). The retinal axon's pathfinding to the optic disk. *Progress in Neurobiology*, 62(2):197–214.

Stuermer, C. A. (1988). Retinotopic organization of the developing retinotectal projection in the zebrafish embryo. *The Journal of Neuroscience*, 8(12):4513–4530.

Swulius, M. T. and Jensen, G. J. (2012). The Helical MreB Cytoskeleton in Escherichia coli MC1000/pLE7 Is an Artifact of the N-Terminal Yellow Fluorescent Protein Tag. *Journal of Bacteriology*, 194(23):6382–6386.

Thanos, S. and Bonhoeffer, F. (1984). Development of the transient ipsilateral retinotectal projection in the chick embryo: A numerical flourescence-microscopic analysis. *Journal of Comparative Neurology*, 224(3):407–414.

Tojima, T., Itofusa, R., and Kamiguchi, H. (2010). Asymmetric Clathrin-Mediated Endocytosis Drives Repulsive Growth Cone Guidance. *Neuron*, 66(3):370–377.

Trowe, T., Klostermann, S., Baier, H., Granato, M., Crawford, A., Grunewald, B., Hoffmann, H., Karlstrom, R., Meyer, S., Muller, B., et al. (1996). Mutations disrupting the ordering and topographic mapping of axons in the retinotectal projection of the zebrafish, Danio rerio. *Development*, 123(1):439–450.

van der Merwe, P. A. and Barclay, N. A. (1994). Transient intercellular adhesion: the importance of weak protein-protein interactions. *Trends in Biochemical Sciences*, 19(9):354–358.

Vitriol, E. A. and Zheng, J. Q. (2012). Growth Cone Travel in Space and Time: the Cellular Ensemble of Cytoskeleton, Adhesion, and Membrane. *Neuron*, 73(6):1068–1081.

Volkmann, K., Chen, Y.-Y., Harris, M. P., Wullimann, M. F., and Köster, R. W. (2010). The zebrafish cerebellar upper rhombic lip generates tegmental hindbrain nuclei by long-distance migration in an evolutionary conserved manner. *The Journal of Comparative Neurology*, 518(14):2794–2817.

Walz, A., Anderson, R. B., Irie, A., Chien, C.-B., and Holt, C. E. (2002). Chondroitin sulfate disrupts axon pathfinding in the optic tract and alters growth cone dynamics. *Journal of Neurobiology*, 53(3):330–342.

Wang, L.-C., Dani, J., Godement, P., Marcus, R. C., and Mason, C. A. (1995). Crossed and uncrossed retinal axons respond differently to cells of the optic chiasm midline in vitro. *Neuron*, 15(6):1349–1364.

Wang, L.-C., Rachel, R. A., Marcus, R. C., and Mason, C. A. (1996). Chemosuppression of Retinal Axon Growth by the Mouse Optic Chiasm. *Neuron*, 17(5):849–862.

Williams, S. E., Grumet, M., Colman, D. R., Henkemeyer, M., Mason, C. A., and Sakurai, T. (2006). A Role for Nr-CAM in the Patterning of Binocular Visual Pathways. *Neuron*, 50(4):535–547.

Williams, S. E., Mann, F., Erskine, L., Sakurai, T., Wei, S., Rossi, D. J., Gale, N. W., Holt, C. E., Mason, C. A., and Henkemeyer, M. (2003). Ephrin-B2 and EphB1 Mediate Retinal Axon Divergence at the Optic Chiasm. *Neuron*, 39(6):919–935.

Wizenmann, A., Thanos, S., Boxberg, Y. v., and Bonhoeffer, F. (1993). Differential reaction of crossing and non-crossing rat retinal axons on cell membrane preparations from the chiasm midline: an in vitro study. *Development*, 117(2):725–735.

Xiao, T. and Baier, H. (2007). Lamina-specific axonal projections in the zebrafish tectum require the type IV collagen Dragnet. *Nature Neuroscience*, 10(12):1529–1537.

Xiao, T., Roeser, T., Staub, W., and Baier, H. (2005). A GFP-based genetic screen reveals mutations that disrupt the architecture of the zebrafish retinotectal projection. *Development*, 132(13):2955–2967.

Xiao, T., Staub, W., Robles, E., Gosse, N. J., Cole, G. J., and Baier, H. (2011). Assembly of Lamina-Specific Neuronal Connections by Slit Bound to Type IV Collagen. *Cell*, 146(1):164–176.

Xu, H., Ye, D., Behra, M., Burgess, S., Chen, S., and Lin, F. (2014). Gβ1 controls collective cell migration by regulating the protrusive activity of leader cells in the posterior lateral line primordium. *Developmental Biology*, 385(2):316–327.

Zolessi, F., Poggi, L., Wilkinson, C., Chien, C., and Harris, W. (2006). Polarization and orientation of retinal ganglion cells in vivo. *Neural development*, 1(1):2.